Autonomous Capillary Systems for Life Science Research and Medical Diagnostics

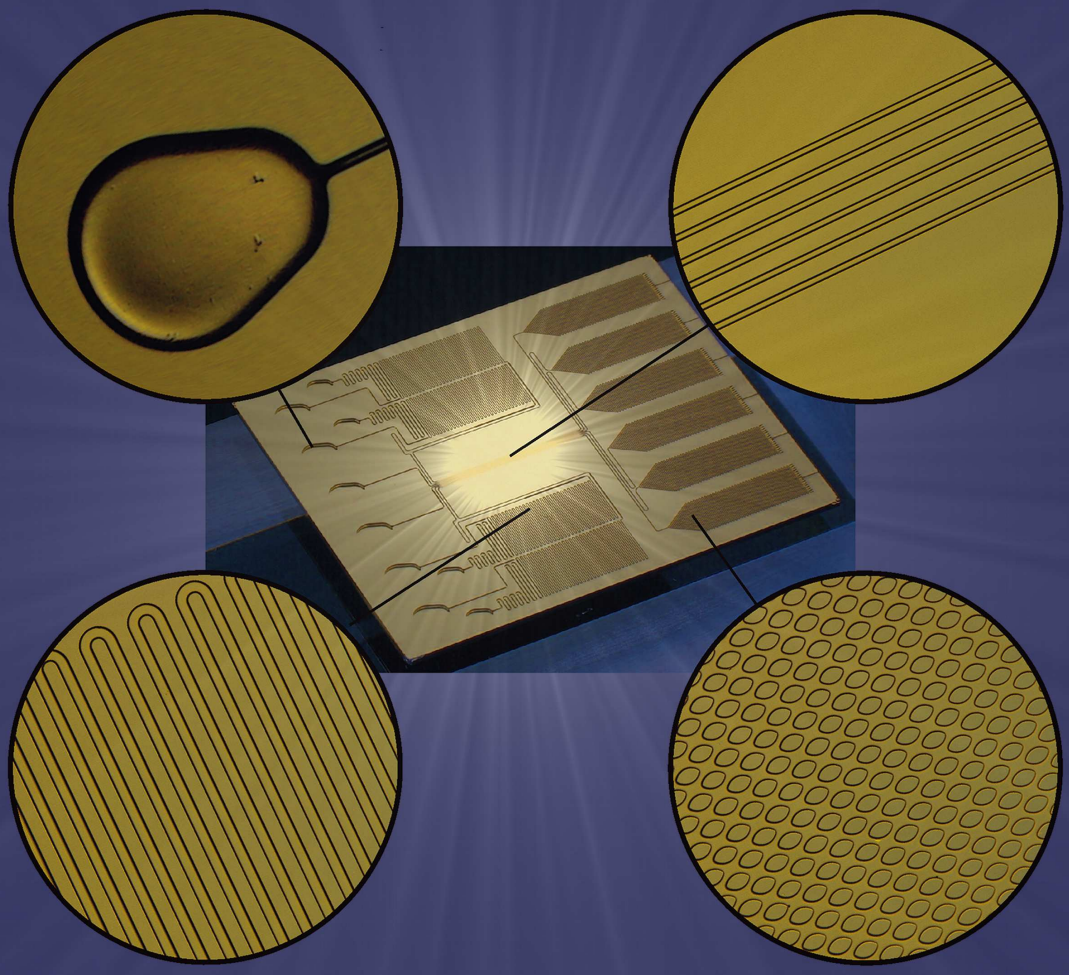

Martin Zimmermann

Autonomous Capillary Systems for Life Science Research and Medical Diagnostics

INAUGRALDISSERTATION

zur Erlangung der Würde eines Doktors der Philosophie
vorgelegt der
Philosophisch-Naturwissenschaftlichen Fakultät
der Universität Basel

von

Martin Zimmermann
aus Heitersheim, Deutschland

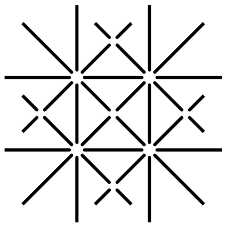

UNI
BASEL

Basel, 2009

Genehmigt von der Philosophisch-Naturwissenschaftlichen Fakultät auf Antrag von:

Prof. Dr. H.-J. Güntherodt (Fakultätsverantwortlicher)
Prof. Dr. N. F. de Rooij (Korreferent)
PD Dr. P. Hunziker (Experte)
Dr. E. Delamarche (Experte)

Basel, den 16. Oktober 2007

Prof. Dr. Hans-Peter Hauri, Dekan

Abstract

In autonomous capillary systems (CS) minute amounts of liquid are transported owing to capillary forces. Such CSs are appealing due to their portability, flexibility, and the exceptional physical behavior of liquids in micrometer sized microchannels, in particular, capillarity and short diffusion times. CSs have shown to be a promising technology for miniaturized immunoassays in life science research and diagnostics. Building on existing experimental demonstrations of immunoassays in CSs, a theoretical model of such immunoassays is implemented, tools and CSs for performing immunoassays are developed, key functional elements of CSs such as capillary pumps and valves are explored experimentally, and a proof-of-concept of the ultimate goal of one-step immunoassays are given in this work.

For the theoretical modeling of immunoassays in CSs a finite difference algorithm is applied to delineate the role of the transport of analyte molecules in the microchannel (convection and diffusion), the kinetics of binding between the analyte and the capture antibodies, and the surface density of the capture antibody on the assay. The model shows that assays can be greatly optimized by varying the flow velocity of the solution of analyte in the microchannels. The model also shows how much the analyte-antibody binding constant and the surface density of the capture antibodies influence the performance of the assay. We derive strategies to optimize assays toward maximal sensitivity, minimal sample volume requirement or fast performance.

A method using evaporation for controlling the flow rate in CSs was developed for maximum flexibility for developing assays. The method allows to use small CSs that initially are filled by capillary forces and then provide a well defined area of the liquid-air interface from which liquid can evaporate. Temperature and humidity are continuously measured and Peltier-elements are used to adjust the temperatures in multiple areas of the CSs relative to the

dew-point. Thereby flow rates in the range from ~ 1.2 nL s^{-1} to ~ 30 pL s^{-1} could be achieved in the microchannels. This method was then used for screening cells for surface receptors.

CSs, that do not need any peripherals for controlling flow rates become even more appealing. We explored the filling behavior of such CSs having microchannels of various length and large capillary pumps. The capillary pumps comprise microstructures of various sizes and shapes, which are spaced to encode certain capillary pressures. The spacing and shape of the microstructures is also used to orient the filling front to obtain a reliable filling behavior and to minimize the risk of entrapping air. We show how two capillary pumps having different hydrodynamic properties can be connected to program a sequence of slow and fast flow rates in CSs. Liquid filling CSs can hardly be stopped, but in some cases it might be beneficial to do so. In a separate chapter we explore how microstructures need to be designed to use capillary forces to stop, time, or trigger liquids.

Besides well-defined flow rates in CSs accurately patterned capture antibodies (cAbs) are key for performing high-sensitive surface immunoassays in CSs. We present a method compatible with mass fabrication for patterning cAbs in dense lines of up to 8 lines per millimeter. These cAbs are used with CSs that are optimized for convenient handling, pipetting of solutions, pumping of liquids such as human serum, and visualization of signals for fluorescence immunoassays to detect c-reactive protein (CRP) with a sensitivity of 0.9 ng mL^{-1} (7.8 pM) from 1 µL of CRP-spiked human serum, within 11 minutes, with 4 pipetting steps, and a total volume of sample and reagents of <1.5 µL.

CSs for diagnostic applications have different requirements than CSs that are used as a research tool in life sciences, where a high flexibility and performance primes over the ease of use and portability of the CSs. We give a proof-of-concept for one-step immunoassays based on CSs which we think can be the base for developing portable diagnostics for point-of-care applications. All reagents are preloaded in the CSs. A sample loaded in the CSs redissolves and reconstitutes the detection antibodies (dAbs), analyte-dAb-complexes are formed and detected downstream in the CSs. A user only needs to load a sample and measure the result using a fluorescence

microscope or scanner. C-reactive protein was detected in human serum at clinical concentrations within 10 minutes and using only 2 μL of sample.

Contents

List of Acronyms

Abs	antibodies
BSA	bovine serum albumin
cAbs	capture antibodies
COC	cyclic olefin copolymer
CP	capillary pump
CRP	C-reactive protein
CRV	capillary retention valve
CS	capillary system
dAbs	detection antibodies
DMSO	dimethylsulfoxide
DRIE	deep reactive ion etching
FACS	fluorescence activated cell sorting
FITC	fluorescein isothiocyanate
HDT	hexadecane thiol
HS-PEG	thiolated poly(ethyleneglycol)
IgG	immunoglobulin G
LOC	lab-on-a-chip
MFN	microfluidic network

μTAS	micro total analysis system
PBS	phosphate-buffered saline
PDMS	poly(dimethylsiloxane)
PEG	poly(ethyleneglycol)
SEM	scanning electron microscope
TNF-α	tissue necrosis factor-α
TRITC	tetramethylrhodamine isothiocyanate

List of Tables

List of Figures

List of Publications

Parts of this work have been published in journal papers or have been presented at conferences.

Journal Papers

M. Zimmermann, E. Delamarche, M. Wolf, P. Hunziker, Modeling and Optimization of High-Sensitivity, Low-Volume Microfluidic-Based Surface Immunoassays, *Biomedical Microdevices* **7**:2, 99–110, **2005**.

M. Zimmermann, S. Bentley, H. Schmid, P. Hunziker, E. Delamarche, Continuous Flow in Open Microfluidics using Controlled Evaporation, *Lab Chip*, **5**, 1355–1359, **2005**.

M. Zimmermann, H. Schmid, P. Hunziker, E. Delamarche, Capillary Pumps for Autonomous Capillary Systems, *Lab Chip*, **7**, 119–125, **2007**.

M. Wolf, M. Zimmermann, E. Delamarche, P. Hunziker, Screening Cell Surface Receptors using Micromosaic Immunoassays, *Biomedical Microdevices*, **9**, 135–141, **2007**.

J. Ziegler, M. Zimmermann, P. Hunziker, E. Delamarche, High-performance immunoassays based on through-stencil patterned antibodies and capillary systems, *Analytical Chemistry*, **80**, 1763–1769, **2008**.

M. Zimmermann, P. Hunziker, E. Delamarche, Valves for autonomous capillary systems, *Microfluidics and Nanofluidics*, **5**, 395–402, **2008**.

M. Zimmermann, P. Hunziker, E. Delamarche, Autonomous capillary system for one-step immunoassays, *Biomedical Microdevices*, **11**, 1–8, **2009**.

Contributions at International Conferences

M. Zimmermann, M. Wolf, C. Jansen, B. Michel, S. Marsch, P. Hunziker, Optimizing Drag Force in Microfluidic-based Immunoassays: Computational Fluid Dynamics Study of a New Approach to Improve Signal-to-noise Ratio of Immunoassays, *7th International Conference on Nanostructured Materials*, Wiesbaden, Germany, June 20–24, **2004**.

M. Zimmermann, P. Hunziker, Computational optimization of microfluidic networks, *International Oberon Meeting*, Basel, Switzerland, July 23, **2004**.

M. Zimmermann, E. Delamarche, M. Wolf, P. Hunziker, Microfluidic-Based Surface Immunoassays for High-Sensitivity and Low-Volume Applications, *8th International Conference on Enabling Technologies for Drug Discovery (Miptec)*, Basel, Switzerland, May 9–12, **2005**.

M. Zimmermann, S. Bentley, D. Juncker, H. Schmid, P. Hunziker, E. Delamarche, Locally Controlling the Environment of a Microfluidic Chip and Programming its Flow Rates, In Proceedings of Micro Total Analysis Systems 2005, *9th International Conference on Miniaturized Systems for Chemistry and Life Science*, Boston, MA, USA, Oct 9–13, **2005**, pp. 578–580.

M. Zimmermann, P. Hunziker, E. Delamarche, Microfluidics for Immunoassays with Sub-microliter Sample Volume, *9th International Conference on Enabling Technologies for Drug Discovery (Miptec)*, Basel, Switzerland, May 8–11, **2006**.

M. Wolf, M. Zimmermann, J. Ziegler, E. Delamarche, P. Hunziker, Receptor–Specific Immobilisation of Cells, *International Conference on Nanoscience and Technology p(ICN+T)*, Basel, Switzerland, July 30–August 4, **2006**.

M. Zimmermann, M. Wolf, P. Hunziker, E. Delamarche, Microfluidic Capillary Systems for Nanobiotechnology, *International Conference on Nanoscience and Technology (ICN+T)*, Basel, Switzerland, July 30–August 4, **2006**.

M. Zimmermann, P. Hunziker, E. Delamarche, Microfluidic Capillary Systems for Diagnostics, *NanoEurope*, St. Gallen, Switzerland, September 12–14, **2006**.

M. Zimmermann, P. Hunziker, E. Delamarche, Advanced flow control of liquids in microfabricated capillary pumps, In Proceedings of Micro Total Analysis Systems 2006, *10th International Conference on Miniaturized Systems for Chemistry and Life Science*, Tokyo, Japan, November 5–9, **2006**, pp. 612–614.

J. Ziegler*, M. Zimmermann*, P. Hunziker, E. Delamarche, Fully autonomous capillary systems for fast and sensitive surface immunoassays, In Proceedings of Micro Total Analysis Systems 2007, *11th International Conference on Miniaturized Systems for Chemistry and Life Science*, Paris, France, October 7–11, **2007**, pp. 101–103.

M. Zimmermann, P. Hunziker, E. Delamarche, Valves for autonomous capillary systems, In Proceedings of Micro Total Analysis Systems 2007, *11th International Conference on Miniaturized Systems for Chemistry and Life Science*, Paris, France, October 7–11, **2007**, pp. 1492–1494.

Luc Gervais, M. Zimmermann, P. Hunziker, E. Delamarche, One-step immunassay on capillary-driven microfluidics, In Proceedings of Micro Total Analysis Systems 2008, *12th International Conference on Miniaturized Systems for Chemistry and Life Science*, San Diego, CA, USA, October 12–16, **2008**.

Invited presentations

Microfluidic capillary systems for immunoassays, *XaarJet Alumni Meeting*, Jarfälla, Sweden, July 7–8, **2006**.

Microfluidics for point-of-care immuno-diagnostics, *Bühlmann Laboratories*, Schönenbuch, Switzerland, May 9, **2007**.

Publications not related to this thesis

W. Voit, M. Zimmermann, M. Alsered, K.V. Rao, W. Zapka, Dispensing adhesive in narrow pattern using a multi-nozzle inkjet head. In Proceedings of *International Microelectronics And Packaging Society (IMAPS) Nordic Conf.*, Stockholm, Sweden, September 29–October 2, **2002**, pp. 64–70.

1. Introduction

Medical diagnostics is the process of identifying a medical condition or disease by its signs, symptoms, and from the results of various diagnostic procedures. Numerous medical tests are commonly performed with patients having abnormal symptoms, such as measuring blood pressure and pulse rate, applying medical imaging methods (e.g. ultra sound imaging), electrical measurements (e.g. electrocardiogram) or analyzing body liquids (blood, urine, saliva, cerebrospinal liquid). A reliable diagnosis is a challenging and complex procedure that typically requires medical professionals to conduct several tests and interpret their results. In some cases, patients perform tests on their own after they have been taught how to interpret the results, such as diabetes patients [1], or if tests are simple to use and self-explaining, such as pregnancy tests [2].

A number of immunoassay tests [3], which are performed to determine antibody and antigen concentrations in body liquids, require skilled operators or complex robotic analyzers to pipette, time and repeat several steps while performing the test. In the case of acute diseases, such as acute myocardial syndrome, fast diagnostic results within a few minutes are essential to start proper treatment early for the patient's benefit. This thesis explores concepts for fast and sensitive immunoassays using capillary systems (CS) in which liquids are moved owing to capillary forces. Such CSs might help improve medical treatments by providing high-sensitive and quantitative results within a short time, with ease-of-use and economy of cost. CSs might also enable applications for life science research, that require immunoassays which can be performed with ultra small sample volumes.

1.1. Trends in Medical Immuno-Diagnostics

Modern immunoassays date back to 1959 when the principle was first described using a radioimmunoassay for insulin [4]. Since then, immunoassays have proved to be one of the most productive technological contributions to medicine and fundamental life science research. Immunoassays have been implemented on various platforms. State-of-the-art clinical random-access analyzers perform bead based immunoassays in tubes. Random-access analyzers are fully automated, allow samples to be loaded at any time, and have a throughput of >200 samples per hour [3]. These analyzers are operated in centralized laboratories. Immunoassays in life science research are performed in microtiter plates having up to 1536 individual wells which enable a higher throughput than clinical analyzers. Robotic liquid handlers fill and aspirate liquids from the wells and tubes according to the protocol of the immunoassay.

The growing demand of fast, accurate, economical and automated analytical systems has emerged the idea of micro total analysis system (μTAS) or lab-on-a-chip (LOC) [5, 6] in the 1990s. The vision of a miniaturized clinical analyzer in the palm of one's hand still persists. LOC benefit from the exceptional physics and behavior of liquids in micrometer sized capillaries and uses these phenomena to process, mix, and capture reagents. Immunoassays in micrometer sized dimensions enable rapid analysis due to short diffusion distances, and require little analyte volumes which also saves precious and expensive reagents. Efficient mass transport and rinsing at the microscale might also ease the simplification and integration of assay steps, such as sample preparation and analysis of results. The small size facilitates the fabrication of handheld analyzers that are suitable for performing urgent test at the point-of-care.

This vision has evolved into the first devices that perform a few critical measurements on-chip. The implemented concept of a portable blood gas analyzer [7] exemplifies the performance of such systems. A single use cartridge, comprising a membrane for cell filtration and a sensor is loaded with a drop of blood and inserted into a handheld analyzer. After a few minutes, results can be read on the screen of the analyzer and transferred to the laboratory information system. Similar devices can be used to perform immunoassays

for cardiac markers [8, 9]. A growing number of companies are active in the production and commercialization of a large variety of miniaturized and effective analytical devices [10], but most of the LOC devices are still far from small due to bulky peripherals [11], or are not yet ultimately fast.

The trend to miniaturized analytical systems is supported by existing fabrication techniques originally applied in the field of microelectronics. Photolithography and 3-dimensional structured silicon wafers are used for microfluidics. We will now discuss the physical properties from which miniaturized analytical systems might benefit.

1.2. Miniaturization Effects

Miniaturization will obviously scale down volumes, but might also change the relative magnitude between forces of different origin. Effects of marginal importance at the macro-scale might dominate at the micro-scale [12]. Figure 1.1 shows a cube having an edge length a. Shrinking a increases the surface-to-volume ratio

$$\frac{A}{V} \propto \frac{a^2}{a^3} = \frac{1}{a} \tag{1.1}$$

of the surface area A and the volume V of the cube significantly. The flow becomes laminar at length scales of millimeters depending on the flow velocity and the viscosity of the liquid. In such small volumes mixing of reagents is provided by convective laminar flow and by diffusion instead of turbulences such as in large volumes [13]. Diffusion is comparably fast at the micrometer scale: A medium sized protein diffuses ∼10 µm within a second compared to 2.7 hours for a distance of 1 mm.

While scaling down the volume of an analyte, its concentration needs to be considered. The absolute number of analyte molecules might statistically get below one analyte molecule per sample if low concentrations of analyte are anticipated and too small sample volumes are used. For example, 1 µL of analyte having a concentration of 1 pg mL^{-1} (10 fM for a protein of the size 100 kDa) contains ∼6000 individual proteins, whereas in 1 nL and 1 pL of the same concentration only 6 and 0.006 proteins are left, respectively.

However, if the area in which the concentration is measured, is reduced

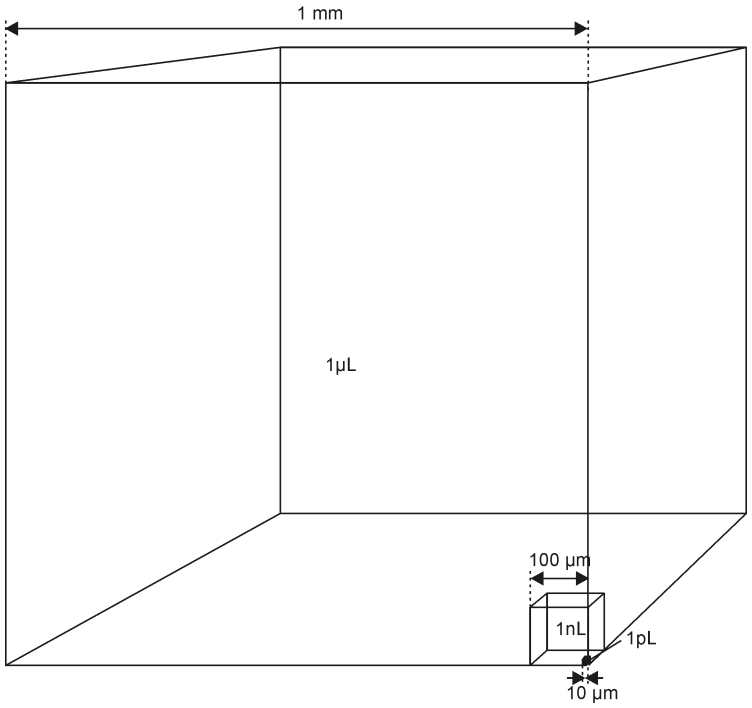

Figure 1.1. Scaling of surface and volumes.

as well, less molecules might be required in order to generate a significant signal. In our micromosaic immunoassays [14] the area in which proteins are captured and quantified using fluorescence techniques can be as small as $30 \times 30\ \mu m^2$. If we assume the footprint of one capture site being the size of $150\ nm^2$ [15, 16] and 10 % active binding sites properly oriented towards the liquids phase [3], 600000 bound and labeled proteins would result in a maximum signal. Depending on the intensity of the fluorophores and the sensitivity of the instrument ∼450 proteins should still be detectable [17].

In the remainder of this section we will discuss constraints which are particularly important for developing and using microfluidic capillary systems.

1.2.1. Surface Tension

Surface tension originates from intramolecular forces and describes the interaction between a liquid and its own gas. Surface tension can shape the surface of microvolumes of liquid, Fig. 1.2. *Young*'s equation relates different interfacial energies σ_{ij} of vapor-solid (vs), liquid-solid (ls), and vapor-liquid

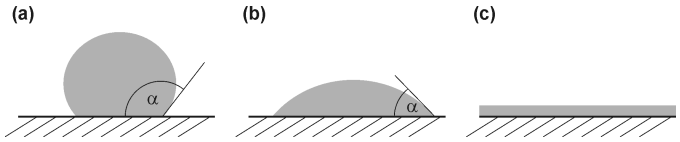

Figure 1.2. Shape of a drop of liquid on solid surfaces in a gas atmosphere. (a) Non-wettable surfaces having a contact angle $\alpha > 90°$ are hydrophobic. (b, c) Wettable or hydrophilic surfaces, respectively, have contact angles $\alpha < 90°$. The surfaces in (a) and (b) are partially wetted and fully wetted in (c) $\alpha = 0°$.

(vl) interfaces via the equilibrium contact angle α of the liquid to the surface: $\sigma_{vs} - \sigma_{ls} = \sigma_{vl} \cos \alpha$. The droplet of liquid in Fig. 1.2a has a poor wettablility on the surface and forms a contact angle $\alpha > 90°$ at the solid-liquid-vapor contact line. This surface is partially non-wettable with this particular liquid. In contrast, the surface in Fig. 1.2b and c having a contact angle $\alpha < 90°$ and $\alpha = 0$ is partially and fully wettable, respectively. A surface is fully wetted when the gain in free energy at the solid-liquid interface is larger than the surface free energy of the liquid. In the case of water a wettable surface is commonly defined as hydrophilic, a non-wettable one as hydrophobic. The difference between the contact angles α_a and α_r of an advancing and receding contact line respectively, is called contact angle hysteresis. Liquids on rough or chemically inhomogenous surfaces tend to have larger contact angle hysteresis than the same liquids on flat and chemically homogenous surfaces. The contact angle is often measured to evaluate the cleanliness of a surface [18, 19]. Organic contamination increases the contact angle which results in poor wettability. CS are wettable on their inner surfaces in order to generate a negative capillary pressure and might have hydrophobic areas in selected regions to prevent contamination or to time liquids [20, 21].

1.2.2. Capillary Flow

In microvolumes forces related to surface tension often dominate gravity, inertia or friction. The conversion of surface tension into capillary pressure is described by the *Young-Laplace* equation [22, 23]. The capillary pressure

$$P_c = -\sigma \left(\frac{\cos \alpha_b + \cos \alpha_t}{d} + \frac{\cos \alpha_l + \cos \alpha_r}{w} \right) \tag{1.2}$$

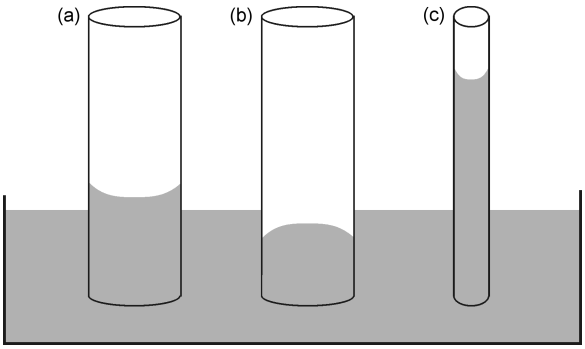

Figure 1.3. Capillary pressure in capillaries of different diameter. The inner surface of the capillaries are hydrophilic (a, c) and hydrophobic (b).

for rectangular capillaries of width w and depth d is a function of the surface tension σ and the contact angles α_i with the indices b, t, l, r referring to *bottom, top, left* and *right* walls, respectively.

Capillaries having hydrophilic surfaces which are partially dipped into a water bath imbibe water, see Fig. 1.3. Thus water levels in hydrophilic capillaries are higher than the water level of the bath. In contrast, the level in a hydrophobic capillary does not exceed the level of the bath. The exact height of the water level inside the capillaries depends on their diameter. Smaller capillaries have larger absolute capillary pressure.

The *Reynolds* number Re quantifies the ratio of inertial to viscous forces and is used to distinguish between laminar and turbulent flow regimes. It is calculated as [24]

$$Re = \frac{\rho v L}{\eta}, \tag{1.3}$$

where ρ is the density, η the dynamic viscosity, and v the mean velocity of the liquid, and L the characteristic length of the flow path. For circular capillaries L equals the capillary diameter and for non-circular cross-section the hydraulic diameter $D_h = \frac{4A}{U}$ where A is the cross-section and U the wetted perimeter of the cross-section is used. A flow is laminar for $Re < 2300$. In microfluidics mostly $Re < 1$ is valid.

The hydrodynamics of a flow of liquid is described by the *Navier-Stokes* equation. In the case of pressure-driven steady laminar flow in a capillary, the solution is known as the law of *Hagen-Poiseuille* which describes the

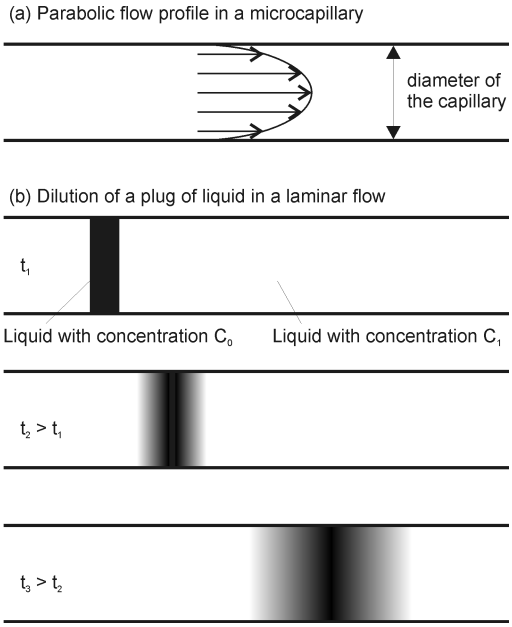

Figure 1.4. Flow and concentration profile in microcapillaries. (a) Characteristic parabolic flow profile in a microcapillary. (b) Effect of the parabolic flow profile on the concentration profile. A plug of liquid having a concentration C_0 which is flowing in-between liquid plugs having the concentration $C_1 < C_0$ is diluted.

characteristic flow velocity

$$v(r) = \frac{\Delta P}{4\eta l}\left(R^2 - r^2\right), \tag{1.4}$$

where r is the distance from the center, R the radius, l the length, and ΔP the difference of the pressure between the inlet and outlet of a capillary. The flow velocity is maximum in the center, and zero at the walls of a capillary. This results in smearing of an analyte concentration C_0 in a plug of liquid which is placed in-between plugs of the same liquid having an analyte concentration C_1, Fig. 1.4. This effect might be useful for mixing of reagents, but also prevents two liquids from flowing sequentially in a capillary without being diluted.

The flow rate I in a capillary can be expressed as

$$I = \frac{1}{\eta}\frac{\Delta P}{R_f}. \tag{1.5}$$

The friction factor R_f times the viscosity η is the hydraulic resistance of the capillary. For a capillary that fills only owing to capillary forces ΔP

corresponds to the capillary pressure. The friction factor is calculated from the geometry of the round capillary

$$R_{f\bigcirc} = \left(\frac{\pi R^4}{8l}\right)^{-1} = \left(\frac{1}{8}\frac{AR_h^2}{l}\right)^{-1}, \tag{1.6}$$

where A is the cross section of the capillary and R_h the hydraulic radius. The friction factor increases while filling the capillary with l corresponding to the filled length.

Capillaries which are etched into silicon using dry-etching have a rectangular cross-section. Such capillaries are termed "microchannels" in this work. The friction factor of microchannels can be derived from a *Taylor* series and be written as a first-order approximation with no more than 10 % deviation from the original value [25]

$$R_{f\square} = \left(\frac{1}{12}\left(1 + \frac{5a}{6b}\right)\frac{AR_h^2}{l}\right)^{-1}, \tag{1.7}$$

with width a and depth b, $a < b$, of the microchannel.

1.2.3. Diffusion

Brownian motion [26], thermally induced random motion of molecules, results in diffusion and in mass transfer in the presence of concentration gradients. The flux of diffusion is described by *Fick*'s law

$$j_i = -D_i \nabla C_i, \tag{1.8}$$

where D_i is the diffusion coefficient, and ∇C_i the concentration gradient of the species i. The *Stokes-Einstein*-relation $D = \frac{kT}{6\pi\eta R_{hydro}}$ is applied to calculate the diffusion coefficient of globular proteins, with the *Boltzmann* constant k, the temperature T, and the hydrodynamic radius R_{hydro} [27]. The diffusion constant D of proteins in aqueous solution typically ranges from $\sim 10^{-7} - 10^{-5}$ cm^2 s^{-1} depending on their size. The average time t_D for diffusing a distance d is given as

$$t_D = \frac{d^2}{2D_i}. \tag{1.9}$$

A protein having the size of 17 kDa has a diffusion coefficient of 10^{-6} cm^2 s^{-1}. It needs 0.05 s for a diffusion distance of 10 µm. Thus reactions in fluidic

microchannels benefit from a short diffusion time of the reactants. In combination with the convective laminar flow described above, reaction rates can be well controlled by supplying more or less reactants with fast or slow flow rates, respectively. Macroscopic reactions can not reach a similar degree of accuracy in controlling a reaction due to the time lag caused by slow diffusion rates and less precise turbulent mixing.

1.3. Principles of Immunoassays

Immunoassays derive their unique characteristics from important properties of antibodies: (i) their ability to bind to an extremely wide range of biomolecules, cells and viruses, (ii) their exceptional specificity for the substance to which each antibody binds and (iii) the strength of the binding between antibody and its target [3]. A widely used variant of immunoassays which forms multiple layers of proteins on a surface is known as sandwich immunoassays. Antibodies, that were immobilized on a surface (capture antibodies, cAb) bind (capture) analytes from solution. Labeled secondary antibodies (detection antibodies, dAb) detect bound analytes. Detection Abs are specific to other binding sites on antigens than cAbs and have radioactive isotopes, enzymes, or fluorescent molecules, as labels, which can be measured. The obtained signal is directly proportional to the concentration of analyte. Typically each species is applied sequentially to the surface and a number of rinsing steps are performed between different steps and before measuring the final result on the surface.

The reaction between antibody and antigen is described by the Law of Mass Action [3]

$$[Ag] + [Ab] \underset{k_{off}}{\overset{k_{on}}{\rightleftharpoons}} [Ag - Ab] \tag{1.10}$$

where $[Ag]$ and $[Ab]$ are the concentration of antigen and antibody, respectively, $[Ag - Ab]$ the concentration of antigen-antibody-complex, k_{on} the association rate constant, and k_{off} the dissociation rate constant. The ratio of the two rate constants give the equilibrium constant $K = \frac{k_{on}}{k_{off}}$, which is also known as the affinity constant.

1.4. Objectives and Structure of this Thesis

This thesis is structured in cumulative chapters which have been published as journal papers. We will give a short outline of the objectives of the chapters and thesis in general.

We are in particular interested in developing tools and methods for fast and sensitive immunoassays which ultimately could lead to portable and easy to use devices operated outside of centralized laboratories or even in ambulances (point-of-care). Such immunoassay tests are required to have no bulky peripherals, ideally be as accurate as clinical laboratory test, and convenient to use. Ideally, only a body liquid would be required to be loaded on a certain region of the device.

In order to design and develop optimal immunoassays and capillary systems a precise understanding of the kinetics of immunoassays in capillary systems is required. The definition of an optimal assay depends on the application: it might be fast, consume ultimately minute volumes, or have a wide range of measurable analyte concentrations. We have developed and implemented a model, which allows to simulate concentration profiles in microchannels and the kinetics of immunoassays performed in such microchannels. The most important parameters leading to optimal assays are comprehensively discussed in Chapter 2.

One of the key challenges is to precisely, reliably and economically control the flow of minute amounts of liquids in microchannels. Capillary systems have the flow rate preprogrammed at the time of fabrication and therefore have limited flexibility. However, while developing assays, flexible systems are desirable in order to easily tune a flow rate depending on the characteristics of the assay. We have set up a platform that allows the user to program a flow rate in microchannels at the time of use. The platform is described in Chapter 3. It is based on the evaporation from a certain region of the capillary system and controls the temperature in different zones of the capillary system relative to the ambient dew point.

In Chapter 4 the platform described in Chapter 3 is used to develop a cell assay. Living cells are flown through the capillary system and screened for specific proteins on their cell membrane. This assay benefits in particular from

the ability to control the temperature in the capillary systems. In addition, the metabolism of living cells is sensitive to temperature and the kinetics of proteins and cells are optimal at 37 °C.

The challenge of controlling the flow of minute amounts of liquid in capillary systems having no peripherals is addressed again in Chapter 5. The components of capillary systems having the highest impact on the flow behavior of liquid in CSs are discussed. Flow resistors are used to tune the flow rate in microchannels and most importantly, large capillary pumps having a reliable filling behavior are developed.

The knowledge gained from designing capillary systems in which liquids move due to capillary forces resulted in the fabrication of chips having six independent capillary systems and suited to displace up to 2 µL of sample volume. In previous work, the method used for immobilizing capture antibodies to perform micromosaic immunoassays required a second microfluidic chip. This method is effective and accurate but requires a microfluidic chip to be cleaned and coated with a hydrophilic monolayer before each use. The handling overhead of such a method is significant and lead to the design of a simplified method that might also be compatible with mass-fabrication. Thus the protocol to perform a CRP-immunoassay using CSs and stencils is discussed in Chapter 6.

Novel microfluidic capillary systems for one-step immunoassays that require only the analyte to be loaded on the CS are investigated in Chapter 7. A method was developed to predeposit the detection antibodies in a dried form in the CS and their reconstitution was investigated.

A liquid that is flowing in a CS can hardly be stopped before the CS is filled or all liquid has been imbibed. However, one could think of circumstances that would benefit form stopping a liquid for a certain time, such as timing, metering, and triggering liquids. Hydrophobic patches in microchannel could stop a liquid but patterning those patches needs additional processing steps. A method using specifically shaped microstructures that stop liquid is investigated in Chapter 8.

Finally, Chapter 9 concludes on the potential of CSs based on the work presented in this thesis.

2. Modeling and Optimization of High-sensitivity, Low-volume Microfluidic-based Surface Immunoassays

Microfluidics are emerging as a promising technology for miniaturizing biological assays for applications in diagnostics and research in life sciences because they enable the parallel analysis of multiple analytes with economy of samples and in short time. We have previously developed microfluidic networks for surface immunoassays where antibodies that are immobilized on one wall of a microchannel capture analytes flowing in the microchannel. This technology is capable of detecting analytes with picomolar sensitivity and from sub-microliter volume of sample within 45 min. This chapter[1] presents the theoretical modeling of these immunoassays where a finite difference algorithm is applied to delineate the role of the transport of analyte molecules in the microchannel (convection and diffusion), the kinetics of binding between the analyte and the capture antibodies, and the surface density of the capture antibody on the assay. The model shows that assays can be greatly optimized by varying the flow velocity of the solution of analyte in the microchannels. The model also shows how much the analyte-antibody binding constant and the surface density of the capture antibodies influence the performance of the assay. We then derive strategies to optimize assays toward maximal sensitivity, minimal sample volume requirement or fast performance,

[1] M. Zimmermann, E. Delamarche, M. Wolf and P. Hunziker, Modeling and Optimization of High-Sensitivity, Low-Volume Microfluidic-Based Surface Immunoassays, first published in *Biomedical Microdevices* **7**:2, 99–110, **2005**.

which we think will allow further development of microfluidic networks for immunoassay applications.

2.1. Introduction

Microfluidics and biochips, which are derived from microfabrication techniques, are emerging as powerful bioanalytical platforms [28, 29]. Microfluidics in particular, have the potential to detect multiple analytes in a small volume of sample and can integrate multiple functionalities for the processing of samples and the generation and acquisition of signals [30]. For these reasons, microfluidic devices are developed and used for detecting disease markers and screening drug candidates as well as for antibody characterization [31]. Different methods can be employed to move liquids in microfluidics, such as pressure-driven flow, electro-osmosis, or acceleration. Ideal microfluidics are simple to utilize, reliable, fast, sensitive, versatile, and cheap. One of the simplest approaches for producing flow in capillaries is to use capillary forces. Capillary-driven flow requires no peripheral equipment, and this concept is used for portable immunodiagnostic tests [32].

We are interested in developing capillary-driven microfluidic chips for diagnostic and bioanalytical applications in which fluorescence surface immunoassays are performed in the microchannels of the chip, samples of 1 μL in volume or less are used, multiple analytes are detected, and sensitivities down to 1 pM concentration of analytes can be achieved. An important step in developing these devices was to employ a hydrophobic elastomeric substrate for the assay and covering the elastomer with a Si microfabricated element having a plurality of microchannels [14]. The assay takes place on the areas of the elastomer that are exposed to the microchannels. Each microchannel starts with a loading pad and ends with a capillary pump [33]. The capillary pressure along the flow path is encoded to secure the unidirectional filling of the liquid from the loading pad to the capillary pump. Therefore, assays are done by loading the necessary reagents (e.g. capture antibody and detection antibody) and samples in the correct sequence in each loading pad. The assay conditions in adjacent microchannels can be varied independently because the elastomer seals the microchannels efficiently. This concept was recently exemplified by

detecting tissue necrosis factor-α (TNF-α) in 0.6 µL volume of cell culture supernatant with 1 pM sensitivity, and up to 170 test sites were made on a 1 mm^2 area of the elastomer [34]. This concept was also qualitatively applied to detect disease markers such as C-reactive protein (CRP) [35]. Because clinically relevant analyte concentrations are often spread over a wide range from micromolar to picomolar concentrations, optimizing the microfluidic devices in terms of covering a large dynamic range for the measurements is important. At the same time, a microfluidic device should also be suited to handle very small concentrations and if possible minute volumes of analyte.

We are interested in examining these previous results analytically to identify the predominant assay parameters and to derive optimization strategies for performing assays with such microfluidics for having optimal sensitivity, minimal sample requirement, or fastest possible times to results.

Like other computational studies on the kinetics of antigen binding in microchannels [36, 37, 38, 39, 40], our computational model of fluid dynamics includes convection, diffusion and receptor-ligand kinetics [41, 42] of capillary-flow-driven microfluidic channels and was implemented using a finite difference approach [43]. Thereby, we solved the steady-state uncompressed *Navier-Stokes* equation, combined with a convection-diffusion model and a fluid-wall interaction model which we describe below.

2.2. Methods

2.2.1. Microfluidic networks used in the analyses

Our model is implemented to describe the binding of an antigen to a surface-immobilized capture antibody in a microchannel, Fig. 2.1, and is based on the geometrical characteristics of microfluidic networks that we used previously [34]. The microfluidic networks had several independent microchannels, and we therefore only need to consider one microchannel. Each microfluidic channel is 20 µm deep, 30 µm wide and 1 mm long. In typical experiments, the capture antibodies are present in the second half of the channel, and the analytes cannot be lost by sticking to the walls elsewhere than at the capture sites because the walls are treated to be protein-repellent [44]. The capture

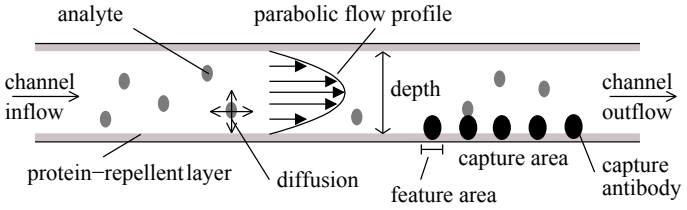

Figure 2.1. Configuration of a surface immunoassay in a microfluidic channel. The liquid enters the channel at the inlet on the left-hand side and flows through the channel under laminar conditions with a parabolic flow profile. The flowing analyte solution contains molecules which are transported in the channel. The molecules are allowed to diffuse perpendicularly to the flow direction and can be captured by the capture antibodies. Wall elements not covered with capture antibodies are protected against unspecific binding, which in the simulation is regarded as perfect.

area is covered by individual capture antibody molecules with a given surface density. We define the "feature area" as the total capture area divided by the number of active capture antibodies. If all capture antibodies were properly oriented and able to bind two antigens each, the feature area would be equal to half the footprint of a capture antibody. In practice, only a fraction of the capture antibodies might be functional and we will therefore explore the influence of the feature area on the assays.

The analyte solution flows into the microchannel at constant flow velocity and flow rate. The flow of an aqueous solution inside a small channel is typically laminar (Reynolds number $\ll 1$) and has a parabolic flow profile. The analyte molecules are transported by convection along the flow direction and in addition are free to diffuse. Each time an analyte molecule reaches a capture site, a standard ligand-receptor binding model is applied to define whether capture occurs. Both the association and dissociation events are modeled. The binding kinetics as well as the convection-diffusion model are described in more detail in the next section.

In the model, we define the analyte exploitation as the ratio between the number of captured analyte molecules and the total number of analyte molecules that were present in a given volume of sample that passed over the capture zone. An assay where all analyte molecules would flow in the microchannel without being captured would have an analyte exploitation of zero

and would generate no signal. Inversely, an ideal assay would have an analyte exploitation of one. The available volume of analyte solution is considered to be unlimited except when the simulation is used to study the exploitation of analyte.

2.2.2. Models

The flow of a liquid in a region over time t is characterized by a velocity vector field $\vec{u}$, a pressure p and a density ρ. For laminar, incompressible and viscous fluids the density is constant. The flow is described by the *Navier-Stokes* partial differential equation system

$$\frac{\partial}{\partial t}\vec{u} + (\vec{u} \cdot grad)\,\vec{u} + grad\, p = \frac{1}{Re}\Delta\vec{u} + \vec{g} \tag{2.1}$$

$$div\,\vec{u} = 0 \tag{2.2}$$

in dimensionless form with the Reynolds number Re and external forces $\vec{g}$. External forces such as gravity can be neglected in such miniaturized systems. For $Re \ll 2100$, flow is considered to be laminar and has a characteristic parabolic flow profile with zero flow velocity at the channel walls and peak flow velocity in the channel center. Here, Re is ~ 0.07 for the maximum flow rates considered.

The bulk concentration C of a solute in a given solution is described by the Convection-Diffusion equation of the form

$$\frac{\partial C}{\partial t} + \vec{u} \cdot grad\, C = D\Delta C + \Theta\,(t, x, y, C) \tag{2.3}$$

with a diffusion coefficient D, a source term Θ and the identical velocity vector field $\vec{u}$ given in Eqn. 2.1. We have applied the Stokes-Einstein-relation $D = \frac{kT}{6\pi\eta R_\mathrm{h}}$, with the hydrodynamic radius R_h, the analyte viscosity η and the Boltzmann constant k to estimate the diffusion coefficient D of the analyte molecule to $D = 10^{-6}$ cm^{2}s^{-1} which we used for all further calculations and which corresponds to the literature [45] where comparable values for small molecules such as TNF-α are reported. The analyte viscosity was set to a high plasma viscosity [46] of 2 mPa s.

The association and the dissociation from the capture site are described by the rate coefficients k, the analyte concentration C and the density of free binding sites $(\Theta_{\max} - \Theta_{\mathrm{t}})$ on the surface, using an ordinary differential equation of the form,

$$\frac{d\Theta_{\mathrm{t}}}{dt} = k_{\mathrm{on}}\, C\, (\Theta_{\max} - \Theta_{\mathrm{t}}) - k_{\mathrm{off}}\, \Theta_{\mathrm{t}} \tag{2.4}$$

for monovalent receptors and ligands. k_{on} is the rate constant for association, k_{off} is the rate constant for dissociation, C is the concentration of free molecules in the fluid, Θ_{t} is the surface density at time t. $\Theta_{\max}$ is the maximum surface density of molecules calculated from the feature area of the individual capture molecules and is assumed to be constant over time. In this simulation we generally used 10^6 M^{-1} s^{-1} for k_{on} and 10^{-3} s^{-1} for k_{off} [47], but in some case these constants were modified.

The set of Eqn. 2.1 - 2.4 is used to implement the model describing the capture of an analyte by a surface-immobilized capture site in a microfluidic channel. This model uses the finite difference approach to calculate the influences of the key parameters on the capture of analyte. The model is detailed in Appendix A, Section A.1, and validated in Section A.2 by comparing results from the simulation with analytical results when the equations could be solved analytically. Eqn. 2.4 in particular can be solved analytically for a constant analyte concentration:

$$\Theta_{\mathrm{t}} = \frac{k_{\mathrm{on}}\, \Theta_{\max}\, C}{k_{\mathrm{on}}\, C + k_{\mathrm{off}}} \left(1 - e^{-(k_{\mathrm{on}}\, C + k_{\mathrm{off}})\, t}\right). \tag{2.5}$$

The maximum binding density $\hat{\Theta}_{\mathrm{bound}}$ of analyte on the capture area depends only on the analyte concentration and the binding constants k_{on} and k_{off} which are also known as the equilibrium constant K:

$$\hat{\Theta}_{\mathrm{bound}} = \frac{k_{\mathrm{on}}\, \Theta_{\max}\, C}{k_{\mathrm{on}}\, C + k_{\mathrm{off}}} \tag{2.6}$$

$$K = \frac{k_{\mathrm{on}}}{k_{\mathrm{off}}} \tag{2.7}$$

$$[K] = \frac{[\mathrm{s}^{-1}\mathrm{M}^{-1}]}{[\mathrm{s}^{-1}]}\ .$$

2.3. Results

The combination of Eqn. 2.1 – 2.4 allows the study of the influence of flow rate, analyte bulk concentration, capture-site surface density and binding-rate coefficients on the binding kinetics. Experimentally, captured analytes might be detected directly using surface-sensitive techniques or by binding them with fluorescently-labeled detection antibodies. We do not need to take the binding between captured analytes and detection antibodies into account because this step is generally not limiting in immunoassays: a high concentration of detection antibodies can be used to ensure fast completion of this binding reaction, for example. First, we need to determine when the capture reaction is reaction-limited or transport-limited.

2.3.1. Reaction-limited versus transport-limited kinetics of capture

One of the key parameters that determine whether the kinetics of capture of analyte is reaction-limited or transport-limited is the velocity of the analyte solution in the microchannel. The capture of the analyte is reaction-limited if the number of molecules binding to the capture site per unit of time remains similar for different flow velocities. In contrast, the capture of the analyte is transport-limited if the number of analyte molecules binding per unit of time is sensitive to the flow velocity of the sample in the microchannel. The analyte exploitation is represented in Fig. 2.2 as a function of the flow velocity. It increases with decreasing flow velocity because insufficient mass transport increases the reaction time for capture. For velocities above 0.5 mm s^{-1}, corresponding to flow rates higher than 18 nL min^{-1} for the channels used in previous experiments, a system with a binding constant K of 10^9 M^{-1} and a feature area of 1500 nm^2 is reaction-limited: the residency time of the analytes on the capture area is short and the analyte exploitation therefore is small ($\sim$ 5 %). At lower flow rates, the analyte exploitation increases but the binding reaction becomes transport-limited because lower volumes of analyte solution are available at the capture area per unit of time and thus fewer molecules have a chance to be captured per unit of time. A flow velocity

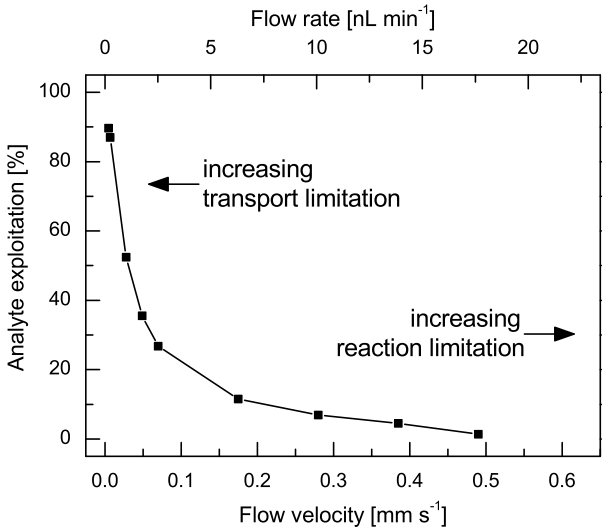

Figure 2.2. Calculated mean analyte exploitation as a function of the flow velocity in the first five minutes of the incubation time with 1 pM analyte concentration. Adjusting the flow velocity (and flow rate) affects the exploitation of the analyte molecules in a sample and is therefore useful to minimize the absolute volume of analyte required for saturation of the capture sites. The line is provided as a guide to the eye. A binding constant of 10^9 M^{-1}, analyte concentration of 1 pM and a feature area of 1500 nm^2 were selected here.

of 0.7 mm s^{-1} was used in previous work [34], and we suggest that these experiments were performed in the reaction-limited regime. We consider this flow velocity as well as lower flow velocities in the remainder of the paper to encompass the different regimes. We specifically choose a flow velocity of 0.07 mm s^{-1}, where transport limitation already occurs, and a flow velocity of 0.007 mm s^{-1}, where the capture according to Fig. 2.2 falls in the transport-limited regime. In this latter case, longer incubation times are necessary to reach an equivalent signal intensity to the reaction-limited case. In contrast to the transport-limited case, the molecules in the sample volume are used more efficiently.

We investigate the influence of the flow velocity and the feature area on the number of analytes captured per unit area, Fig. 2.3. Capture antibodies that are passively adsorbed on a hydrophobic surface have a footprint of ~ 150 nm^2 [15, 16] and it has been suggested that for this mode of deposition ~ 10 % of the antibodies might be correctly oriented and preserved for capturing one

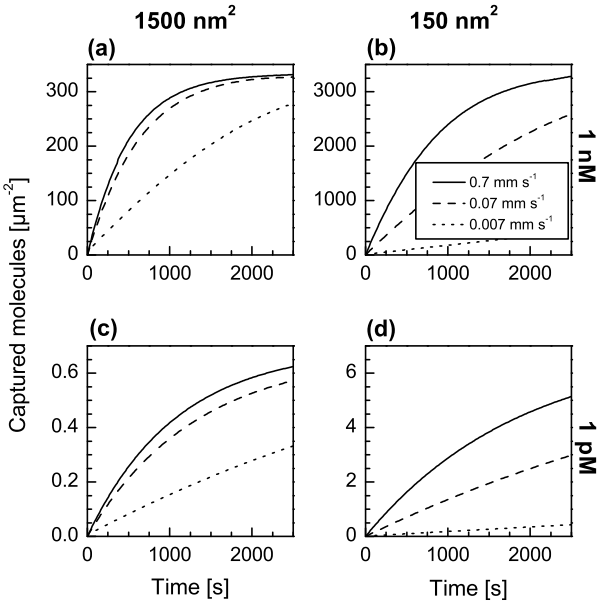

Figure 2.3. Binding of analytes in solution to surface-immobilized antibodies as a function of time and for a concentration of analyte of 1 nM (a, b) and 1 pM (c, d), and for a feature area of 1500 nm^2 (a, c) and 150 nm^2 (b, d). This binding reaction corresponds to the capture step of a surface immunoassay and takes place in a microchannel as shown in Fig. 2.1. The binding reaction is more sensitive to mass transport limitations for the smaller feature areas (b and d) as well as for lower analyte concentrations (c and d). A hypothetical analyte-antibody binding constant of $K = 10^9$ M^{-1} was chosen for these analyzes.

antigen from solution [3], which here would correspond to a feature area of 1500 nm^2. Using oriented antibodies and advanced surface-immobilization strategies, the feature area can be decreased. We consider for this reason a scenario where each capture antibody has a chance to bind one antigen (feature area of 150 nm^2). The model developed here can also be applied to situations with very different feature areas, microchannel dimensions, binding constants, and flow velocities.

Figure 2.3 shows how many analyte molecules are captured per unit area as a function of time for feature areas of 1500 nm^2 and 150 nm^2, various flow rates, and analyte concentrations of 1 nM and 1 pM. We selected 1 nM for the analyte concentration because it corresponds to immunoassays that are relatively sensitive and used for many clinical applications [3]. A concentration of 1 pM represents a practical limit in sensitivity for immunoassays and we want

to use the model developed here to optimize assays done using microfluidics for this analyte concentration. Figure 2.3a and 2.3b show that, as expected, the maximum surface density of captured analyte is inversely proportional to the feature area, but also that the kinetics of capture is affected by the feature area. For a larger feature area (1500 nm^2), it is less important to keep the flow velocity high enough to repopulate the microchannel with new analytes because the assay is reaction-limited. This explains the similar outcomes of assays done using flow velocities of 0.7 and 0.07 mm s^{-1}. The binding reaction becomes transport-limited for a flow velocity of 0.007 mm s^{-1}, as visible in Fig. 2.3a. The graphs in Fig. 2.3b indicate that capture zones having a smaller feature area exploit the solution from analyte faster than those with a larger feature area. As a consequence, the flow rate has a larger influence on the binding kinetics in the case of smaller feature areas.

The surface density of captured analytes decreases dramatically when analytes are at 1 pM concentration, Fig. 2.3c and 2.3d, which is dictated by the equilibrium constant K. The binding reaction is slower than at 1 nM in all cases, and the flow velocity as well as the feature area affect the capture reaction in a similar way as at the higher concentration.

2.3.2. Linear binding saturation curves at very low flow velocities

Biological assays that need a long time to reach equilibrium might have to be stopped early for convenience. The graphs in Fig. 2.3a and 2.3b show that saturation in binding is nearly reached within 1000 s for a flow velocity of 0.7 mm s^{-1}. The binding reactions for lower flow velocities are much slower and show a linear behavior. Although assays done under these conditions yield small signals, they can be conveniently stopped at any point in time, because uncertainties on the incubation time give small errors on the signal. The model predicts that an assay with 1500 nm^2 feature area, 1 nM analyte concentration, and 0.007 mm s^{-1} flow velocity has a relative error of only $\pm$ 4% when the incubation time is 300 $\pm$ 15 s. Interestingly, such an assay leads to having 52 $\pm$ 2 captured antigen per μm^2, which after the binding of detection antibodies should correspond to a signal well above the limit

of detection of conventional fluorescence scanners. The model suggests that assays done with a 1 nM analyte concentration and different conditions have a similar relative error when they are stopped after an incubation time of 300 ± 15 s. The graphs in Fig. 2.3c and 2.3d reveal a similar linear evolution of the signal with time for a 1 pM analyte concentration. However, stopping the assay after an arbitrarily short time for this lower analyte concentration is unlikely to be practical because of the much lower surface density of captured analyte after 300 s (5 min). Long incubation times are therefore crucial for assays with 1 pM analyte concentration.

2.3.3. Influence of the feature area on the binding kinetics

The density of active capture sites in surface immunoassays usually plays an important role in defining the maximum number of analyte molecules that can be captured and therefore the maximum signal surface density that can be reached. Preventing the denaturation of capture antibodies during and after their deposition is therefore important, and methods to orient antibodies so as to have their epitope-binding part exposed at the surface-liquid interface are sometimes employed. As explained above, we based most of our modeling on feature areas of 1500 and 150 nm^2, but now also investigate the role of the feature area on the efficiency of the assay for 1 nM and 1 pM analyte concentration in more detail, Fig. 2.4. We are in particular interested in learning how the feature area affects assays that have critical requirements such as utilizing a very small amount of sample or being fast. We therefore modeled the analyte exploitation for 300 s long assays using the same flow rates as before. As expected, all graphs in Fig. 2.4 show that the surface-density of captured analytes increases with the inverse of the feature area so that the exploitation of analyte is maximal with a feature area of 150 nm^2. The capture and analyte exploitation are particularly sensitive to the feature area for flow velocities ≤ 0.07 mm s^{-1}. The binding constants k_{on} and k_{off} in Eqn. 2.5 enforce the same time to equilibrium for different surface densities of the capture area: the number of capture events per unit of time is larger for surfaces having a higher density of capture sites but the maximum number of capture events is also proportionally larger on these surfaces. As an example,

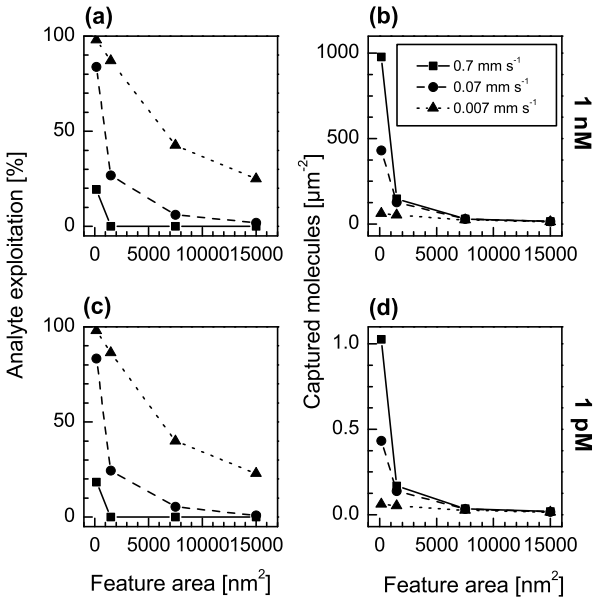

Figure 2.4. Efficiency of the capture of analyte molecules flowing at various velocities in a microchannel as shown in Fig. 2.1 as a function of feature area and analyte concentration and for the first 300 s of the assay. The ratio between analyte molecules flowing in the microchannel and analyte molecules captured defines the analyte exploitation (a, c) and the resulting density of analyte molecules captured on the surface (b, d). The lines are provided as guides to the eye.

an assay where the feature area is 150 nm^2 (first data points) is able to capture ~ 20 % of the analyte molecules when the analyte solution has a concentration of 1 nM and a flow velocity of 0.7 mm s^{-1}, Fig. 2.4a. This corresponds to an analyte exploitation of 20 %. The analyte exploitation falls off dramatically if the feature area is ≥ 1500 nm^2. Reducing the flow velocity will, however, increase the analyte exploitation significantly. The analyte exploitation is ~ 86 % when the feature area is 1500 nm^2 (second data points) and the flow velocity 0.007 mm s^{-1}, for example.

The signal in the assay is proportional to the surface density of captured analytes, and we therefore need to consider what the effect of the feature area on the number of analytes captured per unit area is, Fig. 2.4b. For feature areas ≤ 1500 nm^2, the density of captured molecules is sensitive to the flow velocity and maximum for a velocity of 0.7 mm s^{-1}. We learned from Fig. 2.4b that for these conditions the analyte exploitation is poor, but the

overall number of analyte captured is the highest. The capture step of the assay here is clearly transport-limited. For feature areas $\geq$ 7500 nm^2, the number of captured molecules is small and not sensitive to the flow velocity. Comparing the signals obtained for different flow velocities in the transport-limited regime, a slow velocity of 0.007 mm s^{-1} gives a very small signal compared with that for a velocity of 0.07 or 0.7 mm s^{-1}. Assays done with an analyte concentration of 1 pM exhibit a similar behavior as those with 1 nM analyte concentration, Fig. 2.4c and 2.4d, except that the density of captured molecules is always $\sim$ 1000 times smaller.

We have so far analyzed the performance of the assays done in a microchannel for two key analyte concentrations, and will next explore in more detail how the analyte concentration affects the analyte exploitation, the density of analytes captured on the surface, and the time needed to reach equilibrium. We will also evaluate the influence of the binding constant on the assay.

2.3.4. Effect of the analyte concentration on the analyte exploitation

Both the analyte concentration and the binding constant K determine the maximum density of analytes captured on the surface at equilibrium. Eqn. 2.6 shows that a maximum of 0.1 % of the capture sites can bind an analyte at equilibrium when the analyte concentration is 1 pM and the binding constant 10^9 M^{-1}. This ratio increases to 50 % for an analyte concentration of 1 nM. We take an arbitrary duration of 300 s for the capture step, flow velocities of 0.7, 0.07 and 0.007 mm s^{-1}, and a 1500 nm^2 feature area to investigate how the analyte exploitation and the density of analytes captured on the surface vary with the concentration, Fig. 2.5. At analyte concentrations $\leq$ 1 nM, the analyte exploitation is nearly invariant with the concentration but is strongly influenced by the flow velocity, as already discussed in Fig. 2.2. This situation changes as soon as the analyte concentration becomes larger than K. The analyte exploitation is an important criterion for optimizing the assay when the total number of analyte molecules in a sample is strongly limited, whereas it becomes unimportant for high analyte concentration, Fig. 2.5. 300 s suffice to have nearly all capture sites bound to an analyte when the analyte concentra-

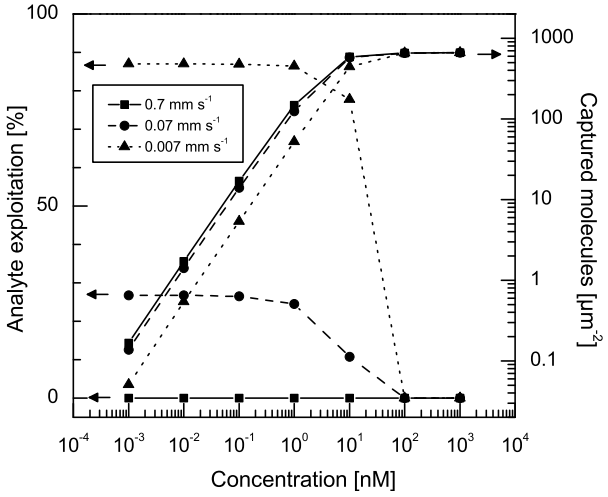

Figure 2.5. Mean analyte exploitation and surface density of captured analytes resulting from a 300 s long assay for various flow velocities and analyte concentrations. The binding constant chosen here was $K = 10^9$ M^{-1}. The lines are provided as guides to the eye.

tion is $\sim$ 10 times larger than the equilibrium constant. Below this concentration value, the surface density of captured molecules diminishes strongly with the concentration of analyte, as expected from Eqn. 2.5. It becomes helpful in this case to employ a flow velocity $\geq$ 0.07 mm s^{-1} to minimize transport limitation. Importantly, the model predicts that there will only be $\sim$ 0.16 captured analyte per μm^2 for a 300 s long assay using a flow velocity of 0.7 mm s^{-1} and an initial analyte concentration of 1 pM. Assays for such a low analyte concentration must be longer and if possible should have a smaller flow velocity. Figure 2.3d showed that a sensitivity of 1 pM can be achieved using an incubation time of $\sim$ 2500 s for the capture, which is consistent with previous experimental work [34].

We now evaluate how strongly high concentrations of analyte affect the time needed to saturate the capture sites, Fig. 2.6. We know from Fig. 2.5 that saturation of the capture sites can be reached for analyte concentrations $\geq$ 10 nM. With analyte concentrations $\geq$ 100 nM, the capture sites are saturated within a few seconds. An assay to detect an analyte at 100 nM concentration, using a 1500 nm^2 feature area and a flow velocity of 0.7 - 0.07 mm s^{-1}, leads to a maximum signal after 45 s, according to our model. This illustrates well the advantage of miniaturizing assays using a microfluidic system. It is preferable

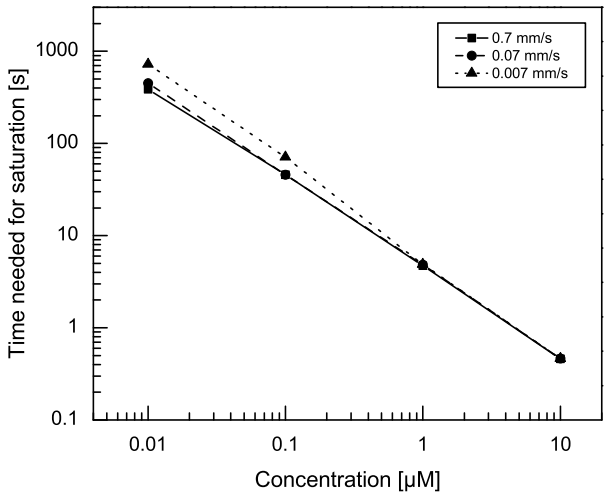

Figure 2.6. Time to complete saturation of the capture sites as function of analyte concentration. At concentrations ≤ 1 μM, time to equilibrium can be increased by reducing the flow velocity and the feature area. For analyte concentrations above 10 μM, the capture sites are saturated in less than 1 s. The lines are provided as guides to the eye.

to reach saturation when the analyte concentration is high, as otherwise variations in the capture duration render the assay imprecise. Conventional assays prevent signal saturation and imprecision due to variations of the incubation time by using a dilution series of the sample. The model shows a relative insensitivity of the assay to the flow velocity for concentrations ≥ 1 μM. The assays are in this case clearly reaction-limited.

2.3.5. Influence of the binding constant on the binding kinetics

The binding constant K between the antigen and the capture antibody plays an important role on the maximum surface density of analyte molecules that can be captured at equilibrium. We have seen above that the assay is very sensitive to the analyte concentration when the concentration falls below K. As we study the time response of the binding, we need to distinguish the different influences of the association and dissociation constants. The key factors giving an antibody high or low affinity are the association constant k_{on} and the dissociation constant k_{off}. The influence of K was therefore investigated

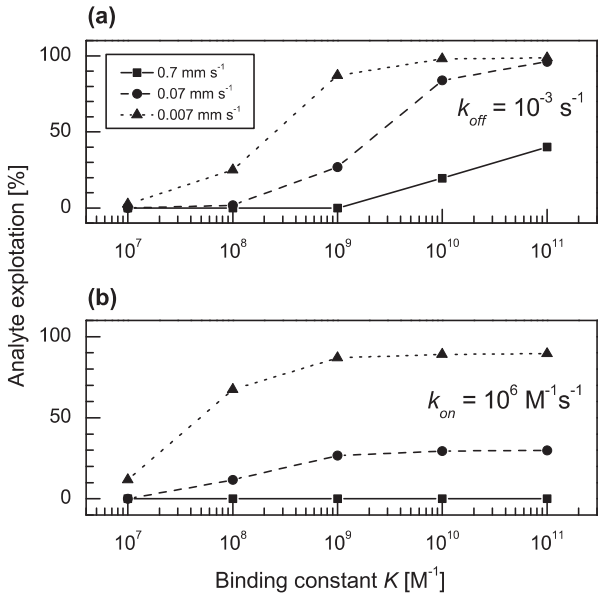

Figure 2.7. Mean exploitation of analyte volume as function of the binding constant in the first 300 s of the reaction. An increasing association constant k_{on} (a) results in increased exploitation of analyte volume, whereas modification of the dissociation rate k_{off} (b) affects the exploitation of a 1 pM analyte only for $K < 10^9$ M^{-1} using a feature area of 1500 nm^2.

for a 300 s long capture step by setting k_{on} from 10^4 to 10^8 M^{-1} s^{-1} while keeping k_{off} unchanged and vice versa. Figure 2.7a shows that the analyte exploitation increases toward 100 % with increasing k_{on}, and the effect of k_{on} on the analyte exploitation convolves with the flow rate. A significant analyte exploitation can be observed even for a high flow velocity of 0.7 mm s^{-1} provided that k_{on} is very high (10^8 M^{-1}s^{-1}). Figure 2.7b shows that when k_{off} is varied and $K < 10^9$ M^{-1}, the analyte exploitation is limited because having $k_{\mathrm{off}} > 0.001$ s^{-1} results in relatively high dissociation rates. For $K \geq 10^9$ M^{-1} the association constant dominates the binding reaction, and the analyte exploitation is only sensitive to the flow velocity.

2.3.6. Comprehensive assay optimizations

The detailed model developed above enables us to propose several strategies to optimize surface assays in which capture antibodies are present on one wall of a microchannel and analytes have a concentration of only 1 pM. We

keep the geometry of the microchannel (30 × 20 μm^2 in cross section), the capture area (500 μm in length), and the binding constant K at 10^9 M^{-1} ($k_{on} = 10^6$ M^{-1}s^{-1} and $k_{off} = 10^{-3}$ s^{-1}) the same as in the previous sections. In the following discussion we consider that the minimum surface density of captured molecules that can be detected using a conventional fluorescence scanner is ~ 0.5 analyte per μm^2 [17]. The remaining parameters influencing the capture step are the flow velocity (or flow rate), the feature area and the time for the capture step, all of which are varied in the next simulations. On a practical level, the flow rate can be changed by varying the evaporation rate of filled capillary pumps or by changing the depth of the channels.

Optimizing assays for fast measurement

We are interested in exploring how fast a sensitive (analyte concentration $\leq$ 1 nM) sandwich fluorescence immunoassay can be. The two important steps in such an assay are the capture of analyte from solution and the binding of fluorescently-labeled detection antibodies to the captured analyte. The capture is likely to be the limiting step because detection antibodies are usually provided at high concentrations (μg mL^{-1}). We therefore focus on the capture step as it was the case in the sections above. First, we assume that the available volume of sample does not limit the assay (e.g. volume $>$ 10 μL), and second, we arbitrarily set the duration of the capture step to 120 s for an analyte concentration of either 1 nM or 1 pM. This duration is $\sim$ 12 times shorter than the capture time used for experiments in which TNF-α was detected with a 1 pM sensitivity [34]. To obtain a sufficient signal in such a short time, the binding reaction must be very efficient and fast, especially for low analyte concentration where only a small fraction of the capture sites can be bound with analytes at equilibrium. A crucial strategy for fast assays is then to have a high flow velocity to prevent mass transport limitations and a small feature area to increase the analyte exploitation. Small feature areas might be achieved by orienting the capture antibody on the surface and/or roughening the surface used for capture. Figure 2.8 predicts the surface density of analytes captured on the surface for 150 and 1500 nm^2 feature areas. The model suggests that generating a strong enough signal in only 120 s is not challeng-

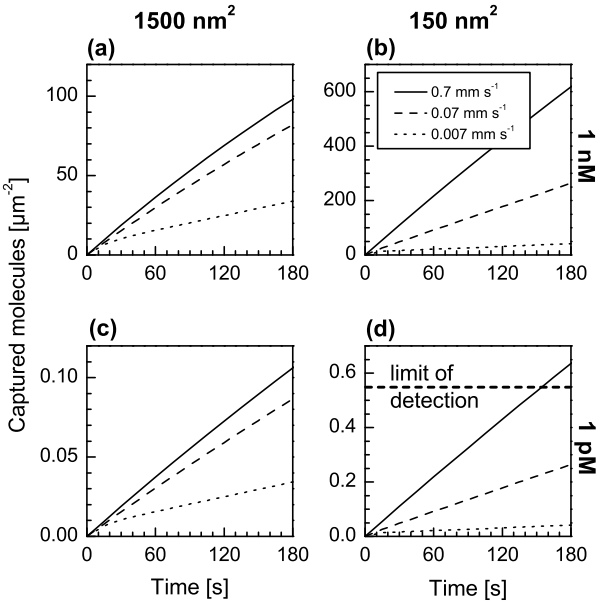

Figure 2.8. Number of captured molecules per μm^2 as a function of time for an analyte concentration in (a), (b) [(c), (d)] of 1 nM [1 pM] and a feature area in (a), (c) [(b), (d)] of 1500 nm^2 [150 nm^2].

ing when the analyte has a concentration of 1 nM, Fig. 2.8a and 2.8b. The density of surface-bound analytes should in this case amount to 422 μm^{-2}. A high flow velocity of 0.7 mm s^{-1} is beneficial in the case of small feature areas. At 1 pM analyte concentration, the limit of detection cannot be reached in 120 s if the feature area is 1500 nm^2, Fig. 2.8c. A smaller feature area is helpful to increase the surface density of captured analytes close to the detection threshold if the flow velocity is 0.7 mm s^{-1}, Fig. 2.8d. If the flow velocity is further increased to 2.8 mm s^{-1} (data not shown), the model predicts that an analyte concentration down to 1 pM can be measured in 120 s, yielding a surface density of captured analytes of 0.68 μm^{-2}.

Optimizing assays using minimal volumes of analyte

For some applications, only very limited amounts of sample analyte might be available and having a fast assay is less important. We now investigate what the smallest volume of analyte solution needed to detect an analyte at a concentration of 1 pM is. In this case, the analyte has to be exploited as much as possible.

We learned from Fig. 2.4c that an exploitation of the analyte of $> 95\%$ can be achieved by using a feature area of 150 nm^2 and a flow velocity of 0.007 mm s^{-1} (flow rate of 0.25 nL min^{-1}). With this feature area and flow velocity, the surface density of captured analytes becomes sufficient for detection after an incubation time of 55 min. This translates into a consumption of only $\sim$ 13.8 nL of sample. If the feature area is 1500 nm^2 and the flow velocity is 0.007 mm s^{-1}, the analyte exploitation is $\sim$ 86 % and the incubation to achieve sufficient signal increases to $\sim$ 85 min. In this case, $\sim$ 21.3 nL of sample is necessary. A higher signal might be desirable and we therefore consider the case where the surface density of captured analytes is 2 μm^{-2}, and the feature area is 150 nm^2: The volume of analyte needed with a 1 pM analyte concentration and a flow velocity of 0.7 mm s^{-1} becomes $\sim$ 263 nL and the assay will take 10.5 min. A slower flow of 0.07 mm s^{-1} would increase the analyte exploitation and require a slightly longer assay and much less sample: 25.5 min and $\sim$ 63.8 nL, respectively.

Increasing the dynamic range of the assay

Many biological assays have a limited dynamic range due to the equilibrium behavior dictated by Eqn. 2.5. Saturation of the capture sites is easily reached for concentrations of analyte (e.g. 100 nM) that are higher than $\frac{1}{K}$, and the surface density of captured analytes diminishes dramatically as soon as the analyte concentration becomes smaller than $\frac{1}{K}$. Sensitive assays will be limited in dynamic range mostly by saturation at which high analyte concentrations lead to a fast and complete coverage of all binding sites, which makes it impossible to distinguish between different elevated concentrations of analyte. The dilution of the analyte sample that solves this problem with assays done using microtiter plates is not an ideal solution for a microfluidic-based immunoassay. We suggest that flushing a solution of analyte through an array of parallel microchannels at different flow rates can expand the dynamic range of the assay. Figure 2.6 suggested that decreasing the flow velocity from 0.7 mm s^{-1} to 0.007 mm s^{-1} will increase the time needed to saturate the capture sites with a 100 nM analyte concentration from 45 to 70 s. The freedom in designing microchannels of various widths and depths in Si could be used to implement this strategy. In our previous work, the dynamic range for a sandwich

fluorescence immunoassay for TNF-α was from 20 pg mL^{-1} to $\sim$ 50 ng mL^{-1}, and we suggest that the upper limit of the dynamic range could be increased to 1 μM using the method described here.

2.4. Conclusions

Microfluidic networks offer several advantages over conventional microtiter plates where the assays are done using much larger volumes. However, to take full advantage of microfluidic networks, it is important to identify the major parameters of assays in microfluidics as well as their interplay. The theoretical model developed here aims at understanding the relative importance of the transport of analyte in a microchannel by diffusion and convection, the binding kinetics between an analyte in solution and a surface-immobilized antibody, and the footprint of a capture antibody on the substrate for the assay. The flow velocity of the analyte solution in the microchannel is probably the parameter that is the most practical to vary using microfluidics with capillary pumps or using forced evaporation. Strategies to increase the surface density and orientation of the capture antibodies can also be applied to enhance the performances of the assays greatly. The substrate for the assay surface could be roughened, for example, or capture antibodies could be immobilized via their Fc part with cross-linkers or protein A or G, or using affinity-contact printing [48]. Many assays would benefit from using very small amounts of sample or from being very fast. As the overall number of analyte molecules in miniaturized assays is typically small ($\leq$ 1 femtomol), it is important to exploit analytes as much as possible. An exciting outcome of this model is the indication that an analyte could be detected with picomolar sensitivity with a capture step of only 2 min duration using appropriately engineered capture sites. Conversely, longer assays and low flow rates might be used to perform 1 pM sensitivity assays using a few tens of nanoliters only. The model presented here and the experimental results obtained previously coincide in showing that microfluidic networks have an excellent potential to miniaturize surface immunoassays that have demanding performances, such as in point-of-care testing where multiple disease markers could be detected at low concentrations in a single drop of sample and within minutes.

3. Continuous Flow in Open Microfluidics using Controlled Evaporation

This chapter[1] presents a method for programming the flow rate of liquid aliquots inside open microfluidic network (MFN)s using evaporation while preventing the undesired evaporation of the aliquots from the MFNs. The MFNs comprise a number of independent capillary systems, each of which has a filling port, a microchannel in which assays can be performed, and a capillary pump (CP) . The capillary systems initially fill owing to capillary forces. Peltier elements placed underneath the functional zones of the MFNs dynamically prevent evaporation in all filling ports using the ambient temperature and relative humidity as inputs, and define the flow rate of the liquid in all microchannels by controlling the evaporation of the liquids from the CPs. This method achieves flow rates in the microchannels ranging from $\sim$30 pL s^{-1} to $\sim$1.2 nL s^{-1}, and is able to keep 90% of a 0.6 µL solution placed in an open filling port for 60 min. It is applicable to numerous assays or chemical reactions that require appropriate flow control of liquids and reagents.

3.1. Introduction

Miniaturized platforms such as microfluidics [49] have recently emerged as powerful (bio)analytical platforms. In particular, the transport of minute

[1] M. Zimmermann, S. Bentley, H. Schmid, P. Hunziker and E. Delamarche, Continuous Flow in Open Microfluidics using Controlled Evaporation, first published in *Lab Chip*, **5**, 1355–1359, **2005**.

amounts of liquids in microchannels has opened new possibilities of integration and parallelization. Microfluidics are used, for example, for cell-sorting and cellular assays, protein crystallization, immunoassays, DNA analysis, and medical applications [31, 50]. Each of these applications requires some sort of pumping mechanism to draw liquids through various functional microfluidic elements. Several pumping methods based on pneumatic pressure, electro-osmosis, capillary pressure, coriolis force and electrostatic or piezoelectric pumps are commonly used for microfluidic applications [51].

A trend in miniaturization is also observed with microtiter plates, which are typically used for pharmaceutical research (*e.g.* drug screening), research in life sciences, and *in vitro* diagnostics. This trend led to an increase in the number of test sites per plate and to a reduction of the total sample volume per test to $\sim$2 µL for a 1536-well plate.

For both microfluidics and microtiter plates, long times often are needed to complete assays with low concentration of analytes: assays in microtiter plates are typically diffusion-limited and necessitate long incubation times, whereas assays in microfluidics can be reaction-rate-limited. The latter case is particularly challenging as it requires (i) displacing a small volume of analyte solution slowly in a microstructure and (ii) preventing undesired evaporation of sample volume from the microfluidics. Therefore means for pumping small absolute volumes of liquids accurately and with ultra-low flow rates are critically required for microfluidics applied to high-sensitivity assays, Chapter 2. Table 3.1 gives the minimal flow rates for a selected number of pumping systems.

A simple and yet efficient approach to program ultra-low flow rates in microchannels is to use controlled evaporation. Examples are the evaporation-driven pumping for chromatography applications [58, 59] and the valveless pump for nonpulsatile flow, [60] where the combination of evaporation with capillary forces generates a continuous ultra-low flow in microchannels.

Continuous low flow rates of $\sim$5 nL min^{-1} were achieved in microfluidic channels, which had integrated heaters and temperature sensors [21]. In that application, a hydrophobic valve [61] was used to align the liquid-air interface of a sample with a heating element, and the evaporation rate was defined by the length of the diffusion path for evaporation. An additional airflow

Pumping principle	Flow rate [nL min^{-1}]	Withdraw	Infuse	Continuous	Periodic	Comments
Syringe pump (PicoPlus)[52]	0.003	×	×	–	×	∼1.5 pL/step, dead volume
Evaporating from open CP (this chapter)	1.80	×	–	×	–	Temperature tracking of the dew point
Transpiration-based[21]	5	×	–	×	–	–
Magneto-hydro-dynamic (MHD)[53]	50	×	×	×	–	Requires strong magnetic fields, pH-dependent
Membrane pumps	100	×	×	–	×	Stroke volume typically 100–150 nL
Electro-hydro-dynamic		×	×	×	–	High voltage required, pump rate depends on conductivity of the liquid
Peristaltic pump[52]	330	×	×	–	×	–
Pumps used for drug delivery:						
Panomat/Accu-chek®,[54, 55]	66	–	×	–	×	Delivers in intervals of 3 min.
Microjet Crono®,[56], Pegasus light®,[57]	165	–	×	–	×	–

Table 3.1. Minimal flow-rates and flow-capabilities of various pumping systems.

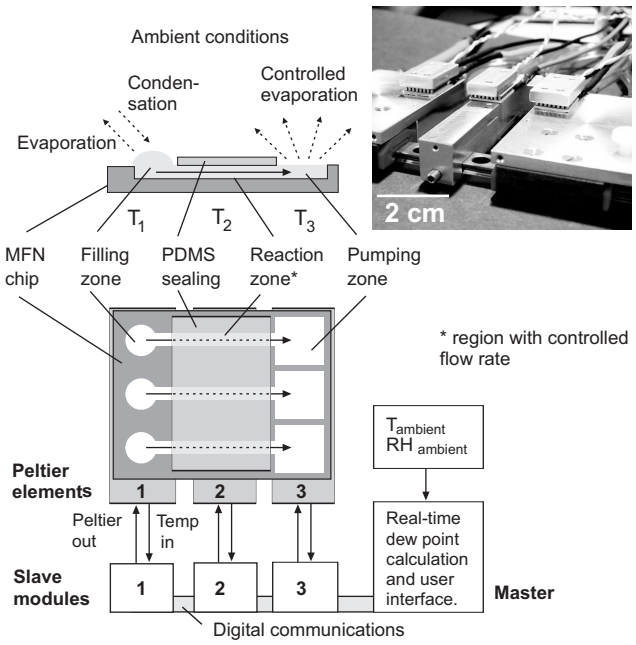

Figure 3.1. Method for controlling the flow of liquids in a MFN. The microfabricated MFN chip comprises independent capillary systems, having as main functional elements a filling zone, a microchannel providing a reaction zone wherein an immunoassay is performed, and a pumping zone. Peltier elements placed underneath these zones prevent undesired evaporation of solution from the filling zone and relay CPs when they are filled with solution. The Peltier elements are connected to a microcontroller, which continuously tracks the ambient conditions, calculates the dew point and provides a user interface. Each Peltier element can be programmed to a certain temperature. The inset shows a picture of the three Peltier elements that can slide sideway to receive chips of various lengths.

maintained a constant relative humidity at the other end of the diffusion path. In another work, a sorption agent was employed as a sink for evaporated liquid to achieve continuous flow rates in microchannels over several hours [62]. This approach required a closed evaporation chamber.

Here, we present a simplified method to produce a continuous ultra-low flow rate in a MFN that we want to use for miniatuized surface immunoassays. This method is based on (i) controlling the evaporation of liquid from an evaporation zone by local control of the temperature and (ii) simultaneously preventing undesired evaporation of solution elsewhere by cooling. This method works with open MFNs, *i.e.* the macroscopic user-interfaces need not be sealed, but are left open and thus accessible for pipetting.

The MFNs used here are ∼2 cm^2 microfabricated Si chips, similar to those previously used for combinatorial surface immunoassays having a sensitivity of ∼1.2 pM and a sample consumption <1 μL per test site [34]. These MFNs were also used to detect cardiac markers from ∼1 μL samples within 10 min [35]. Independent capillary systems in these chips fill owing to capillary forces, which makes the chips simple to fabricate and use. The capillary forces are defined by the geometry and the surface characteristics of the microchannels. A liquid added to a filling port sequentially moves through an appended microchannel and starts filling a CP. A slab of poly(dimethylsiloxane) (PDMS) elastomer placed over the microchannels can optionally serve as the substrate for the assays. Accurately controlling flow rates in filled capillary systems necessitates both the control, or preferably the prevention, of evaporation in the filling ports and the control of evaporation in the CPs. This dual requirement is achieved using Peltier elements onto which the chip is placed, as shown in Fig. 3.1. A first Peltier is used to cool the zone of the chip in which the filling ports are located. A second one allows variation of the temperature in the reaction zone (not used here). Finally, a third Peltier sets the temperature of the CPs to modulate evaporation and thereby to control the flow of solution in the microchannels.

The Peltier elements are driven by individual slave modules, which are programmed by a master module. The electrical part of the system is completely separated from the microfluidic chip, which is just mounted on the temperature-controlling unit. Thus, the microfluidic chip does not require any integrated electrical components for flow control, so that such chips remain simple and easy to fabricate.

3.2. Modeling and Experimental Methods

The master module controlling the slave modules measures the ambient temperature and the relative humidity (RH), and provides a user interface. It calculates the dew point in real time and can command each slave to dynamically track the dew point by a given offset, allowing flexible evaporation and condensation control. In the slave module, shown in Fig. 3.2, a microcontroller controls a Peltier driver unit and receives feedback from a thermocouple. The

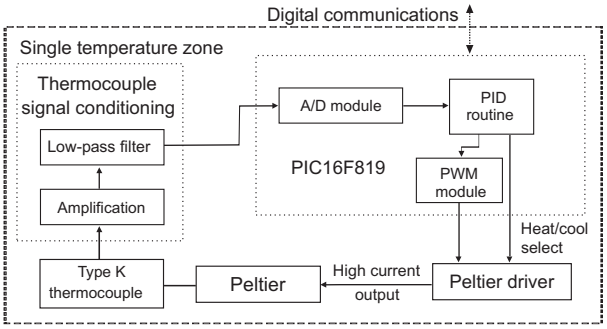

Figure 3.2. Functional structure of the temperature-tracking process in the slave modules. Each slave module receives an individual target temperature value from the master and measures the temperature of its Peltier element. The accuracy of this algorithm was found to be $\pm 0.1^\circ$ of an integer target temperature value.

PID routine in the microcontroller of the slave module accurately keeps the temperature at the programmed offset from the dew point.

If the MFN is completely filled, the evaporation flux $j_\mathrm{e} = MD\frac{\partial C}{\partial x}$ of liquid from the liquid-air interface in an open CP determines the flow rate i_f in the connected capillary system:

$$i_\mathrm{f} = i_\mathrm{e} = MA_\mathrm{e}D\frac{\partial C}{\partial x} = MA_\mathrm{e}\frac{D}{RT}\frac{\partial p}{\partial x} \tag{3.1}$$

where A_e is the evaporation area, M and D are the molecular weight and the diffusivity of the evaporating molecules respectively, x is the distance to the liquid-air interface, and p is the partial vapor pressure of the evaporating liquid [21].

As we do not employ a convective air flow over the evaporation zone to vary the flow rate, the transport of the evaporated liquid is dominated by diffusion and can be calculated using

$$D\nabla^2 p = \frac{\partial p}{\partial t} \tag{3.2}$$

Eqn. 3.1 and 3.2 cover the most important parameters for evaporating a liquid: we modify A_e by varying the coverage of the CP and p by varying the local temperature to regulate the flow. A larger value of p also speeds up the diffusion of vapor. Our boundary conditions are 100% relative humidity at the liquid-air interface and ambient conditions far away from the interface. More detailed models for evaporation from a liquid meniscus or thin films can be found in literature [63, 64].

3.2.1. Experimental

The MFNs used here comprise 11 independent capillary systems and several monitoring ports (*i.e.* filling ports, which are not connected to a flow path) [33, 34]. The structures forming the MFN are produced by vertically etching Si to a depth of 30 μm. Next, the chip is coated with a thin layer of sputtered Au, which is then derivatized with a hydrophilic monolayer of poly(ethyleneglycol) (PEG) (inside the filling structures) and a hydrophobic monolayer (non-filling areas). First, the stability against evaporation of liquids pipetted into monitoring ports is assessed using an optical microscope. In a next step, liquids containing fluorescent beads are added to the filling ports and their velocity is tracked in the microchannels using a fluorescence microscope and the particle-tracking algorithm of a commercial software package (Image Pro Plus).

3.3. Results

3.3.1. Controlling/preventing evaporation in the filling ports

Ideally, evaporation is limited to the evaporation zone: If evaporation of liquid occurs elsewhere (*e.g.* in the filling ports), the concentration of analytes and reagents will increase and variable flow rates will occur in the capillary systems.

The evaporation of a 0.6 μL droplet of deionized water placed in a monitoring port is shown in Fig. 3.3. The diameter and the height of the droplet were measured by viewing it from the side and its volume was calculated. A droplet that is dispensed in a monitoring port evaporates within 10 min if there is no temperature tracking of the dew point. Evaporation is significantly reduced if the dew point is tracked at $\Delta T = 2$ K. In this case, 75% of the droplet still remains in the port after 15 min. If the offset from the dew point is further reduced ($\Delta T = 0$ K) 75% of the volume remains in the port after 30 minutes. At temperatures below the dew point, small droplets start to condense around the ports. We observed that for $\Delta T = -2$ K these droplets typically do not

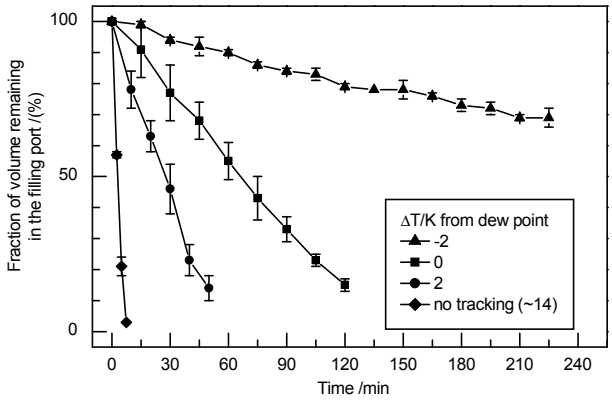

Figure 3.3. Evaporation of a 0.6 µL droplet dispensed in a monitoring port, which is maintained at a temperature ΔT from the dew point. The lines are provided as guides to the eye.

coalesce, and the droplet placed in the monitoring port does not grow for tracking periods of up to an hour. A temperature gradient probably increases the effective temperature at the surface of these "large" (2-mm-high) droplets and accounts for these observations. With $\Delta T = -2$ K, 90% of the dispensed sample volume remains in the filling port after 60 minutes. Such a duration should be sufficient for assays requiring long incubation times without leading to detrimental changes in analyte concentration. Longer durations sometimes resulted in the coalescence of droplets, which occasionally made contact with the liquid in the filling port, thereby providing a pathway for sample loss from the filling port or for dilution.

3.3.2. Programming the flow rate

Dispensing a sample of liquid into the filling port of a capillary system results in the filling of the microchannel and CP connected to the filling port. The flow rate of the solution in the microchannel is defined by the capillary pressure exerted by the CP and the flow resistance of all filled parts. Evaporating liquid from the CP by raising the temperature in the pumping zone to a value above the dew point introduces a small flow in the connected microchannel, which was monitored by tracking the 2.5 µm large fluorescent beads flowing in the microchannels, Fig. 3.4. The beads were moving at constant velocity and in

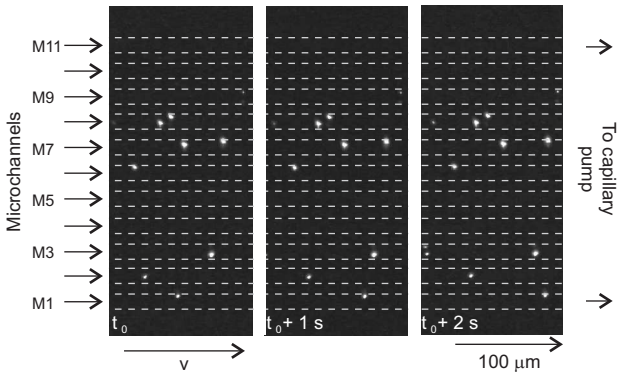

Figure 3.4. Tracking the flow of liquid in microchannels using fluorescent beads. The 2.5 µm large latex beads are tracked over time, and the velocity is measured. The mean flow velocity was estimated using the fitted peak velocity of the beads.

stable position within the channel. A video camera recorded the movement of these beads while the temperature in the evaporation zone was being modified to vary the flow rate in the microchannels.

The flow in the microchannels is laminar and has a parabolic flow profile, which was used to estimate the peak flow velocity, Fig. 3.5. A flow rate of $\sim$10 pL s^{-1} can be achieved in the 30 $\times$ 30 µm^2 wide microchannel while keeping the pumping zone at a temperature equal to the dew point (ΔT = 0 K). Here, the CPs are not covered and the air-liquid interface is $\sim$1 mm^2. Tracking the dew point using ΔT = 30 K increases the flow rate to 1.2 nL s^{-1}. Larger flow rates can of course be obtained by increasing the liquid-air interface of the CPs. If we use the modeled assumptions and combine Eqn. 3.1 and 3.2, we obtain flow rates that compare well with those achieved in the experimental part (calculations not shown), even hough the model does not consider three-dimensional diffusion and thermal flow at the interface. The slightly parabolic relationship between ΔT and the flow rate i_f provides convenient control of the flow rate in the microchannels.

A further adjustment of the flow rate can be achieved by partially covering the CPs using a PDMS layer. In Fig. 3.6, for example, the 11 CPs of a MFN were covered from 0 to 90% of their surface area. This resulted in a sixfold difference in speed between the microchannels with the most and the least covered CPs when the tracking temperature was between 2 and 30 K

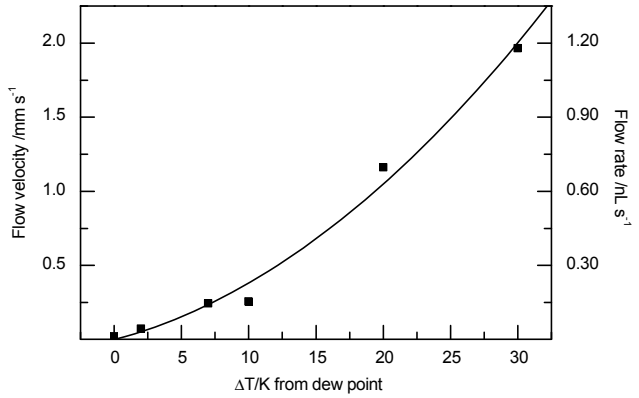

Figure 3.5. Mean flow velocity and flow rate of a solution moving in a microchannel and filling the CP wherein liquid is evaporated by changing ΔT.

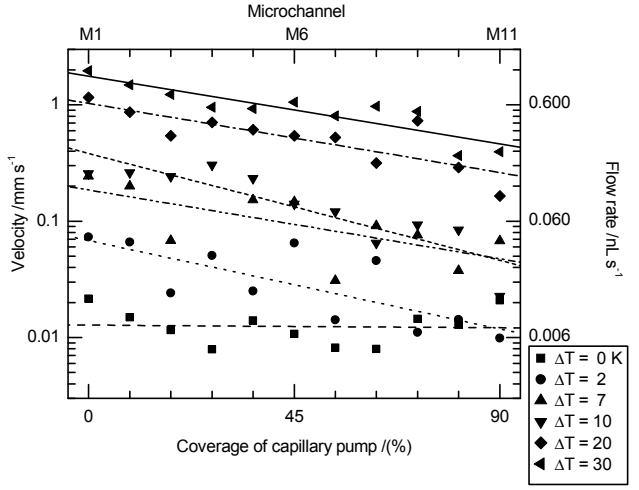

Figure 3.6. Partially covering a CP will reduce its evaporation area as well as the flow velocity in the corresponding microchannel. A gradient of flow velocities in the 11 microchannels of a MFN chip is achieved by covering the CPs with a layer of PDMS. The lines are provided as guides to the eye.

above the dew point. Taking an evaporation area of ∼0.4 mm^2 and setting the temperature at $\Delta T = 7$ K from the dew point results in a flow rate of ∼30 pL s^{-1}. We observed that 90 s only were needed to reduce or increase the flow rate by a factor 10 by varying the tracking temperature. This time was sufficient to maintain the temperature of the Si chip and a 5 mm thick aluminum block between the chip and the Peltier element.

3.4. Conclusions

Temperature-controlled evaporation is well suited to control flow even at very low flow rates in open MFNs provided that evaporation is prevented in those areas of the MFNs where liquids are initially loaded. The design of CPs and their sealing can be combined to define the upper and lower ranges of the flow rates. Ultra-small flow rates (*i.e.* < 100 pL s^{-1}) provide a unique opportunity to perform high-sensitivity assays using microliter volumes of sample. A sample with a volume of 2 µL, which can be used with 1536-well microtiter plates, could flow in a MFN for more than 9 h at a flow rate of 60 pL s^{-1}. With the same flow rate and using a sample of 50 nL, an assay could still last for ∼14 min and simultaneously provide sufficient time for performing immunoassays having sub-nanomolar sensitivity.

It is also possible to modulate the flow rates in the microchannels by adjusting the evaporation in the CP to optimize the time needed for reaction with each successive reagent. To set the flow rates of liquids in the microstructures, MFN chips require neither integrated components nor expensive peripherals. This method therefore expands the versatility and hydrodynamic performance of MFNs without departing from the original goal of developing a flexible technology for ultraminiaturized biological assays. This method could also be used to study how cells immobilized in microchannels respond to slowly delivered substrates.

4. Screening Cell Surface Receptors using Micromosaic Immunoassays

This chapter[1] presents a general method for screening cell surface receptors using so-called micromosaic immunoassays. This method employs a microfluidic chip having n ($n = 11$) independent flow paths to move cells over m ($m = 11$) lines of surface-patterned antibodies for screening individual cells in a parallel, combinatorial, fast and flexible manner. The antibodies are patterned as 30 μm wide lines on a poly(dimethylsiloxane) layer used to seal the area of the chip in which screening is being monitored. Mouse hybridoma cells having CD44 cell surface receptors and anti-CD44 antibodies were used to establish a proof-of-concept for this method. Both the capture antibodies and the cells were fluorescently labelled to allow the position of the cells to be accurately tracked over the binding sites using an inverted fluorescence microscope. The chips and cells were maintained at a constant temperature between 20 to 37 °C, and flow velocities of the cells over the capture areas were 100–280 μm s^{-1}, resulting in a ∼0.1–0.3 s residency time of the cells on each of the eleven 30 × 30 μm^2 capture areas. Binding of the cells appeared to be specific to the capture areas, with a yield of ∼30 % when the assay was performed at a temperature of 37 °C and with a slow flow velocity. We suggest that this proof-of-concept is broadly applicable to the screening of cells for medical/diagnostic purposes as well as for basic research on the interaction of cells with surfaces.

[1] M. Wolf, M. Zimmermann, E. Delamarche and P. Hunziker, Screening Cell Surface Receptors using Micromosaic Immunoassays, first published in *Biomedical Microdevices* **9**, 135–141, **2007**.

4.1. Introduction

Cellular assays are used to study how chemicals, biomolecules and factors such as electrical and mechanical stimuli, radiation, and heat affect the viability, metabolism, differentiation, cytoskeleton, motility, adhesion, receptor trafficking, and apoptosis processes of cells [65]. Cellular assays therefore are of fundamental importance in biology, medicine, pharmacology, and biotechnology. They are used both at a fundamental research level as well as for diagnostics. Whereas many assays focus on changes in the morphology, activity, or colour (due to staining) of cells, several assays aim at identifying cell membrane receptors to classify cells, detect diseases, or elucidate biological pathways [66].

Cellular assays are also increasingly being used to test the safety of drugs and to identify potential drugs for cellular receptors. Cellular assays can require testing thousands of compounds at various concentrations, using individual compounds or a combination of compounds [67]. Clearly, these assays can benefit from miniaturization by decreasing the size and cost of the infrastructure and equipment needed [68, 69]. In addition, cells such as stem cells and cells from some mammalian cell lines are available in very limited quantities only.

Microfluidics are emerging as a powerful class of devices for performing miniaturized cellular assays [70, 71, 72], patterning cells, [73, 74] and controlling cellular environments [75, 76, 77]. These devices can accommodate microliter and sub-microliter volumes of samples and reagents, can provide faster time to results than conventional technologies, can effect multiple assays in parallel or serial assays with high throughput, and sometimes are portable. We have developed a class of microfluidics in which liquids move under the action of capillary forces [78, 79]. These microfluidic chips are autonomous and do not need pumping elements. They can be used without peripherals for actuation. We call one independent flow path on such a microfluidic chip a capillary system (CS) [33]. CSs can be cloned and arrayed so as to move a number of solutions independently and run assays in parallel. Key to using these chips is the accurate patterning of receptors for analytes on the surface of a PDMS elastomer, which reversibly seals sections of the CSs.

Assays based on this approach can be two-dimensional and combinatorial. A first microfluidic chip with n CSs can be used to pattern n types of capture antibodies (Abs) on PDMS as parallel lines. A second chip having m CSs can be used to bring m samples over the surface-immobilized capture Abs. Ligand-receptor interactions between the capture Abs and their antigens from solution result in a maximum of $n \times m$ binding interactions, which can be displayed as a "micromosaic" of fluorescence signals if fluorescently-tagged detection Abs are used to reveal where antigens are captured on PDMS [14]. Similar approaches for the combinatorial screening of clinical analytes [80, 81, 82] and single-stranded DNA analytes have been developed [83]. A matrix of surface binding interactions can also be used to detect flowing antigens with a serial dilution strategy [84].

In this chapter, we explore how the concept of micromosaic immunoassays [14] can be applied to the screening of cells. Several reasons motivate this work. First, micromosaic immunoassays are efficient. One microliter of sample or less is sufficient to screen eight or more types of analyte. The short paths for diffusion of analytes in microchannels can greatly accelerate diffusion-limited steps. The flow of solutions in microfluidics is typically laminar and makes rinsing steps short and effective. A fluorescent sandwich immunoassay having ∼10 steps can be done in less than 10 min for detecting analytes at a concentration level of ∼10 nM or in ∼45 min for analytes at concentrations down to 1 pM [34, 35]. This method suggests that cells can be screened rapidly and using small volumes of sample. Second, using microfluidic chips the PDMS substrate for the assay can be patterned in a flexible manner prior to analyzing samples [49]. The accurate patterning of capture Abs on a PDMS surface limits the depletion of analytes from a small volume of sample and facilitates the reading of a large number (up to several hundreds) of fluorescent signals. The PDMS layer can be readily removed from the microfluidic chip at the end of the assay and the signals analyzed using a fluorescence scanner or microscope. With respect to cellular assays, it should then be possible to localize the interaction of cells with surface-bound receptors accurately. Third, the possibility to conduct assays and calibrate them simultaneously using reference samples may yield a better consistency and smaller intra-assay variation than assays do that are done as independent experiments.

Similarly, it should be possible to screen different types of cells in parallel using a micromosaic format. In the remainder of this chapter, we first review how a micromosaic immunoassay for screening cells can be set up and then provide a proof-of-concept by analyzing the trajectories of individual cells passing in microchannels over surface-immobilized antibodies.

4.2. Experimental

4.2.1. Chemicals and cells

Chemicals were purchased from Sigma-Aldrich or Fluka (Buchs, Switzerland) unless otherwise stated. Cells from the mouse hybridoma cell line PK136 were used for this work. Briefly, these cells secrete mouse IgG2a monoclonal antibody, which reacts with mouse natural killer cells. These hybridomas were obtained by fusion between SP2 myeloma cells and spleen cells (C3H × BALB/c) immunized with mouse spleen cells [85, 86]. The cells were cultured and prepared using phosphate-buffered saline (PBS) with pH 7.4, bovine serum albumin (BSA), Tween 20, fluorescein diacetate, dimethylsulfoxide (DMSO), Iscove's Modified Dulbecco's Medium (Gibco, Invitrogen, Switzerland), foetal calf serum, normal mouse serum, hyaluronidase, and propidium iodine. The cells were cultured with 5 % atmospheric CO_2 at 37 °C in Iscove's Modified Dulbecco's Medium, which was supplemented with 10 % foetal calf serum, in a cell incubator.

Anti-CD44 monoclonal antibodies (BD Biosciences, San Jose, CA), either conjugated with fluorescein isothiocyanate (FITC) or Phycoerythrin, were used as capture antibodies for the microfluidic-based assays (see below) as well as for fluorescence activated cell sorting (FACS). FACS (FACScan, BD Biosciences, San Jose, CA) was used to verify the presence of CD44 on the PK136 cells before performing microfluidic-based assays as follows. First, cells were taken from the cell culture and washed, resuspended in PBS at a concentration of 2.5×10^6 cells mL^{-1}, and 200 µL of the suspension was loaded into the wells of a 96 microtiter plate (Falcon), which corresponds to ∼500,000 cells per well. The cell aliquots were centrifuged, and their Fc receptors (a potential nonspecific cellular receptor for antibodies) blocked using 100 µL solution

of mouse serum in PBS (1:50) for 15 min at room temperature. To label the CD44 cellular receptors fluorescently, the cells were centrifuged again and incubated in a 1:200 solution of antibody (anti-CD44-Phycoerythrin conjugate) in 0.1 % normal mouse serum in PBS for 15 min at room temperature. The cells were centrifuged and resuspended in 200 µL of PBS twice. Immediately prior to FACS, propidium iodine was added to sort out nonviable (necrotic) cells. Viable cells were assessed using FACS scatter plots by gating on propidium iodine-negative populations.

Cells for the microfluidic-based assays were handled and stained as follows. A suspension of PK136 mouse hybridoma cells was taken from the cell culture and incubated for 1 h at 37°C with hyaluronidase (5000 IU per $\sim 5 \times 10^6$ cells mL^{-1}) to prevent hyaluronic acid-mediated cell aggregation [87]. To visualize the cells during the assays, 0.1 µL of a 5 mg mL^{-1} solution of fluorescein diacetate in DMSO was added to 1 mL of cell suspension. After 30 min of incubation at room temperature, the cells were washed three times with PBS, resuspended in a 2 % solution of normal mouse serum in PBS, and used after a minimum resting time of 15 min.

4.2.2. PDMS and microfluidic chips

The prepolymers of PDMS (Sylgard-184, Dow Corning, Midland, MI) were mixed at a 10:1 ratio using a Dopag Mixer (Cham, Switzerland), dispensed on the bottom of a Falcon Petri dish, and cured for at least 24 h at 60°C. PDMS slabs of desired dimensions were then cut and used to prepare lines of capture Abs or simply to seal some areas of the chips during the assays.

The microfluidic chips were microfabricated using photolithography. A chrome mask was used to pattern a photoresist on 4" silicon wafers and to etch selectively 20 µm of silicon using a deep reactive ion etcher (STS ICP, Surface Technology Systems plc, Newport, U.K.). After removal of the photoresist, the wafers were coated with Ti (10 nm) and Au (150 nm), and then diced to yield individual chips. Each microfluidic chip had 11 independent CSs [34]. The top surface of each chip was microcontact-printed with octadecanethiol to form a hydrophobic coating (advancing contact angle with water of $\sim 115°$). The chips were then immersed in a 10 mM ethanolic solution of

thiolated poly(ethylene glycol) (ABCR, Karlsruhe, Germany) for 30 s to make the recessed areas of the chips wettable (advancing contact angle with water of ∼40°) and protein-repellent. Used chips were cleaned prior to reuse by immersion in a "Piranha" solution (H_2SO_4:H_2O_2, 3:1, CAUTION) [88], after which the chips were copiously rinsed with deionised water and dried under a stream of N_2. The surface of the chips was freshly prepared before each use.

4.3. Patterning of Capture Antibodies and Screening Assays

Capture Abs were patterned on PDMS by covering the microchannels of a chip with a ∼1-mm-thick slab of PDMS and filling the loading pads of the chip with 0.5 μL of a 0.1 mg mL^{-1} PBS solution of anti-CD44 Ab conjugated with FITC . After 2 min, most of the Ab aliquots had passed through the microchannels, which were flushed by adding (i) 0.5 μL of a 1 % solution of BSA in PBS and (ii) 0.5 μL of PBS to the loading pads. Finally, the PDMS layer was removed manually from the chip, rinsed with deionised water and blown dry under a stream of N_2.

Next the PDMS layer was brought into contact with a second microfluidic chip so as to expose the lines of capture Abs orthogonally to the microchannels of the second chip. A slab of PDMS was used to seal the capillary pumps. The chip was then placed on a thermally conductive adhesive, which covered a thermoelectric element. The cellular assays proceeded by filling the loading pads of the chip with ∼0.5 μL of a 1 % BSA solution in PBS and ∼0.5 μL of a 10^7 cells mL^{-1} suspension of PK136 hybridomas. During the filling of the capillary pumps, air trapped in the pumps slowly diffused through PDMS, which resulted in a slow and homogenous flow rate of solution in all microchannels. After dispensing the cells, two cover glass slides separated by a 1-mm-thick PDMS frame were quickly placed over the chip and its thermoelectric element. The thermoelectric support with the chip and glass slides were turned upside down and placed on the stage of an inverted fluorescence microscope (Axiovert 100, Zeiss, Switzerland). A thermo-regulator (TC2812, Minco, Niederuzwil, Switzerland) with pulse-width modulation and thermo sensor was used to

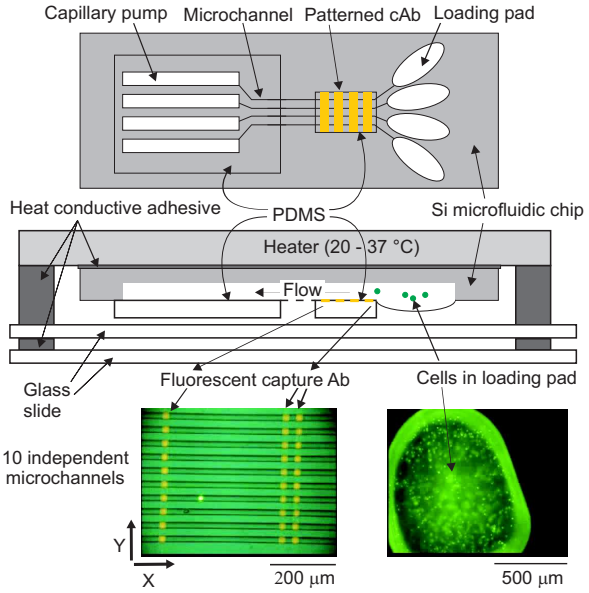

Figure 4.1. Experimental setup for a micromosaic immunoassay screening of cells. Aliquots of cell suspensions are placed in the loading pads of independent capillary systems, from where they fill the microchannels and capillary pumps of the capillary systems. As the cells cross lines of capture Abs, which are patterned on a sealing PDMS layer, capture of some cells may occur. A heater, two glass slides, and conductive foil spacers form a chamber inside which the microfluidic chip and the cells are maintained at a constant temperature; moreover evaporation of water from the loading pads is negligible. The trajectory of the cells in the region of the capture sites is monitored in the X- and Y-directions using an inverted fluorescence microscope and recorded as a video for analysis. The fluorescence microscope images show (left) three lines of capture Abs (orange) and a cell (green) moving in one microchannel and (right) ∼300 nL of cell suspension in one loading pad.

regulate the temperature of the thermoelectric element and chip from 20 to 37 °C. A digital camera (Coolpix E990, Nikon) was used to record the trajectory of cells flowing over the region in which the capture Abs are located. The focal plane of the microscope was set to the lines of capture Abs. The videos showing the trajectories of the cells were analyzed after the assay using the software Image Pro and its object-tracking functions.

4.4. Results and Discussion

The influence of the environmental parameters (e.g. culture medium, pH, temperature, shear stress) on the metabolism of living cells and the tendency of cells to sediment require the adaptation of micromosaic immunoassays to the particular needs of living cells. The setup used for screening cells using CSs is displayed in Fig. 4.1. It consists of a microfluidic chip of silicon, covered with a thin layer of Au and self-assembled monolayers, and has two separate blocks of PDMS. One block serves as the substrate for the assay: it is patterned with lines of capture Abs and placed on the region in which the microchannels of the CSs run parallel. The second PDMS block covers the capillary pumps of the CSs. It helps to maintain a reproducibly low flow rate in the microchannels when the solutions added to the loading pads progressively displace air from the CS and fill the capillary pumps. To prevent cell lyses due to fast cell flow in the microchannels, a small volume of buffer is added first to each loading pad so as to fill the microchannels up to approximately the inlet of the capillary pumps. During the assay, the air compressed by the filling liquid permeates through the PDMS, resulting in a slow flow of solution inside the microchannels. The microfluidic chip is placed on a heat-conductive adhesive and heating device. Once the solutions with cells are loaded on the chip, the chip and its heating element are placed upside down on the stage of an inverted fluorescence microscope. Two glass slides separated by ∼1-mm-thick slabs of PDMS insulate the chip from the microscope stage to prevent condensation of water in front of the microscope's optical path. The chip was maintained at a constant temperature between 20 and 37 °C for the assays. Sedimentation of cells resulted in cells coming into contact with the capture sites. The fluorescence images in Fig. 4.1 show cells labelled with fluorescein (green) and capture sites on PDMS having antibodies labelled with R-phycoerythrin (orange).

For the proof-of-concept shown here, we selected mouse hybridoma cells having a CD44 cell surface receptor. These cells partly derive from white blood cells, and CD44 is involved in numerous cell-cell interactions important for lymphocyte activation, hematopoiesis, and tumour metastasis. In addition, the transmigration of blood vessel walls by white blood cells is a physi-

ological process, which is mediated by rolling and tethering through receptor molecules in the cell membranes [89, 90]. This cell-binding mechanism guides immunocompetent cells to inflammatory target areas. The receptor profile expressed and displayed by the endothelial cells provides specificity for subpopulations of white blood cells that can be differentiated by their membrane protein expression, that is their cluster of differentiation (CD) [89]. Using a micromosaic immunoassay and specific antibodies, it should be possible to imitate the capture of a subpopulation of white blood cells on the surface of blood vessels to a certain extent: depending on the combination of antibody and receptor, rolling, tethering or firm binding of leukocytes to a surface may occur under a certain shear rate. In clinical medicine, the examination of white blood cell subpopulations is crucial for diagnosis and treatment of diseases, e.g. AIDS. A device capable of separating subpopulations would allow further examination of these cells or an isolated ex vivo treatment of these cells and their reinsertion into the blood stream. In current clinical practice, conventional FACS machines require incubating the cell sample to be examined with fluorescently labelled antibodies for at least half an hour.

The cellular assays consist in following the real-time trajectories of the cells in each microchannel along the main axis of the microchannel (X-coordinate) and orthogonal to the microchannel (Y-coordinate). Fig. 4.2 shows the trajectory of cells in 11 independent microchannels with the microfluidic chip maintained at 20 °C. First, ∼140 cells are tracked during 42 s and their Y-positions are analyzed, Fig. 4.2a. Short segments in this graph correspond to cells entering and leaving the channels without noticeable interaction with the capture Abs. On average, the cells remain ∼2.5 s in the length of the microchannels that is visible in the field of view and their mean velocity in the microchannel is ∼280 $\mu m\, s^{-1}$. Note that the curvature of the segments reflects an optical artifact and not a curved trajectory of the cells in the microchannels. In addition, several cells bind to the capture areas and become immobile during this experiment. The graph in Fig. 4.2b shows the trajectory of selected cells along the main axis of the microchannels as a function of time. Cells flow along the microchannels at a steady speed until they become bound to one of the 11 capture zones they cross.

Figure 4.3 shows selected frames of a video in which the trajectory of cells

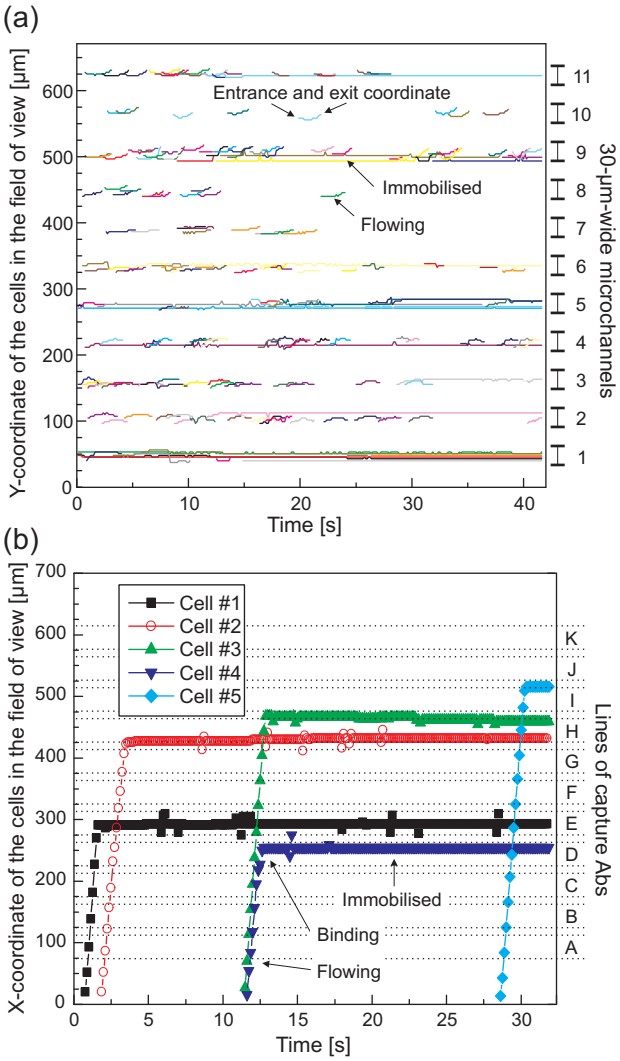

Figure 4.2. Trajectories of PK136 hybridoma cells having CD44 surface receptors and flowing inside microchannels across patterned lines of anti-CD44 Abs. (a) Graph showing the lateral positions of the cells inside the microchannels as a function of time. The entrance and exit coordinates of one cell flowing through a microchannel without binding are marked. Following a binding event, cells acquire an invariant Y-coordinate. (b) Graph showing the longitudinal position of cells along the microchannels as a function of time. Cells flow over 11 areas having capture Abs. The trajectories of only a few binding cells are depicted for better clarity.

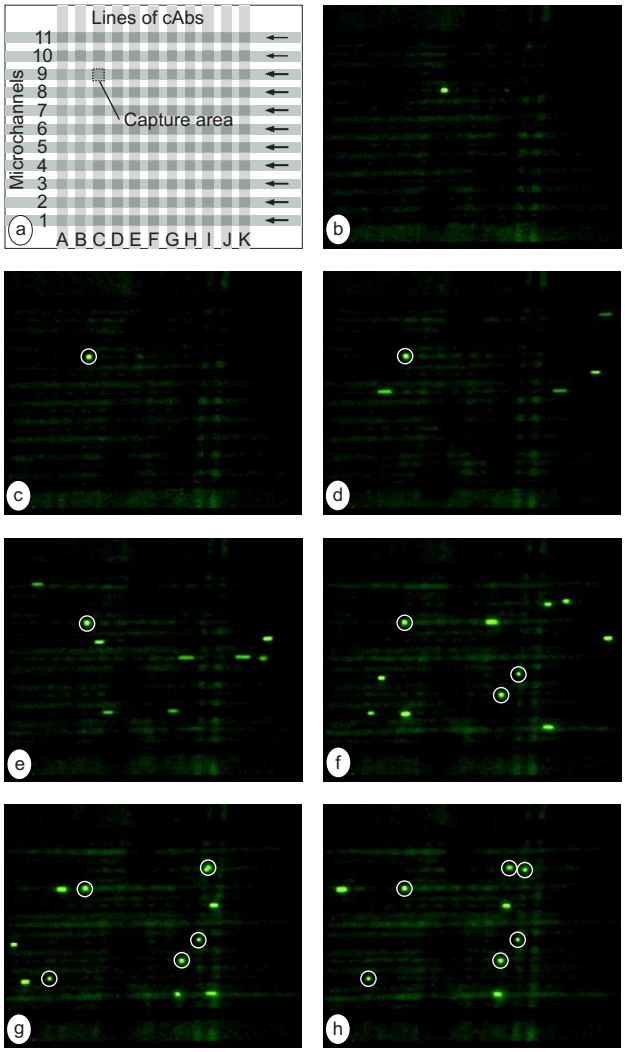

Figure 4.3. Outline (a) and movie frames (b - h) illustrating a micromosaic immunoassay with cells as recorded using a fluorescence microscope and video camera. The cells are PK136 hybridomas, have CD44 surface receptors, and are labelled with a fluorescein dye (green). Anti-CD44 Abs labelled with fluorescein, which are patterned as lines on a PDMS layer used to seal the microchannels, form the capture areas. The cells flow from left to right inside 30 μm wide microchannels. The cells binding to anti-CD44 Abs are circled. The video corresponding to this assay is provided as supplementary material [91].

over the capture areas was followed. This experiment was done at 37 °C to optimize the chances of binding of the cells. The fluorescently-labeled capture Abs appear faint as a result of photobleaching, whereas cells appear as bright green ∼10–15 μm wide spheres. The frames cover a timeframe of ∼20 s during which the cells flowed with an average velocity of 150±45 μm s^{-1} or equivalent flow rate of ∼0.15 nL s^{-1}. This range of velocities is mainly due to the laminar flow profile, which transports cells positioned in the center of the microchannel faster than those positioned elsewhere. The average residence time of one cell above one 30 × 30 μm^2 capture area is 0.2 s. A basic analysis of the trajectories and binding of the cells using commercial vision software revealed that ∼30 % of the cells were captured on one of the 11 capture sites aligned in each microchannel. A more detailed analysis would require the identification of the three-dimensional position of the cells in the microchannels and the calculation of the specific velocity and residence time on the capture areas for each cell. Such an analysis could for instance use methods known from particle image velocimetry, which requires a high-speed imaging setup. Interestingly, the retardation of some cells passing over surface-immobilized receptors can yield insight into the protein expression of retarded cells [92]. This suggests that qualitative cellular assays can provide useful information without the need for full parameterization of the factors governing the interaction between the cells and the receptors.

The flow rate of the cell suspension may be varied using peripheral equipment having several heating/cooling elements placed in contact with the microfluidic chip, Chapter 3, to study the effect of hydrodynamic forces on the behavior of immobilized cells [93]. The direction of flow, for example, can be changed back and forth to obtain statistical information on the binding of one cell over one type of capture area. In addition, micromosaic immunoassays for screening cell surface receptors can be combined with an interrogation of the mechanical properties of cells (size and elasticity) to identify particular cells, such as cells that are infected with parasites [94].

4.5. Conclusions

The proof-of-concept shown here can be further refined. First, many types of capture Abs may be used to screen for various types of cells or receptors simultaneously. This may require using cells that are labeled differently in a first step when developing the assay. Second, the geometries of the microchannels and capture sites can be varied to capture cells at particular locations. This could minimize or prevent the risk of collisions and interferences between flowing and surface-immobilized cells. Third, "advanced" capillary pumps can be designed, see Chapter 5, so as to vary the flow conditions in the microchannels and to study the influence of the flow rate on the statistics of binding. In this paper, the emphasis was to miniaturize the assays and screen individual cells from microliter volumes of samples. Larger volumes of sample can of course also be used, and capture sites can be made much larger and continuous, for example. The setup, microscope, camera and chemicals used here are relatively standard and did not require any particular modification for the assays, except for holding the microfluidic chips on an element having a controlled temperature.

We believe that the work shown here is broadly applicable and provides a flexible and efficient method for screening cell surface receptors. This concept may be used for histocompatibility testing to screen human leukocyte antigens. It can also be used for blood typing and for verifying the presence of cells in routine applications in which samples are available in limited volumes. There is a number of diagnostics that require the analysis of the number and type of white blood cells, and the status of some diseases such as HIV can be monitored by counting CD4-T-cells, for example. Although we are mainly interested in developing simple research and diagnostic platforms based on capillary-driven microfluidics, actuation mechanisms may be added to the microfluidic chips used here for sorting cells [95, 96]. In general, multidimensional assays are needed when testing large numbers of cells and compounds to obtain statistically meaningful results. It is therefore desirable to have cell assays that can screen cell/compound interaction in parallel (i.e. multiplexed assays), a task at which micromosaic assays excel.

5. Capillary Pumps for Autonomous Capillary Systems

Autonomous capillary systems (CSs), where liquids are displaced by means of capillarity, are efficient, fast and convenient platforms for many bioanalytical applications. The proper functioning of these microfluidic devices requires displacing accurate volumes of liquids with precise flow rates. In this chapter,[1] we show how to design capillary pumps for controlling the flow properties of CSs. The capillary pumps comprise microstructures of various shapes with dimensions from 15–250 μm, which are positioned in the capillary pumps to encode a desired capillary pressure. The capillary pumps are designed to have a small flow resistance and are preceded by a constricted microchannel, which acts as a flow resistance. Therefore, both the capillary pump and the flow resistance define the flow rate in the capillary system (CS), and flow rates from 0.2–3.7 nL s^{-1} were achieved. The placement and the shape of the microstructures in the capillary pumps are used to tailor the filling front of liquids in the capillary pumps to obtain a reliable filling behaviour and to minimize the risk of entrapping air. The filling front can, for example, be oriented vertically or tilted to the main axis of the capillary pump. We also show how capillary pumps having different hydrodynamic properties can be connected to program a sequence of slow and fast flow rates in a CS.

5.1. Introduction

Microfluidic devices are promising for applications that require precise displacement of small amounts of liquids or that can benefit from peculiar be-

[1] M. Zimmermann, H. Schmid, P. Hunziker and E. Delamarche, Capillary Pumps for Autonomous Capillary Systems, first published in *Lab Chip*, **7**, 119–125, **2007**.

haviours that liquids and chemical reactions exhibit at the micrometer length scale [97]. At small scale, for example, diffusion times of reactants and analytes are short, surface-to-volume ratios are large, and surface tension forces dominate gravitation forces [98, 99]. Accurate control of the flow of liquids in microfluidics is key to their proper functioning and can be achieved with either actuated or passive microfluidics. In actuated microfluidics, the flow is controlled using an external power source or pump and is driven mostly by displacement, centrifugal, electric-field or magnetic-field pumping mechanisms [51]. Actuated microfluidics are most powerful in pumping on demand milli- and microliters of liquids for a long time and with a high flow rate. In passive microfluidics, flow rates are encoded in the design of the microfluidics. Typical driving forces for propelling liquids in passive microfluidics are, for example, chemical gradients on surfaces, osmotic pressure, degassed PDMS [100], permeation in PDMS [101] or capillary forces [102, 103]. Such microfluidics fill spontaneously and are appealing owing to their portability, low dead volume and small power consumption. A combination of actuated and passive control for moving liquids in microfluidics has also been demonstrated [104]. There, pressurised gas chambers embedded in a plastic chip were separated from a liquid via thin membranes. Opening these membranes irreversibly using a thermal actuator caused the liquid to be pushed pushed through hydrophobic microfluidic channels at flow rates defined by the geometry of the channels. We are mainly interested in developing passive microfluidics driven by capillary forces for use in bioanalytics and for patterning biomolecules on surfaces [49]. We call such microfluidics capillary systems (CSs) [33]. Passive microfluidics have also been used for micromoulding in capillaries to study the dynamics of wetting of liquid prepolymers in rectangular capillaries [105] or to deposit locally enzymes within capillaries [106]. Passive microfluidics which require the displacement of large volumes of liquid or very low flow rates can be enhanced by peripheral equipment, Chapter 3. As the flow rate of a liquid in passive microfluidics is predefined, minor device variations can compromise their operation. For this reason, modelling the filling dynamics [107, 108] of liquids in capillaries is desirable, but for capillary-force-driven microfluidics the computational fluid dynamic methods require extremely high grid resolution or adaptive grid refinement algorithms to track the movement

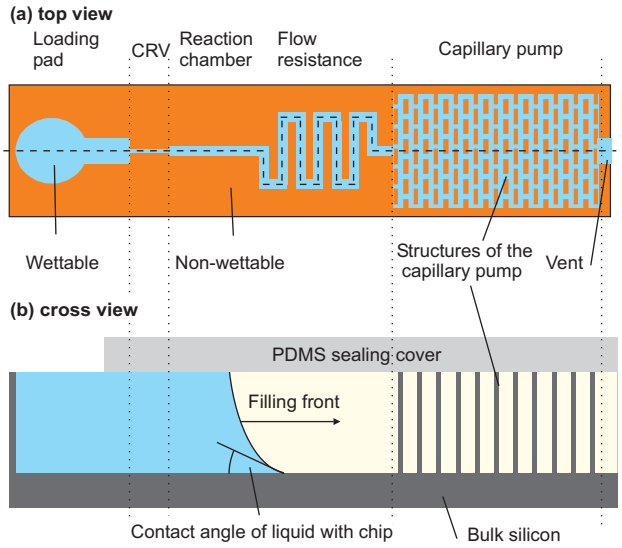

Figure 5.1. Encoding flow rates of a liquid in a CS using a capillary pump. (a) The capillary pump is the principal structure determining the flow rate of the liquid in the CS and can therefore be designed to program this flow rate. A chip having one or several CSs has a typical area of 1 cm^2. The capillary retention valve (CRV) prevents the reaction chamber from drying out. (b) The pumping power of a capillary pump depends on the contact angles of the filling liquid with its walls and the characteristic dimensions of its structures. The various parts in the scheme are not to scale.

of the liquid filling front [109, 110]. Therefore, a high computational effort is necessary to apply these methods. An alternative method is to use a constraint energy minimization approach, but such a method cannot describe the dynamics of filling [111].

In this chapter we are interested in extending the performance of CSs by understanding and governing the filling dynamics of liquids in CSs better. We therefore designed, fabricated and tested a range of CSs, and compared their experimental filling behaviour with a simple analytical model. We use CSs that are microfabricated into silicon chips and sealed with PDMS. The CSs comprise a loading pad, a capillary retention valve (CRV) and a reaction chamber, in which an immunoassay can be performed, as well as a flow resistance and a capillary pump with a vent, see Fig. 5.1. Surface-immunoassays can be performed directly on the sealed chip by patterning receptors for analytes on the PDMS layer [34]. Given the importance of capillary pumps on the

hydrodynamic performance of CSs, we focus on designing and implementing new types of capillary pumps in this work. As will be shown below, a flow resistance in front of the capillary pump can also be used to modulate the filling behaviour of liquids in capillary pumps. The flow rate Q of a liquid in a CS is determined by the wettability of the CS, the viscosity of the liquid, the total flow resistance and the capillary pressure in the capillary pump, and can be expressed as

$$Q = \frac{1}{\eta}\frac{\Delta P}{R_{\mathrm{F}}} \tag{5.1}$$

where η is the viscosity of the liquid, ΔP the difference in pressure inside and in front of the liquid, and R_{F} the total resistance to flow of the flow path. In CSs such as that shown in Fig. 5.1a, a microchannel of variable length dominates the flow resistance. The resulting capillary pressure P_{c} of a liquid-air meniscus in such a rectangular microchannel is

$$P_{\mathrm{c}} = -\gamma\left(\frac{\cos\alpha_{\mathrm{b}} + \cos\alpha_{\mathrm{t}}}{a} + \frac{\cos\alpha_{\mathrm{l}} + \cos\alpha_{\mathrm{r}}}{b}\right) \tag{5.2}$$

where γ is the surface tension of the liquid, $\alpha_{\mathrm{b,t,l,r}}$ are the contact angles of the liquid on the bottom, top, left, and right wall, respectively, and a and b are the depth and width of the microchannel, respectively.

The flow resistance of such microchannels is a geometric term with a Fourier series and can be approximated by a linear term [25]

$$R_{\mathrm{F}} = \left[\frac{1}{12}\left(1 + \frac{5}{6}\frac{a}{b}\right)\frac{abR_{\mathrm{H}}^2}{L}\right]^{-1} \tag{5.3}$$

satisfying the condition $a < b$. Here L is the length of the microchannel and R_{H} is the hydraulic radius of the microchannel, $R_{\mathrm{H}} = \frac{2A}{P} = \frac{ab}{a+b}$, with P being the perimeter and A the area of the cross section of the microchannel.

The flow in a microchannel can thus be estimated by the capillary pressure divided by the flow resistance that continually increases as the channel is being filled. In the case of capillary filling, spontaneous filling of a liquid inside a microstructure results from the interaction between the surface tension of the liquid and the chemistry and geometry of the surfaces of the microstructure. In the following sections, we review how to design capillary pumps for CSs and show how the capillary pumps enable advanced flow control in CSs.

5.2. Experimental

The CSs were fabricated in silicon using photolithography and dry etching. Briefly, photoplotted polymer masks [112] (Selba S.A., Versoix, Switzerland) with a resolution of 25400 dpi were used to pattern a photoresist on silicon wafers. The CSs were etched 30 µm deep into the silicon using a deep reactive ion etcher (STS ICP, Surface Technology Systems plc, Newport, U.K.). On some CSs the flow resistor was then coated by hand with resist and the remainder of the CS was etched to a total depth of 60 and 90 µm. Unless otherwise noted, we will discuss the 30 µm CSs in detail. After removal of the photoresist, the wafers were coated with Ti (10 nm) and Au (150 nm), and then diced to produce individual CSs.

The Au surface of the CSs was cleaned in a UV-ozone chamber (UV-Ozone Photoreactor PR-100, Ultra-Violet Products, Upland, CA) for at least 20 min. The CSs were then immersed for 30 s in a 2 mM ethanolic solution of thiolated poly(ethylene glycol) (HS-PEG 12750-4, Rapp Polymere, Tübingen, Germany) to make the Au surface hydrophilic. The CSs were rinsed with ethanol and dried under a stream of N_2. The resulting Au surface had an advancing contact angle of 40° with deionised water, to which a food colorant was added (Food Colour bordeaux, Werna W. Schweizer AG, Wollerau, Switzerland). Contact angles were measured using the sessile drop method on flat surfaces. A few millimetre thick layer of cured PDMS (Sylgard-184, Dow Corning, Midland, MI) was used to seal the CSs from the capillary retention valve to the vent. The advancing contact angle of deionised water with PDMS was 115°. All surface treatment and sealing steps were executed in a laminar flow box.

The CSs were used within 5 to 45 min after derivatization of its surface and sealing. Coloured deionised water was used as a model liquid in the experiments for this paper. The CSs showed comparable filling characteristics when other liquids having similar contact angles and viscosities as water were used (data not shown). To prevent evaporation of liquid from the loading pads, the sealed CSs were placed on a Peltier stage in a closed chamber and maintained at a temperature of 1 K above dew point (∼10 °C). The chamber was briefly opened to pipette liquid into the loading pads. The flow rate was

determined based on the time it required to fill a capillary pump completely. This time ranged from 45 s to a few minutes. The filling of liquids in the CSs was observed using a stereomicroscope (Wild Heerbrugg, Switzerland) equipped with a digital camera (Coolpix E990, Nikon).

5.3. Results and Discussion

5.3.1. Designing advanced capillary pumps

A CS starts filling upon pipetting a liquid into its loading pad. After the liquid has filled the capillary retention valve, the reaction chamber and the flow resistor, the liquid front reaches the capillary pump. The total volume of the elements in a CS located before the capillary pump is generally negligible compared with the volume of the capillary pump. The capillary pump therefore dictates the flow conditions of the largest volume fraction of liquids pipetted in the loading pad. Ideally, capillary pumps should be able to generate a smooth flow of liquid in a CS, to induce flow rates ranging from micro- to picolitre per second and to fill the CS entirely without entrapping air. In practice, these requirements can be difficult to meet. This is the case for CSs that are used to miniaturize surface immunoassays and in which the long (up to 10 mm) and narrow (cross section $\leq$ 30 $\times$ 30 μm^2) reaction chambers possess a significant flow resistance and thus required capillary pumps having low flow resistance and high capillary pressure. A large flow resistance can also build up in a capillary pump that has a large volume capacity. If capillary pumps having different characteristics are to be connected, it is important to fill the first capillary pump completely before the liquid proceeds to the next one. Control over the filling front of a liquid in a capillary pump is therefore desirable and may also be advantageous if some of the liquid present in the capillary pump must be retrieved for further analysis or processing.

Figure 5.2 shows different implementations of capillary pumps. The simplest possible capillary pump is a microchannel having a sufficient volume to accommodate the volume of liquid that needs to be displaced. The next simplest capillary pump is a cavity, which can have supporting posts to prevent collapse of the soft PDMS sealing cover ("Posts" capillary pump in Fig. 5.2a)

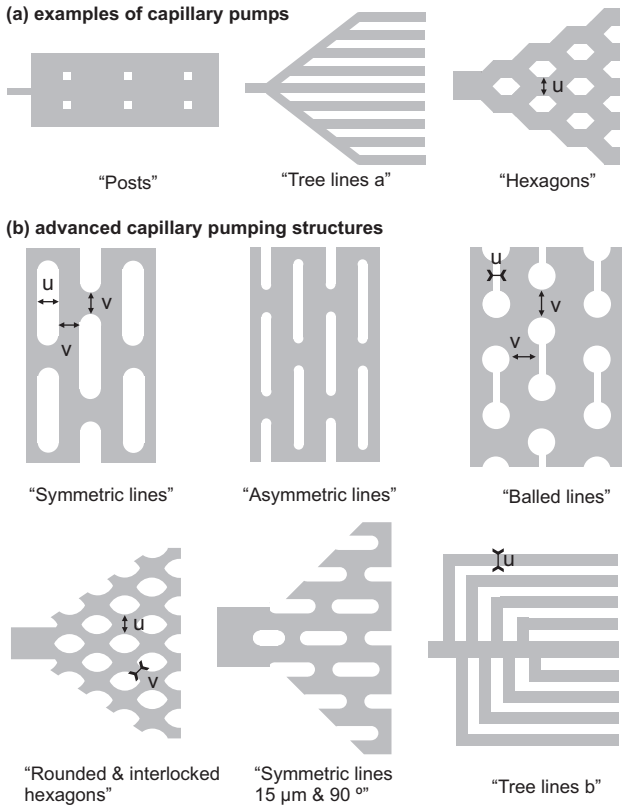

Figure 5.2. Examples of capillary pumps. (a) The characteristic dimensions of the structures generating capillary pressure in a capillary pump can be varied by changing the density ("Posts"), shape ("Hexagons"), relative positioning, and continuity ("Tree lines") of these structures. (b) Examples of capillary pumps described in depth in this work. All capillary pumps are shown with a filling direction from left to right.

[79]. Capillary pressure in the capillary pump can be increased by splitting the capillary pump into smaller parallel microchannels ("Tree lines a" in Fig. 5.2a) [33]. We previously used such capillary pumps to encode a high capillary pressure in autonomous CSs [33]. The total flow resistance of such capillary pumps, however, can significantly increase when the microchannels in the capillary pump are long. An alternative design is to place microstructures, such as hexagons, at regular intervals inside the capillary pump. These capillary pumps have a comparatively lower flow resistance because of the large number of parallel flow paths. They can thus be used when "large" volumes of liquid must be pumped at constant flow rate [34].

Advanced capillary pumping structures as shown in Fig. 5.2b can further enhance the pumping capabilities of CSs. Elongated microstructures can be used to control the filling front of a liquid by imposing various time constants for the progression of a liquid along different directions of the capillary pump. A straight filling front can be achieved by using lines, as shown in Fig. 5.2b. Changing the width (u) of the structures compared with their spacing (v) affects the progression rates of the liquid in the vertical and horizontal directions: the liquid moves quickly in between two parallel lines, whereas it spreads more slowly elsewhere. The areas separating microstructures act as pinning sites, which can delay the progression of the filling front for considerable amounts of time. It is preferable to have microstructures with a round periphery to minimize the occurrence of pinning of the liquid. Reducing the width of the microstructures in the region where they run parallel ("Balled lines" in Fig. 5.2b) increases the storage capacity of a capillary pump.

It is important to connect the capillary pump correctly to the remainder of the CS to ensure that the capillary pressure is sufficiently high everywhere in the connecting region to draw liquid efficiently from the CS to the capillary pump. This can be done by gradually expanding the lateral dimension of the capillary pump and centring one microstructure in the connecting channel at the entrance of the capillary pump. Interlocked structures, such as the rounded hexagons in Fig. 5.2b, reduce the time needed for a liquid to move along the sidewalls of the microstructures and to bridge them. Moreover, the edges of the capillary pump can be made long and similar to the microstructure lattice to minimize the risk of having the liquid shortcutting

the capillary pump by rapidly wetting its edges. The last type of capillary pump shown in Fig. 5.2b ("Tree lines b") has branched filling regions, which, once filled, become disconnected from the central flow path. With this type of geometry, capillary pumps can be programmed to have zones that generate different capillary pressures and that can be filled one after the other without continuously adding flow resistance to the CS.

From the set of capillary pumps described in Fig. 5.2, we implemented the most promising ones into CSs using various characteristic dimensions, measured their flow rate and characterized their filling behaviour, Table 5.1. We chose characteristic dimensions to obtain flow rates of a few nanoliters per second. Such flow rates are typical for high-sensitivity and low-volume assays [34]. Table 5.1 summarizes the findings for CSs, in which the capillary pumps have characteristic dimensions of 15–250 µm and which draw liquid with rates from ∼2 to 4 nL s^{-1}. As expected, the fastest CSs have capillary pumps with the smallest characteristic dimensions. The "symmetric line"-type capillary pump with a typical dimension of 15 µm, however, has a smaller flow rate than expected from the calculations. A reason is probably the high number of sites in which the meniscus at the liquid front is pinned. A liquid filling this capillary pump exhibits a random filling front – similar to a liquid filling a porous medium [113] – but this random filling front can be changed to a straight one by rotating the microstructures in the capillary pump by 90°. "Symmetric line"-type capillary pumps having larger characteristic dimensions, and "asymmetric line"-type capillary pumps have a straight filling front, which is oriented perpendicular to the main axis of the capillary pump. Liquid that fills "hexagon"-type capillary pumps sometimes runs preferably along the capillary edges, which is typical for most capillaries [114]. Flow rates in "rounded hexagon"-type capillary pumps are very uniform, because the microstructures are interlocked so that liquid is less pinned. A reproducible filling front can be observed in the tree-line capillary pump: Liquid in this capillary pump fills the individual branches one after the other. All capillary pumps have an absorption capacity (filling factor) of ∼60 to 75 % of their total volume and can accommodate ∼0.02 µL mm^{-2} of liquid for a depth of 30 µm. In our experiments, the capillary pumps typically had a total volume of 0.3 µL on an area of 15 mm^2. From the analytical model based on Eqn. 5.1–5.3, we

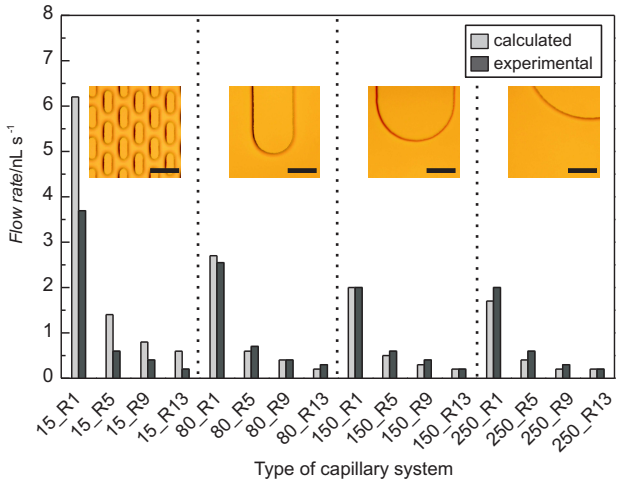

Figure 5.3. Calculated and experimental flow rates of water in "Symmetric line"-type capillary pumps. For each type of CS, the first number refers to the spacing (in μm) between the microstructures of the capillary pump and the last number indicates the length (in cm) of a flow resistor having a cross section of 30 × 30 μm^2 and placed before the capillary pump. The insets are optical micrographs showing the relative size of the microstructures in the capillary pumps. The scale bars are 50 μm.

estimated a flow rate of 1.7–8.7 nL s^{-1} for the "symmetric line"-type capillary pumps. The capillary pumps were modeled as networks of parallel and serial resistors, each resistor representing a small channel of the capillary pump. The total resistance was derived using the equivalent network approach and Ohm's Law. We assumed a flow resistance of 3.6×10^{-14} m^{-3}, which includes the exit channel of the loading pad, three parallel, 10 μm wide capillary retention valves, the reaction chamber, and a 30 μm wide and 1 cm long flow resistor. In Eqn. 5.3 we used a corrected width of $b = \sqrt{v^2 + 4v^2} = v\sqrt{5}$, which we observed from the experiments as the typical width of the moving meniscus in the "symmetric line"-type capillary pumps. We will now discuss the influence of the flow resistance in front of the capillary pump on the flow rate and compare the experimental with the estimated flow rates.

Capillary pumping structure	Characteristic dimensions / μm	Experimental flow rate / nL s^{-1}	Calculated flow rate / nL s^{-1}	Filling factor (%)	Volume / μL mm^{-2}	Comments
Hexagons	$u = 60$	2.1	–	59	0.018	Good filling, risk of shortcutting along the edges of the pump
Sym. line	$u = v = 15$	3.7	6.2	65	0.02	Random filling front
Sym. line	$u = v = 80$	2.6	2.7	63	0.019	Straight filling front, straighter with smaller flow resistance
Sym. line	$u = v = 150$	2	2	62	0.019	”
Sym. line	$u = v = 250$	2	1.7	65	0.02	”
Asym. Line	$u = 40$, $v = 80$	2.4	–	74	0.022	Good filling like for sym. line pumps
Balled line	$u = 20$, $v = 80$	2.1	–	75	0.023	Preferred filling from the side
Rounded Hexa.	$u = 60$, $v = 30$	2.6	–	60 c	0.018	Filling front moves continuously
Rounded Hexa.	$u = 30$, $v = 15$	3	–	60 c	0.018	”
Sym. line	$u = v = 15$, 90	3.6	–	65 c	0.02	Straight filling front, tilted by 45°
Tree line b	$u = 30$	3.2	–	61	0.018	Subsequent filling of the branches

Table 5.1. Characteristics of advanced capillary pumps.

5.3.2. Connecting capillary pumps using microchannels of different lengths

It is convenient to change the flow rate of a CS without changing the design of the capillary pump by simply varying the flow resistance in front of the capillary pump. For example, we varied the flow resistance in CSs using "symmetric line"-type capillary pumps. The flow rates for these CSs are displayed in Fig. 5.3 for four different total flow resistances. A capillary pump has a maximal flow resistance when it is almost fully filled. This resistance can however be neglected as it is very small and at least 2–3 orders of magnitude smaller than the total flow resistance of the CS. The predominating flow resistors used here precede the capillary pump and had a length of 1, 5, 9 and 13 cm and are abbreviated R1, R5, R9 and R13, respectively. For these CSs, experimental flow rates varied by a factor of ∼18 and ranged from 0.2–3.7 nL s^{-1}. Flow rates were determined with an accuracy of ±0.1 nL s^{-1} or better. In the CSs with the smallest flow resistance (R1), the liquid filled the capillary pumps with the largest flow rate, namely 2.0–3.7 nL s^{-1}. A larger flow resistance (R5) slowed down the flow rate to 0.6–0.7 nL s^{-1}. By further increasing the flow resistance (R9, R13), flow rates down to 0.2–0.4 nL s^{-1} could be achieved. Irrespectively of the preceding flow-resistance area, the capillary pump with the smallest characteristic dimension of 15 µm exhibits an experimental flow rate that is significantly smaller than expected from the calculations. For the other CSs, experimental results fit the predicted flow rates with a deviation of ∼10 %. Large flow resistances (R9, R13) can predominate the flow rate, whereas the capillary pump determines the flow rate when flow resistances are small (R1), see CS 15_R1 and CS 250_R1 in Fig. 5.3. Although the internal structure of the capillary pump seems to be less important for the flow rate than the flow resistance, it can be relevant to ensure a proper filling as we will show next.

Time series of typical filling fronts of coloured water in various types of CSs are shown in Fig. 5.4. The liquid fills the capillary pumps from the left to the right. The exact shape of the filling front depends on the total flow resistance and the type of capillary pump. A low flow resistance (R1, R5) in front of a "symmetric line"-type capillary pump results in a filling front that is parallel

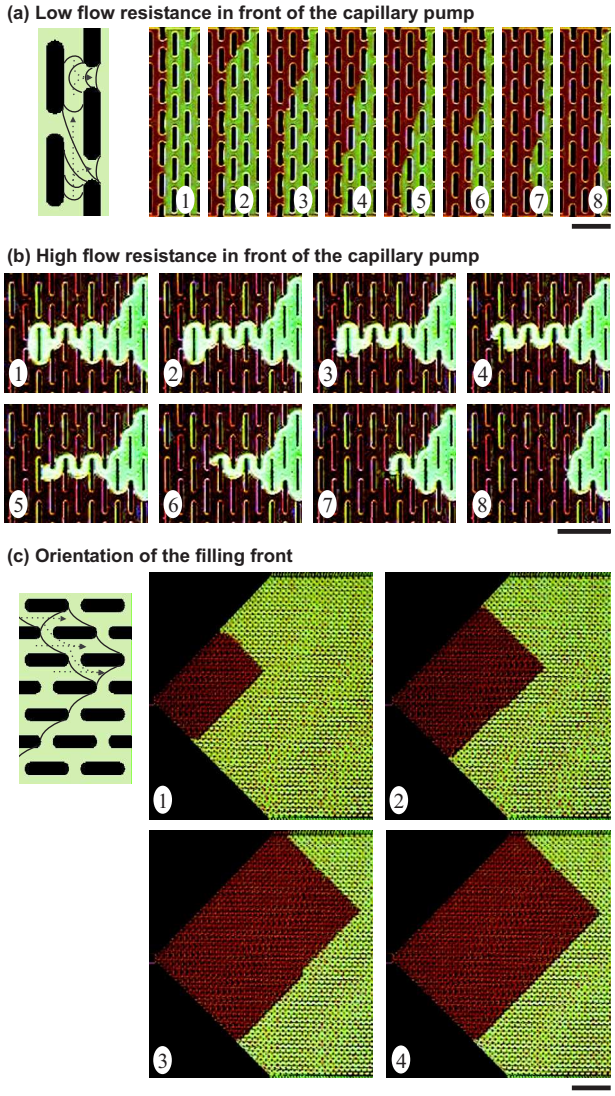

Figure 5.4. Time series of optical micrographs showing the typical filling fronts of coloured water in various types of capillary pumps. Liquid flows from left to right. (a) Flat filling front in a capillary pump that is preceded by a low-flow resistor and corresponding scheme showing how the water menisci (plain lines) progress from structure to structure (dashed arrows). (b) Capillary pump preceded by a high-flow resistor that has a meandering filling front. Such a capillary pump is designed to minimize the risk of entrapping air. (c) Example of a capillary pump designed to control the shape and orientation of the filling fronts in the capillary pump. The scale bars are 500 µm. These results are also available as videos [115].

to the microstructures, Fig. 5.4a. The liquid spreads preferably along the edge of the capillary pump into the next row of microstructures and is then drawn by the slightly higher capillary pressure into the space between two parallel lines, and fills the entire width of the capillary pump. This overall straight filling front moves consistently along the main axis of the capillary pump. In Fig. 5.4b the capillary pump has the same capillary pressure as in Fig. 5.4a but the flow resistance is larger (R13), which reduces the flow rate and changes the filling behaviour. Here spreading of liquid along the edge of the capillary pump predominates. In the case of a sealed capillary pump, such a filling behaviour increases the risk of incomplete filling and enclosing air. This risk is minimized when using the "symmetric line"-type of capillary pumps in which two filling fronts of liquid converge from the edges of the capillary pump toward its centre without entrapping air. For small characteristic dimensions (15 µm) in the capillary pump, Fig. 5.4c, the filling line is rotated by 45° compare with the large structures in Fig. 5.4a. The capillary pump shown in Fig. 5.4c has two main parts, namely, of a triangular entrance and a rectangular main body. Spreading of liquid along the edges of the capillary pump is slowed down in the entrance of the capillary pump because the entrance sidewalls are indented. In the rectangular part of the capillary pump, the microstructures are parallel to the sidewalls and these walls are therefore not indented. Accordingly, the microstructures vicinal to the sidewalls are placed 25 µm instead of 15 µm away from the walls to reduce the capillary pressure in this region and to prevent undesired spreading of liquid along the peripheral walls.

5.3.3. Serial connection of capillary pumps

Biological assays typically comprise multiple incubation and rinsing steps, which can differ in duration. Because liquids in CSs flow in a laminar manner, a brief rinsing step can be an efficient way to remove a preceding liquid from a reaction chamber [33]. In contrast, the time needed to capture antigens from solution or to bind detection antibodies to a surface-immobilized antigen necessitate minutes [34]. Matching the flow rates during an assay to the optimal durations of individual steps is desirable to shorten the time to result

when using microfluidic systems, Chapter 2, [34].

A sequence of steps can be optimized using a capillary pump with multiple zones, each generating a slightly different flow rate. It is easy to design a CS in which a first capillary pump is followed by a second, slower one because the high flow resistance of the second capillary pump does not affect the filling of the first capillary pump. The reverse case is more challenging for two reasons. First, the filling behaviour of the liquid in the capillary pumps must be carefully controlled to prevent the first (slow) capillary pump from being bypassed. The second challenge for accelerating a liquid in a CS using serial capillary pumps is the additive effect of flow resistances of serial microfluidic elements. Bypassing, as has been shown above, occurs preferentially along the peripheral edges of the capillary pump and might lead to an only partial filling of the first capillary pump. The risk of bypassing can be greatly reduced by selecting a capillary pump having indented peripheral walls, Fig. 5.5. In addition, the liquid at the end of the first capillary pump can gradually be directed to a single connexion channel using a series of hierarchical bridges, Fig. 5.5a. Here, the capillary pressure in the successive bridges diminishes (in absolute value) and favours the complete filling of the small bridges over that of the larger ones. The geometry of the junction between smaller and larger bridges also helps pinning a liquid that fills a bridge from only one side until the liquid has also filled the second branch. We found such hierarchical structures very efficient for the CSs designed here. In addition, these structures have a relatively small footprint. The increase in resistance of serial capillary pumps can be compensated by augmenting the capillary pressure in the second capillary pump compared with that in the first one. The serial capillary pumps shown in Fig. 5.5b are connected via hierarchical bridges, do not entrap air, are not bypassed by the spreading of liquid along the capillary pump edges, and the second capillary pump generates a flow rate that is about twice as fast as the first one.

5.4. Conclusions

The work presented here enhances the capabilities of autonomous CSs by showing how to program their filling properties. The possibility to slow down

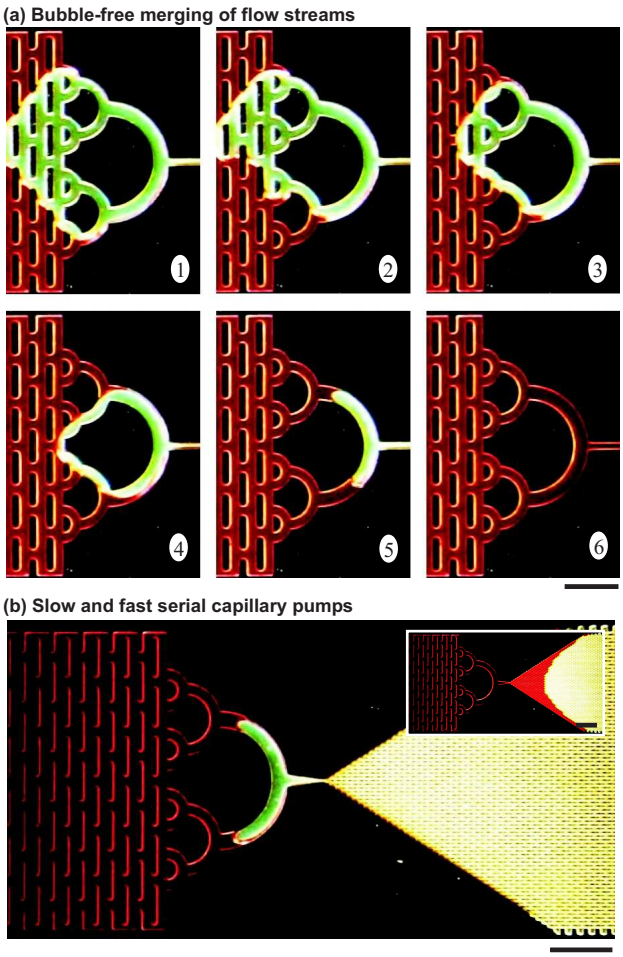

Figure 5.5. Optical micrographs showing (a) the consolidation of liquid streams at the end of a capillary pump to prevent entrapping air or incomplete filling of a capillary pump, and (b) a liquid moving from a completely filled, slow pump to a second faster pump. The inset shows the same region observed a few seconds later when liquid starts filling the second pump. The scale bars are 500 μm.

or even temporarily stop the flow of liquid in a CS makes it possible, for example, to fill a reaction chamber, perform an incubation step or enzymatic assay, and flush the reactants and products for a next test in the same CS. Enzyme-linked immunosorbent assays as well as other types of assay could in principle be implemented on CSs using appropriate types of capillary pumps. These CSs would certainly lead to sensitive and versatile platforms for point-of-care testing [116]. Here, we studied capillary pumps in combination with flow resistances, in which the capillary pressure was defined solely by the geometry. Such CSs can also have tailored surface chemistry [117] to further enhance their flow behaviour or to add new functionalities such as hydrophobic valves and metering channels. Other functions that can be added to CSs are filters for cells or particles, mixers, chambers with immobilized cells, and surface-immobilized binding sites for analytes. The small form factor of CSs, their simplicity in term of utilization, and the possibility to tailor their hydrodynamic properties using advanced capillary pumps may help to promote their use for a large number of applications in which miniaturization provides a benefit to performing biological assays.

6. High-performance Immunoassays Based on Through-stencil Patterned Antibodies and Capillary Systems

Autonomous capillary systems (CSs) are self-powered microfluidics that can be used for detecting multiple analytes in sub-microliter volume of sample, within minutes and with picomolar sensitivity, i.e. CSs enable high-performance immunoassays. We present a simple method to pattern capture antibodies (cAbs) on PDMS with high accuracy and in a manner compatible with mass fabrication for use with CSs.[1] Capture antibodies are patterned in dense lines of up to 8 lines per millimeter of PDMS and used with CSs that have been optimized for convenient handling, pipetting of solutions, pumping of liquids such as human blood serum, and visualization of signals for fluorescence immunoassays. The detection of CRP with a sensitivity of 0.9 ng mL^{-1} (7.8 pM), in 1 μL of CRP-spiked human serum, within 11 minutes, using four pipetting steps and a total volume of sample and reagents of 1.35 μL exemplifies the high-performances that can be achieved using this approach and an otherwise conventional surface sandwich fluorescence immunoassay. This method is simple and flexible and should therefore be applicable to a large number of immunoassays.

[1] J. Ziegler, M. Zimmermann, P. Hunziker, E. Delamarche, High-performance immunoassays based on through-stencil patterned antibodies and capillary systems, first published in *Analytical Chemistry*, **80**, 1763–1769, **2008**.

6.1. Introduction

Immunoassays are widely used for diagnostics, research in life sciences, therapy monitoring, environmental monitoring, and food safety [3]. These assays rely on the specific interaction between antigens and antibodies to detect analytes (antigens or antibodies) of interest in body fluids or other samples. Even for a single type of application, the requirements for having informative and efficient immunoassays can vary strongly. There is for example a notable difference between platforms used for portable immunoassays done near a patient and for a clinical analyzer from the central laboratory of a hospital. The first platform must be simple to use and provides results within minutes whereas a clinical analyzer typically runs a large number of possible tests and can process samples (i.e. filtration, dilution, thermal treatment, spinning, etc.) to optimize the sensitivity and accuracy of the test. Immunoassays, that are used for research in life sciences are usually more specialized and customized than for diagnostics. The signal of the assay can be based on radioactivity, light (emitted or absorbed), a current, [118] fluorescence, or even changes in the index of refraction [119] or mass of a sensing surface [120]. These assays comprise numerous incubation and rinsing steps with volumes of solution ranging from a microliter to hundreds of microliters. These steps can last for a few seconds, for example, when rinsing or adding reagents, to hours, for example for ligand-receptor binding reactions for high-sensitivity assays. The diversity of platforms, [121] formats, and steps performed for immunoassays in research suggests that new platforms should be versatile and flexible in the number of steps and volumes of solutions, they can accommodate.

We pioneered the concepts of microfluidic networks and then CSs with the goal of providing convenient platforms for high-performance immunoassays [49]. Key to these concepts is the use of a PDMS substrate patterned with receptors for analytes that can reversibly seal microfluidic structures [78]. The microfluidic structures are accurately prepared by means of microfabrication using Si wafers or in plastics using replication techniques. CSs extend microfluidic networks by implementing a more precise control over filling behavior of liquids entering the microstructures [33]. They typically have loading pads inside which reagents and samples are pipetted, reaction chambers cov-

ered by PDMS, and capillary pumps. Valves and flow resistances can also be added to reduce evaporation of liquid, meter liquid, or delay the progression of a liquid in the different parts of the CS, Chapter 5, [33]. Importantly, the geometry and wetting properties of the microstructures encode a capillary pressure in the various parts of the CSs, which permits drawing a desired amount of liquid in a CS with a controlled flow rate without requiring actuated pumping systems. The merit of CSs for immunoassays is the possibility to detect rapidly multiple analytes in samples smaller than 1 μL in volume [34]. Here, the patterning of cAbs on PDMS plays a critical role by providing well-defined areas where analytes are captured. These areas, which are typically a few tens of micrometers in lateral dimensions, help limiting the depletion of analytes [29] and can be spaced so as to provide many contiguous signals and controls, which is useful for the combinatorial screening of analytes, [35] imaging data in one step, and achieving assays with small intra-assay variations [34]. These assays, called "micromosaic immunoassays", utilize two microfluidic chips for patterning cAbs and dispensing samples [14].

We present in this chapter a method for accurately patterning Abs on PDMS using stencils that fit well with improved CSs for achieving high-performance immunoassays in a flexible manner. We first describe the functions of the CSs for immunoassays and the use of the stencils for delivering Abs to a PDMS surface, and then assess the characteristics of sandwich fluorescence surface immunoassays. These immunoassays were performed with stencil-deposited cAbs, the new CSs, and human serum spiked with CRP. CRP is a protein rapidly synthesized by the liver in response to many conditions including infection, inflammation, and cardiovascular diseases [122, 123].

6.2. Experimental Section

6.2.1. Reagents and Proteins

Solutions of PBS (tablets P4417, Sigma) and BSA (Sigma) were reconstituted in ultra pure water (Millipore Simplicity 185, Bedford MA) and filtered prior to use with a 0.20 μm syringe filter (Sartorius, Epsom UK). Solutions of alkanethiols were prepared in ethanol (puriss. = 99.8 %, Fluka) using

thiolated poly(ethyleneglycol) (HS-PEG) (CH_3O-(CH_2CH_2O)n-SH, molecular weight of 750 g mol^{-1}, Rapp Polymere GmbH, Tübingen, Germany) and hexadecane thiol (HDT) (HS-$(CH_2)_{15}$-CH_3, Fluka). PDMS prepolymers (Sylgard 184, Dow Corning, Midland MI) were mixed at a ratio of 1:10 using a DOPAG mixer (Cham, Switzerland), poured onto planar polystyrene Petri-dishes (Greiner BioOne), and cured over night in a oven at 60 °C. The cured 3-mm-thick layer of PDMS was cut into 8×8 mm^2 pieces. Abs were patterned on the surface of the PDMS that faced the Petri-dish.

Lyophilized goat anti-rabbit immunoglobulin G (IgG) (R2004, Sigma-Aldrich) and rabbit anti-guinea pig IgG tetramethylrhodamine isothiocyanate (TRITC)-labelled (T7153, Sigma-Aldrich) were reconstituted in PBS at concentrations of 125 and 250 μg mL^{-1}, respectively. Human CRP (8C72), anti-CRP (4C28-C2, 4C28-C6), anti-CRP-FITC (4C28F-C6) and human CRP free serum (8CFS) were bought from HyTest (Turku, Finland) and diluted in PBS. Human CRP-free serum was spiked with human CRP to the desired CRP concentration. The anti-CRP-C6 Abs were labelled using an Alexa Fluor 647 labeling kit (Alexa Fluor 647 Monoclonal Antibody Labelling Kit, Molecular Probes). The number of fluorophores per protein was measured to be four using an Eppendorf BioPhotometer.

6.2.2. Handling of Microfluidic CS and Templates

The microfluidic CSs and the stencil templates were etched in Si using photolithography and deep reactive ion etching. The CSs were sputtered with Au and diced to yield individual microfluidic chips having each 6 CSs each.

Prior to each use, the microfluidic chips were cleaned in an UV-ozone reactor (UV-Ozone Photoreactor PR-100, Ultra-Violet Products, Upland, CA) during 60 min. A planar PDMS stamp having the size of a microfluidic chip was inked with a 2 mM solution of HDT in ethanol for 30 s, rinsed with ethanol, and dried under a stream of N_2. The PDMS stamp was applied manually to the chip for 30 s to make its top surface hydrophobic. The chip was then covered with a 2 mM solution of HS-PEG in ethanol for 30 s, rinsed with ethanol, and dried under a stream of N_2 to render the CSs wettable and the surfaces protein-repellent. The derivatized chips were stored in a dry environment and

typically used within 6 h.

The Si wafers with the stencils were diced into 12 × 12 mm^2 individual templates having 16 or 24 stencils. Each stencil comprises a loading pad connected to a 2-mm-long line. The templates were cleaned in O_2-plasma (Tepla Microwave-Plasma System 100, PVA Tepla, Asslar Germany) during 2 min at 200 W and 0.7 Torr before they were placed on the PDMS block. The stencils were filled with a solution of cAbs for a 15-min-long deposition of cAb on PDMS at room temperature. The stencils in contact with PDMS were rinsed under a stream of PBS and ultra pure water. The PDMS surface was separated from the stencil using tweezers, exposed to a blocking solution of BSA for 15 min, rinsed with PBS, ultra pure water, and dried under a stream of N_2. The templates were rinsed and cleaned in an O_2-plasma before reuse.

The PDMS block was placed on the CSs in such a way that the lines of cAbs were oriented perpendicularly to the reaction chambers of the CSs. A non-patterned block of PDMS was used to seal the capillary pumps. Immunoassays were performed by pipetting the solution of analyte into the loading pads of the CSs, followed by a solution for rinsing, and a solution containing detection antibodies (dAbs). CRP-free human serum was then placed around the PDMS substrate, which was removed from the CSs. The PDMS was rinsed under a stream of PBS and ultra pure water, dried under a stream of N_2 and imaged. Fluorescence micrographs were obtained using a fluorescence microscope (Eclipse 90i, Nikon, Japan), which was equipped with a 100 W halogen lamp for excitation, and a digital camera (DS-1QM, Nikon) cooled to -30 °C for imaging. Fluorescence micrographs were analyzed using the software NIS-Elements (Nikon). After the experiments, the microfluidic chips were rinsed with PBS, ultra pure water and ethanol, dried under a stream of N_2, and cleaned again in the UV-ozone reactor.

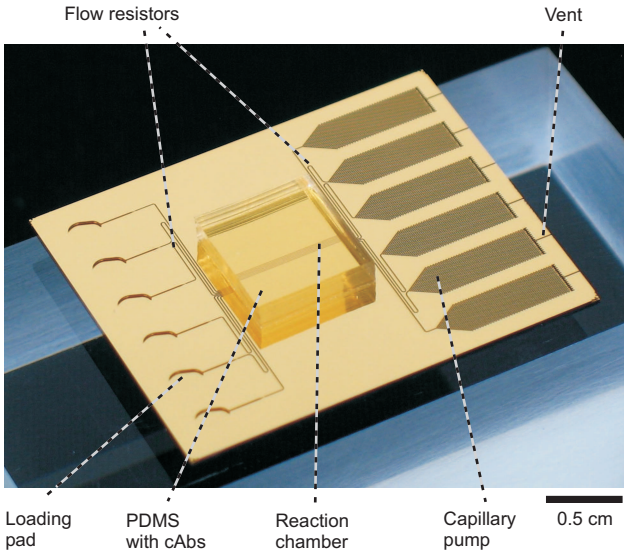

Figure 6.1. Photograph of a Au-coated silicon microfluidic chip having six independent CSs. Up to 6 independent surface immunoassays can be performed using such a chip. Assays are performed by successively loading samples and reagents in the loading pads and capturing analytes flowing in the reaction chambers using cAbs, which are patterned on a sealing block of PDMS.

6.3. Results and Discussion

6.3.1. Capillary Systems

Figure 6.1 shows a microfluidic chip having six independent CSs with their reaction chambers sealed with a block of PDMS. All structures of the CSs have a depth of 180 µm, except for the reaction chambers, which are 20 µm deep. A depth of 180 µm enables loading pads and sealed capillary pumps to hold a total volume of 2 µL without requiring too large a footprint on the chip. When 2 µL of solution are pipetted into a loading pad, most of the solution protrudes outside of the pad without spreading toward adjacent pads because the top part of the chip is covered with a hydrophobic self-assembled monolayer. These pads are approximately twice as large as those of the previous CSs [33] to ease the loading of solutions using manual micropipetting. The depth of the reaction chambers provides a good compromise between having an efficient transport of analytes to the capture sites, Chapter 2, keeping the hydraulic resistance of the reaction chamber low, and preventing the collapse

Average flow rates in the reaction chambers	Sample viscosity / mPa s	Reaction chamber 20 µm deep / nL s^{-1}	CV /%	30 µm deep / nL s^{-1}	CV /%
Water	1	1.9	4.7	4.2	4.8
PBS + 1% BSA	1	1.9	5.0	4.0	3.4
Solution of 20% hum. albumin	4	0.5	12.0	1.5	11.9

Table 6.1. Characteristic flow rates of samples filling CSs and corresponding coefficients of variation (CV).

of the PDMS into the chamber [124]. The reaction chambers are 30 µm wide, 9 mm long, and are separated from each other by 120 µm. Their length permits the convenient manual placement of a block of PDMS having numerous lines (> 20) of cAbs and their spacing allows having six rows of signals per millimeter. Grouping the reaction chambers in the center of the chip facilitates imaging the results of assays because the fluorescence signals on the surface of PDMS can be acquired in one imaging step [34]. The total volume of 2 µL of the capillary pumps was selected based on previous work, in which 600 nL of sample were used for high sensitivity assays, [34] and based on the maximum volume of dAbs and rinsing solution estimated to be necessary for completing the assay. The pumps have a vent to prevent the entrapment of air. The use of large pads and pumps and the grouping of reaction chambers in the middle of the chip make the CSs asymmetric: CSs at the periphery of the chip have longer distances between pads, pumps, and reaction chambers. For this reason, meandering channels are added to the inner pads on both sides of the reaction chamber to equalize the hydraulic resistance of all CSs.

A sample added to a loading pad of a CS flows through the reaction chamber and moves into the capillary pump at a flow rate depending in part on the surface tension and viscosity of the sample, Table 6.1. Water and a solution of 1 % BSA in PBS, which has a similar viscosity as human serum (1 mPa s), flow at 1.9 nL s^{-1} with variations ±5 % through CSs having 20 µm deep reaction chambers. Reducing the hydraulic resistance of the CSs by using 30 µm deep reaction chambers increases the flow rate to 4.2 nL s^{-1} for water and 4 nL s^{-1}

for PBS containing 1 % BSA. Blood or blood plasma, which might be used in point-of-care applications, have higher viscosities than serum. The blood viscosity depends on the hematocrit and can amount to 3 to 8 times the viscosity of water, with typical values being 3 to 4 [125]. As blood is a non-Newtonian liquid, the viscosity therefore depends also on its velocity [126]. The viscosity of plasma is ∼1.8× higher than that of water. We chose a solution of 20 % human albumin as a model liquid to measure the flow rate of a liquid having a viscosity of 4 mPa s in CSs. As expected, such a liquid flows slower than less viscous solutions with flow rates of 0.5 nL s^{-1} and 1.5 nL s^{-1} in CSs having 20 µm deep and 30 µm deep reaction chambers, respectively. The coefficient of variation is ∼12 % in both cases, which might be improved by optimizing the internal structures in the capillary pump to have finer and more continuous structures. In the experiments described next, CSs having 20 µm deep reaction chambers are used, in which 0.9 µL of human serum flow within ∼8 min.

6.3.2. Patterning of Capture Antibodies Through Stencils

Figure 6.2 shows a template that is used to localize antibodies to specific areas of a PDMS surface as well as fluorescence images of the resulting patterns. The template was microfabricated in Si and has zones with four stencils. The template can readily be rendered hydrophilic or cleaned for reuse by using an O_2-based plasma. The template is placed manually on a block of PDMS, and the conformal contact occurring between the PDMS and the template seals the stencils. The stencils are accessible from above and can be filled individually by manual pipetting. The pads and stencils are laid out in such a way as to ease the addressing of each pad while keeping the stencils grouped as much as possible to keep the assay signals as contiguous as possible. Using a pitch of 1 mm for the loading pads and keeping the solution of antibody solution that is pipetted into the pads to values smaller than 0.3 µL help prevent pad overflow and crosstalk when pipetting manually. We found that a deposition time of 15 min was sufficient to saturate the PDMS surface with a layer of Abs using a 125 µg mL^{-1} solution of Abs in PBS. The filled template was kept in a humid environment during deposition to prevent evaporation of solution from the

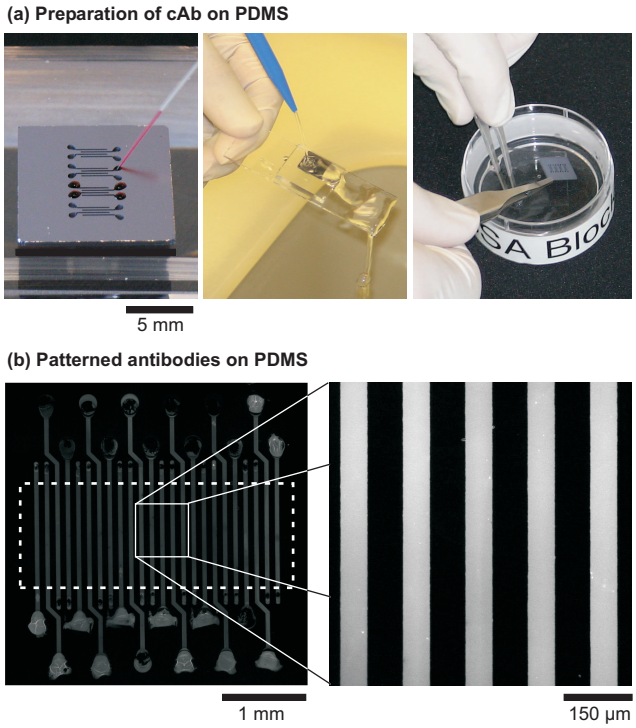

Figure 6.2. Local delivery of Abs to PDMS areas using microfabricated stencils. (a) The 2-mm-long stencils of a silicon template can be filled individually with a solution of Abs, rinsed under a stream of PBS and deionised water. The PDMS is then separated from the template under a blocking solution of BSA and dried. (b) Fluorescence micrograph showing the accurate delivery of TRITC-labeled Abs through stencils onto a PDMS surface homogeneously covered with cAbs.

stencils. All stencils were rinsed for a few seconds using a flexible dispensing bottle filled with PBS and with the jet of PBS being in the direction of the stencils, Fig. 6.2a. The template adhered well to the PDMS, even during intense rinsing involving multiple steps. The template was separated from PDMS in a BSA bath to quickly cover any area of PDMS left free of Abs with BSA. The fluorescence images in Fig. 6.2b show an example of delivering Abs locally to PDMS areas using 60 µm wide stencils. In this case, cAbs (anti-rabbit IgGs) have been homogeneously applied from solution to PDMS and 0.3 µL aliquots of TRITC-labeled rabbit IgGs were locally provided in each stencil. The homogenous fluorescence signals observed in the inner area of the template (dashed rectangle in Fig. 6.2b) underline the homogeneous, local delivery of Abs to the PDMS surface. Having a pad at the beginning of each stencil not only facilitates the addressing of the stencil but also helps localize imperfections (drying artifacts, entrapment of air bubble) away from the area used for the assay.

Stencils can greatly vary in size and be several hundreds micrometer wide, [127] a few micrometers in diameter, [128, 129] or even just 100 nm in size [130]. Here, we looked for stencils that were (i) easy to microfabricate even with micrometer accuracy, (ii) small enough to enable the delivery of approximately 6 to 10 solutions of proteins per millimeter across capture areas and to allow the use of sub-microliter volumes of protein solution, and (iii) made from a material that can withstand strong oxidizing conditions so that cleaning them and removing proteins from the template would be easy using ozone, oxidative plasmas, or oxidants in solution. The length of the stencils provides the possibility of patterning long lines of cAbs on PDMS, thereby preventing issues involved in aligning the reaction chambers of CSs with the patterned cAbs. The width of the stencils defines one lateral dimension of the mosaic of fluorescence signals. We were not able to fill stencils individually by hand if their pads had a pitch of 0.6 mm. Pipetting robots can in principle be used for filling higher-density stencils and/or preparing PDMS substrates in mass for miniaturized immunoassays. In the remainder of the chapter, cAbs for CRP are patterned onto PDMS using 16 stencils as shown in Fig. 6.2a, with

a pitch of 1 mm between pads and 120 to 270 μm wide stencils. These assays have a potential maximum of 96 test sites when combined with a microfluidic chip having six independent reaction chambers.

6.3.3. Immunoassays for c-reactive protein in capilary systems

A first series of immunoassays was performed in CSs using human serum spiked with 0.1 μg mL^{-1} CRP to determine the homogeneity of the fluorescence intensity in adjacent capture areas and CSs, Fig. 6.3. This immunoassay was also developed with the goal of using minute volumes of solutions and brief incubation times. A volume of 1 μL of CRP-spiked human serum was added in each pad of the CSs, except in CS No. 2, in which CRP-free human serum was loaded to provide a control. After a quick rinsing step with CRP-free human serum, 0.25 μL of a solution of Alexa-647 labeled dAbs was flown through the CS for 2 min followed by a second brief rinsing step, Fig. 6.3a. After 11 min the assay was finished and the block of PDMS separated from the CSs in the presence of human serum. The PDMS surface was rinsed, dried, and the fluorescent signals were imaged. A fluorescence image of a block of PDMS having three rows of cAbs (A, B, C, deposited using the stencils) that are crossed by six CSs (1 - 6) is shown in Fig. 6.3b. CRP in the CSs passed over rows A, B, and then C. The 15 zones of signal shown in Fig. 6.3b are accurate rectangles, having a width of 30 μm (corresponding to the width of the reaction chamber in the CS) and a length of 120 μm (corresponding to the width of the stencils). No signal was generated in CS 2 or outside the areas of PDMS, where no cAbs had been patterned, as expected. A detailed comparison of the fluorescence intensities of the individual areas, Fig. 6.3c, reveals that corresponding areas A1-A6, B1-B6 and C1-C6 in independent CSs have similar intensities, whereas the areas A, B, and C in the same CS have decreasing intensities. The first areas of cAbs (A) that were passed by CRP exhibit a larger fluorescence intensity than subsequent areas (B, C). This decrease of the fluorescence intensity originates from a slight depletion of CRP analyte in the reaction chamber during the capture step. In Fig. 6.4, 14 lines of cAbs and 5 CSs were used, and CRP was omitted in one of the CSs to provide a control. An intensity profile of the fluorescence

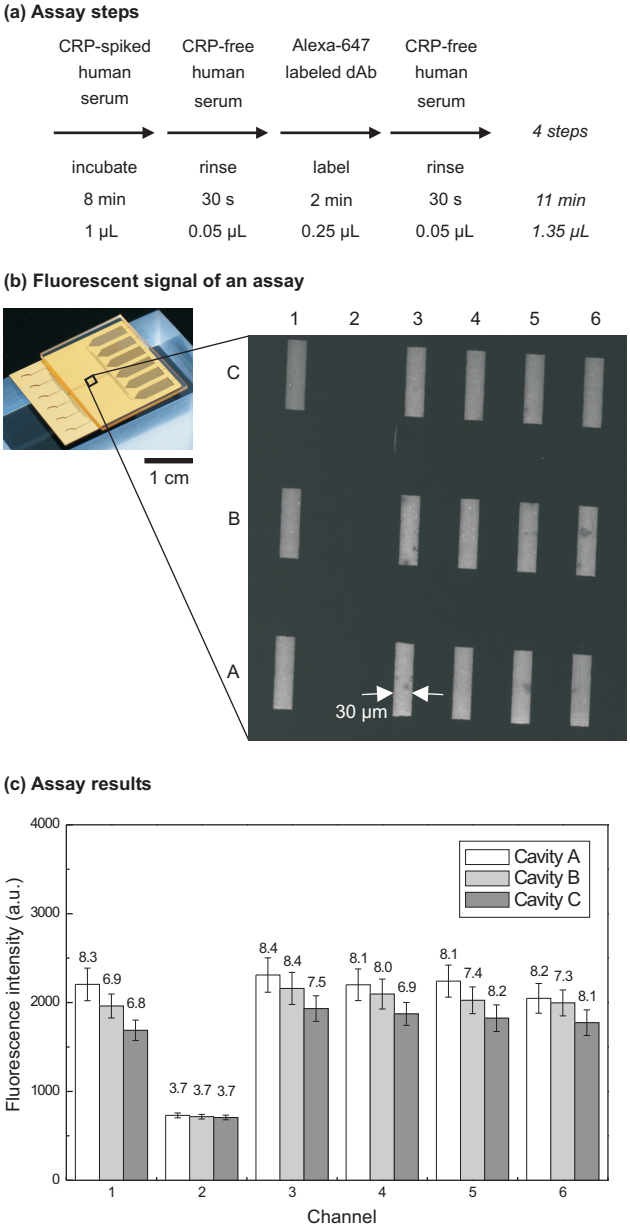

Figure 6.3. Fluorescence surface immunoassays for CRP performed in CSs using cAbs patterned on PDMS using a stencil template. (a) The immunoassay comprises four pipetting steps for incubation of the analyte, rinsing of non-captured analytes, binding dAbs to captured analytes, and rinsing excess dAbs. (b) The CSs were sealed with PDMS from the beginning of the reaction chamber to the end of the capillary pumps. The PDMS was patterned with lines of one type of cAbs (CRP-C2, 125 µg mL^{-1}) which are crossing the reaction chambers of the CSs. The optical micrograph shows the fluorescence signal of Alexa-647-labeled dAbs (CRP-C6, 250 µg mL^{-1}) after 5 identical assays (CRP, 0.1 µg mL^{-1}) were performed in each CS except in channel 2, in which the analyte was free of CRP. (c) The bar chart shows the mean fluorescence intensity of the signals shown in (b) with the standard deviation (not to scale).

signal corresponding to a concentration of CRP of 1 μg mL^{-1} is shown in Fig. 6.4b. The fluorescence intensity of the signals slowly decreases from the first area of cAbs to the last one, and it decreases faster along one area of cAb. This reflects the depletion of CRP along the reaction chamber, but also the enrichment in CRP of the depleted boundary layer during the 0.22 s it takes the sample to reach the next capture area. After the fourth capture area, the mean fluorescence signals of the remaining areas are equal, which suggests that the depletion layer in proximity to the surface has grown and a steady state has been reached between the diffusive and convective mass transport of CRP to the cAbs areas and the binding of CRP to the cAbs.

Figure 6.5 shows a micromosaic immunoassay for CRP using CSs and stencil-deposited cAbs that results from using three lines of cAbs (120 μm wide stencils) and six CSs (30 μm wide reaction chambers). The flow rate in this assay was controlled entirely by the capillary pump, and no particular precaution had to be taken to prevent evaporation of the liquids added to the pads. The fluorescence intensity of the signals on each row was averaged and used to make a reference curve of for the assay. A total of six independent experiments were performed to obtain the reference curve shown in Fig. 6.5b. The calculated sensitivity of the assay (smallest concentration more than three times larger than the standard deviation of the zero analyte concentration) is 0.9 ng mL^{-1}, i.e. 7.8 pM. The coefficients of variation are < 8 % for concentrations ≤ 0.1 μg mL^{-1} and 12 to 15 % for smaller concentrations. The sensitivity of the CRP assay shown here is impressive considering that 1 μL of sample for multiple test areas, 11 min, and a conventional immunoassay format were used. This assay is notably fast, sensitive, and economical of sample compared with commercially available ELISA assays for CRP [131]. The sensitivity might be further improved by employing signal amplification strategies similar to the work by Hosokawa et al. [132] although this would be at the expense of making the assays longer, using more reagents, and adding numerous pipetting steps. PDMS has a refractive index of 1.47, is transparent and has a low autofluorescence for wavelengths below 600 nm [34]. It is therefore possible to measure the fluorescent signals of the mosaic directly through PDMS without having to remove PDMS from the CSs and drying the PDMS surface. Preliminary experiments showed similar relative intensity of fluores-

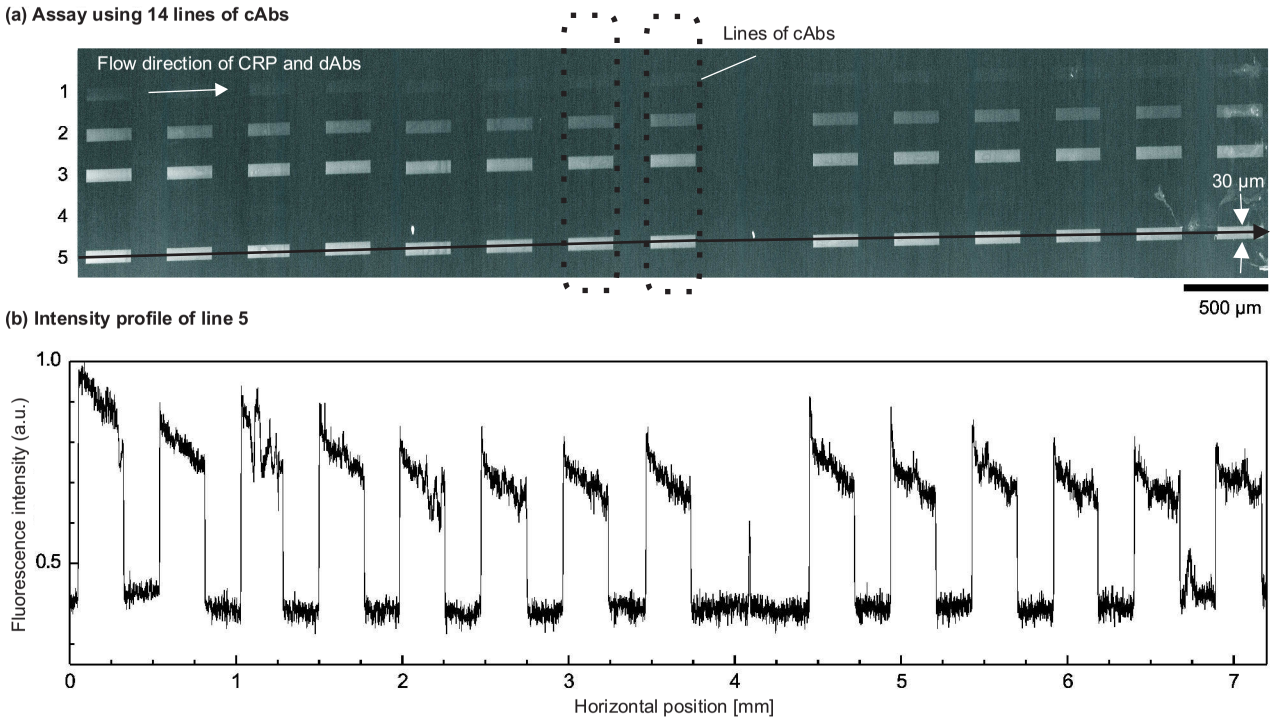

Figure 6.4. Micromosaic immunoassay for CRP performed in CSs and using cAbs patterned on PDMS through a stencil (a) patterned using a capture area having a total length of 3.7 mm and 14 lines of cAbs on PDMS. Optical micrograph showing the fluorescence signals of the assay where 14 lines of cAbs were crossed horizontally by CRP diluted in PBS and then FITC-labelled dAbs in PBS. The cAbs were deposited from solution onto PDMS using two concentrations (125 and 250 µg mL^{-1} on, respectively, the left 8 and right 6 columns). The CRP concentration was 0.04 (CS 1), 0.2, 0.5, 0, and 1 µg mL^{-1}. The concentration of dAbs was 250 µg mL^{-1}. (b) Fluorescence intensity profile of surface bound dAbs along the center of channel 5.

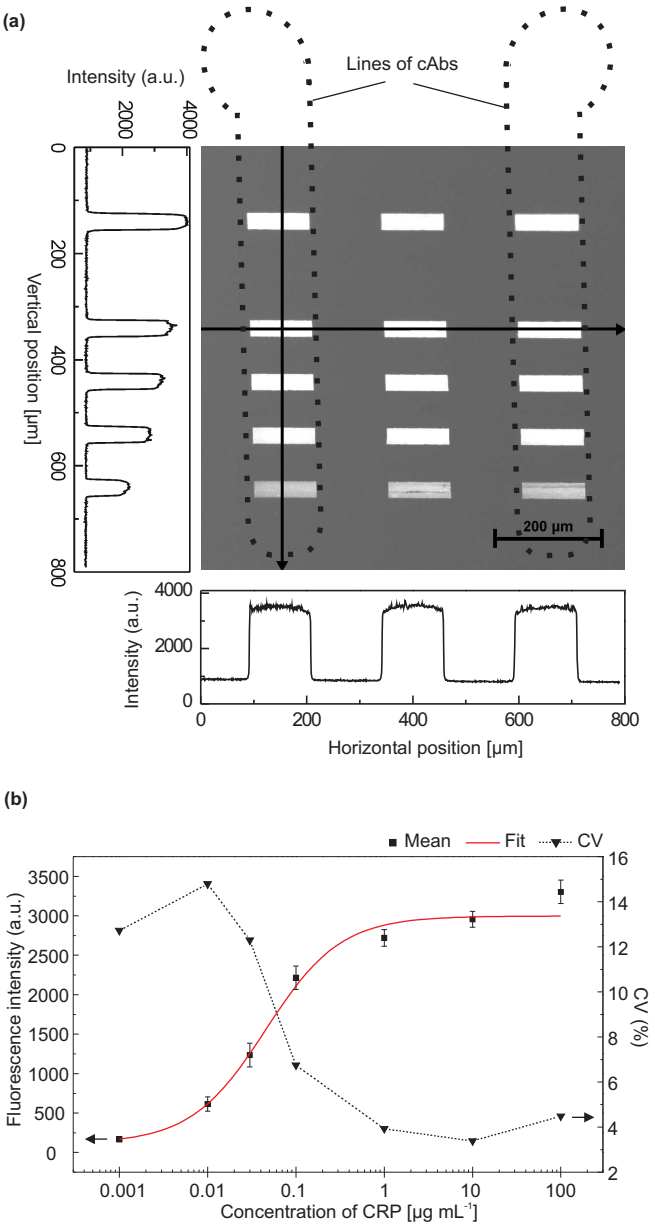

Figure 6.5. Micromosaic immunoassay and reference curve for CRP in human serum. (a) Optical micrograph showing a mosaic of fluorescence signals corresponding to the detection of CRP using cAbs (125 µg mL^{-1} in PBS) deposited onto PDMS using stencils. CRP spiked CRP-free human serum and FITC labelled dAbs (250 µg mL^{-1} in CRP-free human serum) were provided horizontally in independent CSs. The CRP concentration was 10 (top row), 0, 3, 1, 0.3, and 0.1 µg mL^{-1}. Each concentration of CRP results as a fluorescence intensity as can be seen in the vertical graph on the left. The horizontal intensity profile shows fluorescence intensity of a particular CRP concentration over different lines of cAbs. (b) The fluorescence intensities obtained from assays done with different concentrations of CRP (■) and their coefficient of variation (▲) are plotted. The fluorescence intensities are fitted with a sigmoidal curve (-). Error bars correspond to the standard deviation. This assay has a calculated sensitivity of 0.9 ng mL^{-1}. The line (···) is provided as a guide for the eye.

cence but less sharp images probably due to optical effects (data not shown), see Chapter 7. The in situ detection of CRP, and potentially many other markers, is nevertheless promising for further simplifying the use of CSs and encoding immunoassays on microfluidic chips for point-of-care diagnostics.

6.4. Conclusions

Stencil-based patterning of cAbs on a PDMS substrate is a convenient method to immobilize cAbs on PDMS in a manner that should be compatible with techniques used for the mass fabrication of diagnostic devices. We regard the accurate patterning of cAbs as key to achieving high-performance surface immunoassays that do not require complex or cumbersome peripherals, surface engineering, or signal-amplification methods. By following the examples provided here for stencils and CSs, we suggest that users interested in detecting antigens in microliters or less of samples should easily be able to set their own assays using standard reagents, pipetting methods, and fluorescence readers.

7. Autonomous Capillary System for One-step Immunoassays

Autonomous capillary systems (CSs), in which liquids are transported owing to capillary forces, have been previously used to perform fast and sensitive multi-step immunoassays using minute volumes of analyte. CSs for diagnostic applications have different requirements than CSs that are used as a research tool in life sciences, where a high flexibility and performance prevail over ease of use and portability. In this chapter,[1] a proof-of-concept for one-step immunoassays based on CSs is demonstrated. This proof-of-concept is based on preloading detection antibodies (dAbs) on the flow path of analytes and redissolving these antibodies to form dAb-analyte complexes, which can be detected using fluorescence downstream on accurately patterned capture antibodies (cAbs). A user therefore only needs to load a sample at the beginning of a CS and obtains the result of the assay using a conventional fluorescence microscope or scanner. As an example, c-reactive protein (CRP) was detected in human serum at clinical concentrations within 10 minutes and using only 2 μL of sample.

7.1. Introduction

Immunoassays are widely used for detecting analytes (antigens) for diagnostics [3], environmental monitoring [133], therapy monitoring [134], research in the life sciences and food safety [135], for example. Platforms for immunoassays differ widely, from clinical analyzers ran by expert staff to lateral flow tests used at home for pregnancy testing [3]. Novel platforms for immunoassays

[1] M. Zimmermann, P. Hunziker, E. Delamarche, Autonomous capillary system for one-step immunoassays, first published in *Biomedical Microdevices*, **11**, 1–8, **2009**.

are emerging with the advent of miniaturization and microfluidics in which multiple functions, such as metering and preprocessing of a sample, analysis, recording and calibration of the results, can all be done on a portable platform [136, 137]. We are interested in applying the concept of autonomous CS to the detection of disease markers for point-of-care testing of patients, with the ultimate goal of detecting a few related disease markers in less than approximately 10 min, with 2 μL of sample or less, and with only one step of handling. Another important goal is to devise a flexible approach where the volume of sample, the number of analytes to be detected, and the flow conditions of the assays can easily be adjusted by only a minor redesign of the CS.

Ideally, for point-of-care diagnostics, the handling of a CS should be as simple as it is for pregnancy tests [138] or for glucose measurements for diabetes management [139]. Immunoassays that provide results within minutes outside of a clinical laboratory are based on lateral-flow, flow-through, agglutination, or solid phase technology. Lateral-flow tests, also called immunochromatographic strip tests, are used for qualitative or semi-quantitative detection of analytes in a body fluid. Lateral-flow tests only require the addition of the sample. With flow-through tests, the analytes and solutions for washing and detection can be flown sequentially through a porous membrane or, in modern tests, through a channel. The latest versions of such flow-through tests all have the reagents integrated on-chip [140]. In agglutination tests, the sample is placed on a substrate and analytes are detected following the binding of analytes with colored particles having analyte-specific receptors. Point-of-care agglutination tests can therefore hardly be miniaturized nor can they have integrated reagents. Solid phase tests have cAbs immobilised on a non-porous substrate, are dipped into the analyte, and then into solutions for washing and detection. Solid-phase tests in general have less sensitivity for detection of antigens than lateral-flow tests do. All of the tests described provide fast, qualitative or semi-quantitative measurements of analytes in resource-poor environments at a moderate price.

Testing of multiple parameters from the same drop of sample might be desirable for precise diagnostic of myocardial infarction, for instance, where cardiac troponin, CK-MB, and myoglobin are of interest [32]. These three markers

can be qualitatively measured on a single chip, but the chip in fact has two qualitative lateral-flow tests integrated into a single chip having two openings for the blood sample, both of which need to be filled [141]. Quantitative flow-through assays can be performed on-chip for each of the cardiac markers in combination with portable reader instruments [8, 9]. The chips are assembled using a filter membrane for filtering cells from the blood plasma in front of a microfluidic channel and contain all the reagents. The reagents might be embedded in the filter membrane [140] or in a cavity [142] from where the reconstituted reagents are delivered within a certain time span. The markers are detected in separate chips using gold-labelled immunochemistry assays [8], or immunofluorescence assays [9]. Quantitative results are typically obtained within 15 minutes from 150 μL of sample volume.

Other platforms in which immunoassays could be performed to detect multiple parameters and that might be suitable for point-of-care are the Lab-CD [143], T-sensors [144, 145], and structurally programmable microfluidic system (sPROMs) [104]. Lab-CDs are used in a CD-reader-type instrument, can pre-process samples by centrifuging them, and can have multiple immunoassays integrated [143]. But complex and large rotational forces are critical and make CDs that have biological reagents integrated difficult to fabricate. T-sensors need to have active pumps for controlling the flow rates of liquids [144], and sPROM devices have pressurized air chambers integrated that are electrically activated for driving the liquid through the channel system [104].

7.2. The One-step Concept

A CS is an ensemble of connected microstructures in which one or multiple liquids are displaced by means of capillary forces. Key elements of a CS are the sample loading interface, the reaction chamber inside which the immunoassay takes place and the signal is measured, and the capillary pump, which draws the sample at a programmed flow rate. CSs are well suited for performing fluorescence sandwich surface immunoassays when they are sealed with a PDMS cover onto which cAbs have been patterned. In this case, independent reaction chambers can be defined and/or different types of cAbs can be used simultaneously for detecting several of antigens from one sam-

ple. The small dimensions of the CS structures make paths for diffusions short and rinsing steps very efficient owing to the laminar flow of liquids at low-Reynolds-number flow.

The concept of a one-step immunoassay using a CS is sketched in Fig. 7.1. The CS contains the pair of antibodies (cAbs and dAbs) needed to effect a surface sandwich immunoassay. After loading a sample into a CS, the microstructures of the CS determine the flow rates and incubation times needed to (i) dissolve dAbs and reconstitute them in solution, (ii) form the dAb-analyte complexes, (iii) move and bind the dAb-analyte complexes to the surface-immobilized cAbs, and (iv) rinse excess dAbs using some of the sample in which no dAbs dissolved. The fluorescence signal corresponding to the cAb-analyte-dAb complex can then be measured using a fluorescence reader or microscope. The assay time for such a one-step assay is predefined at the time of manufacturing of the CS by defining the hydraulic resistance and wetting properties of the structures. Some functional elements for preprocessing the sample as well as reagents for control purposes can be added [140]. A membrane for filtering cells and particulates can, for example, be stacked at the beginning of the CS [146]. Alternatively, microstructures in the CS can be used to filter samples such as blood [147]. The time needed for preprocessing the sample, reconstituting the dried dAbs, and binding them to analyte molecules in the sample are ideally kept short while the step of binding dAb-analyte complexes to cAbs is kept sufficiently long to improve the sensitivity of the assay.

7.3. Experimental

The microfluidic CSs were fabricated using photolithography, deep reactive ion etching, and silicon wafers. The etched wafers were sputtered with 10 nm Ti and 150 nm Au, and then diced to yield individual microfluidic chips each having six independent CSs. The CSs are 180 μm deep, except the reaction chambers, which are only 20 μm deep. The reconstitution chamber is a 60 μm wide microchannel and large enough for 2 μL solution of proteins. We have also fabricated shallow, 30 μm deep reconstitution chambers for 0.3 μL, but unless indicated otherwise, the deep ones were used. The capillary pumps were

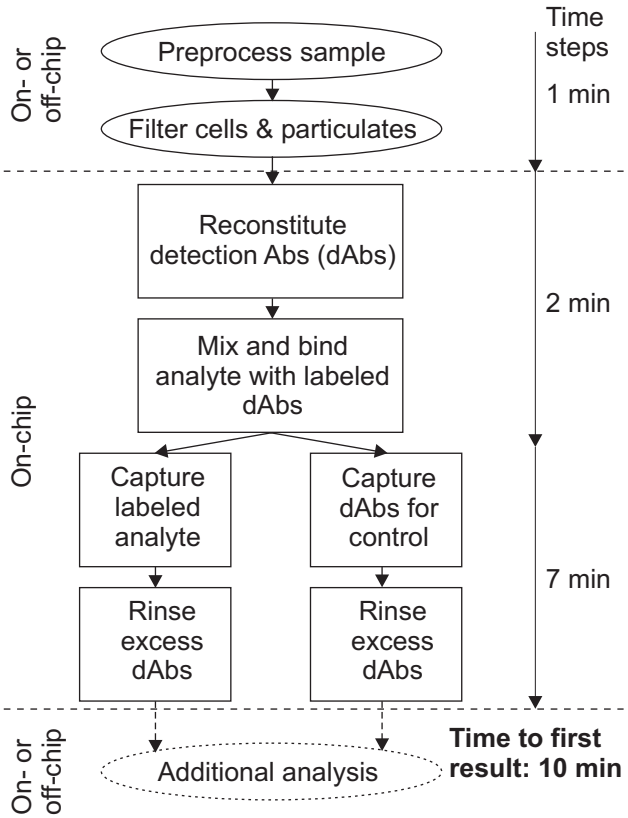

Figure 7.1. Concept of a one-step assay using a microfluidic CS.

designed for pumping 2 µL of liquid and have a vent to prevent compression of air when the CSs are sealed. The reaction chambers were designed a few millimeters away from the rest of the CS to allow the manual alignment of 2 mm long lines of capture antibodies on PDMS orthogonal to the reaction chambers, as discussed in Chapter 6.

The Au surface was cleaned in a UV-ozone chamber (UV-Ozone Photoreactor PR-100, Ultra-Violet Products, Upland, CA) for at least 20 min. PDMS stamps (Sylgard-184, Dow Corning, Midland, MI) approximately as large as the microfluidic chips were coated with a 2 mM ethanolic solution of hexadecanethiol (52270, Fluka, Buchs, Switzerland) for 30 s, rinsed with ethanol, and blown dry under a stream of N_2. A UV-cleaned microfluidic chip was then microcontact printed with the inked PDMS stamp for 30 s to make the top Au surface of the chip hydrophobic. A 2 mM ethanolic solution of thiolated poly(ethylene glycol) (HS-PEG 12750-4, Rapp Polymere, Tübingen, Germany) was placed on the microfluidic chip for 30 s to make the Au-coated walls of the CSs hydrophilic. The microfluidic chips were rinsed with ethanol and dried under a stream of N_2.

Detection antibodies (CRP-C6, HyTest, Turku, Finland) labelled with Alexa-647 (Labelling kit A-20186, Molecular Probes) were prepared in a 60 mM solution of D(+)-trehalose (90208, Fluka, Buchs, Switzerland) containing 20 mg mL^{-1} L-phenylalanine (78020, Fluka). For quicker dissolution and reconstitution of the lyophilisate, the solution of dAbs was diluted by a factor of 2 for some experiments. Chips were either not sealed at all or partially sealed with a 1–2 mm thick layer of cured PDMS. The solution was pipetted into the six CSs of the microfluidic chip and, after it had flown in the microchannels, immediately frozen at -18 °C or -196 °C. A Petri dish was filled with dry ice (-78 °C) onto which the frozen microfluidic chips were placed. The Petri dish was put into a second, larger Petri dish and loaded into a freeze-dryer (Alpha 1-2, Martin Christ, Osterode am Harz, Germany). Alternatively, the frozen chips were put on a metal block cooled to -18 °C. Open CSs were freeze-dried for 24 h; sealed ones for 2–3 days. After taking the box containing the chips out of the freeze-dryer, the box was sealed with tape and left for at least 30 min until it reached room temperature. Microfluidic chips were typically used within half a day after they had been taken out of

the freeze-dryer. Freeze-dried dAbs were observed in a scanning electron microscope (SEM) (LEO 1550, LEO Electron Microscopy Inc., Thorwood, NY). The PDMS on sealed CSs was removed prior loading the CSs into the SEM. Some minor fractions of lyophilisate stuck to the PDMS and were pulled out of the CSs.

Capture antibodies (CRP-C2, HyTest, Turku, Finland) were patterned as 2-mm-long lines on a layer of PDMS, which was cured in a Petri dish and cut to the size of the microfluidic chips. The PDMS surface was then blocked with bovine serum albumin (A7906, Sigma), rinsed with deionized water, dried under a stream of N_2, and stored in a dry Petri dish containing a dessicant ($CaCl_2$) until it was placed over the CSs of a microfluidic chip having freeze-dried dAbs. The lines of cAbs on the PDMS surface were aligned orthogonally to the reaction chambers of the CSs, and the entire CSs were sealed except for the loading pads. The CSs were used within 1 h after sealing with PDMS. Human serum spiked with CRP was pipetted into the loading pads. The redissolution of the dAbs and reconstitution in the human serum was observed using a fluorescence microscope (Eclipse 90i, Nikon, Tokyo, Japan), which was equipped with a 100 W halogen lamp for fluorescence excitation and a digital camera (DS-1QM, Nikon) for imaging. To prevent evaporation of the sample from the loading pad, the chip was observed in a humidified chamber.

7.4. Results and Discussion

We focus in a first step on a method to deposit dAbs in a CS and to reconstitute them in a sample, and then verify that CRP, a non-specific marker for inflammatory responses, [122] can be detected from human sera with a clinically relevant sensitivity. Figure 7.2 shows the layout of a typical CS for a one-step immunoassay. A main loading pad having a maximum capacity of 2 μL starts the CS and is connected to a reconstitution chamber. This chamber holds dAbs (in dry state) and is connected to (i) a reaction chamber sealed with a PDMS slab having lines of cAbs and (ii) an overflow chamber, which is connected to a secondary pad. The functional elements of this CS have a defined capillary pressure P_i, and a liquid moves spontaneously from a zone with a low capillary pressure (absolute value) to a zone of higher cap-

illary pressure. A strategy for depositing dAbs in the flow path of the sample is depicted in Fig. 7.2b. A solution containing dAbs is added to the secondary pad, from where it flows preferentially through the reconstitution chamber to some extent toward, but not into, the main pad because $|P_1|$, $|P_2| < |P_3|$, $|P_4|$. The reconstitution chamber is the zone exerting the highest capillary pressure and therefore fills preferentially at the expense of the other structures; it has a total volume of 2 µL. The overflow chamber has the purpose of accommodating the volume fraction of solution of dAbs that exceeds the volume of the reconstitution chamber. This ensures having a controlled and reproducible amount of dAbs preloaded into the reconstitution chamber of the CS. Only proteins preloaded in the reconstitution chamber finally reach the reaction chamber. The interplay between the reconstitution and the overflow chamber acts as a metering unit, leading to an estimated accuracy of the aliquot of dAbs, which will be reconstituted, of better than ±5 nL. The typical error of ±4 % or ±80 nL for micropipetting by hand a volume of 2 µL is in comparison much larger. The reconstitution and the overflow chamber have the shape of a meandering channel to minimize their footprint on the chip while keeping flows laminar and preventing having structures with dead volumes.

A sample placed in the main pad flows through the reconstitution chamber, where dAbs dissolve and bind to analytes, Fig. 7.2b. The dAb-analyte complexes flow to the reaction chamber and bind to specific cAbs. Detection Abs are in excess compared with the analyte molecules and reconstitute in only a fraction of the volume of sample. Free dAbs are therefore rinsed away from the zones with the cAbs, similarly to how immunoassays in lateral flow tests are performed. An external fluorescence reader excites the fluorescent dyes conjugated to the dAbs and measures the emitted fluorescence, which relates to the concentration of analyte in the sample. The capillary pump at the end of the CS holds at least 2 µL of liquid, determines the flow rate of most of the liquid flowing through the CS, and has a venting structure at its end. We found it convenient to load the solution of dAbs to the secondary pad to determine the best conditions for depositing the dAbs to the chip (volume, composition of the solution, and concentration of dAbs). The dAb solution can also be added directly to the main pad. In this case, an overflow chamber is required if the volume of the dAb solution exceeds the total volume of the

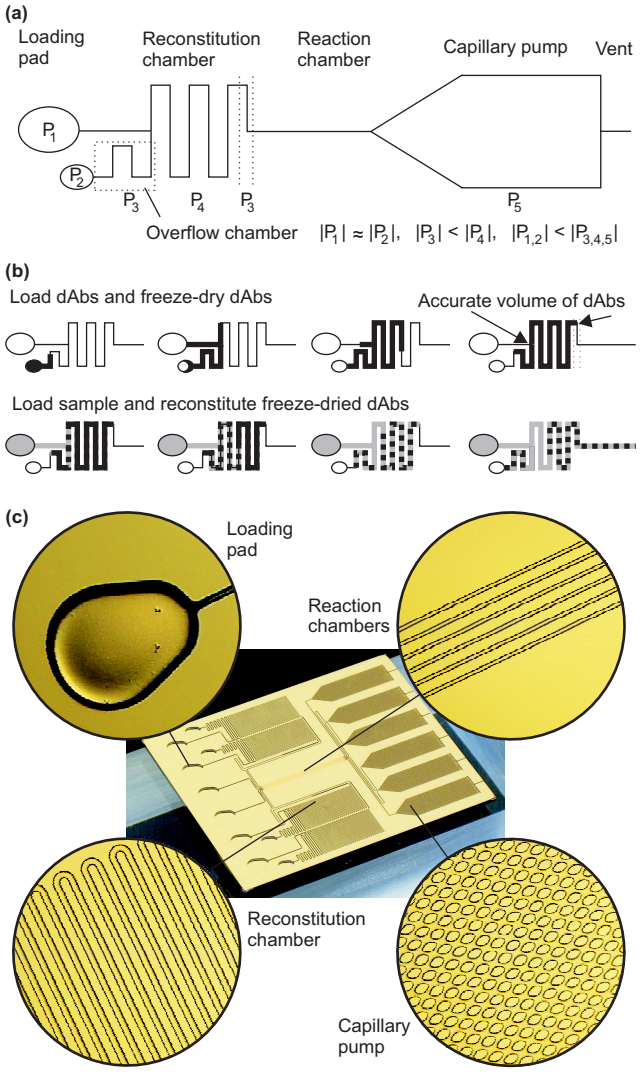

Figure 7.2. (a) Scheme of a one-step CS. (b) Scheme showing the filling procedure and metering of dAbs and sample, and the reconstitution and mixing of dAbs with sample. (c) Optical micrographs of a microfluidic chip in Si having six one-step CSs, two of which (the middle ones) have no overflow chamber and a very small reconstitution chamber. The chip is 28 × 22 mm^2 and is covered with Au, with the top surface beeing hydrophobic and the inner surface of the microstructures being hydrophilic.

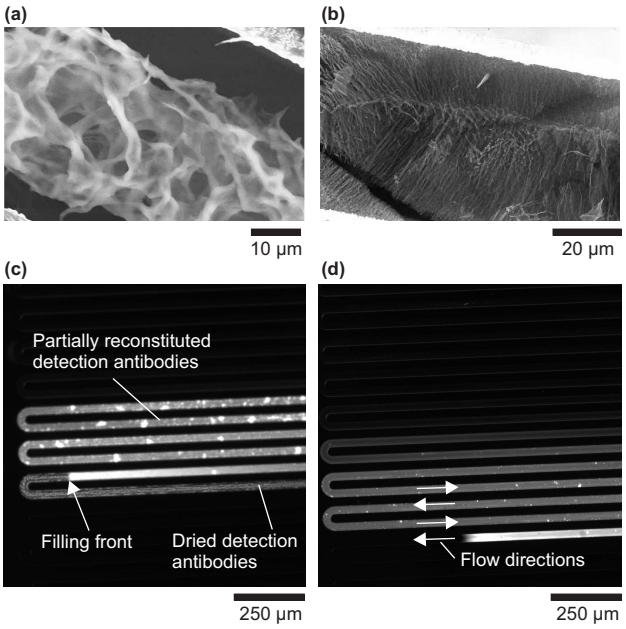

Figure 7.3. SEM images (a), (b) and optical fluorescence micrographs (c), (d) of dAbs, trehalose, and phenylalanine in microchannels of a reconstitution chamber that were frozen (a) at -18 °C and (b) at -196 °C and freeze-dried. Detection antibodies as shown in (b) are redissolved and reconstituted in human serum (c) 8.25 min and (d) 9 min after loading the human serum into the loading pads of the CS.

microfluidic elements between the main pad and the reaction chamber. The microfluidic chip shown in Fig. 7.2c possesses six independent CSs, four of which have an overflow chamber and secondary pad, as sketched in Fig. 7.2a. The meandering microchannels located before and after the reaction chambers act as hydraulic resistors to give all CSs an equivalent hydraulic resistance. The reaction chambers on this chip are microchannels with a crossection of $30 \times 20\ \mu m^2$ (width $\times$ depth) and a length of 9 mm. These microchannels run parallel in a region of the chip where a PDMS block having lines of cAbs would normally be present during an assay.

7.4.1. Predeposition and reconstitution of labelled detection antibodies

Besides the amount of dAbs preloaded on the CS, the volume of sample in which the dAbs reconstitute is key for obtaining reproducible and sensitive

assays. Figure 7.3 shows a lyophilisate containing dAbs that was dried in a CS and the reconstitution of dAbs in a stream of human serum advancing in the reconstitution chamber. The dAbs were freeze-dried in a matrix of phenylalanine and trehalose, which is frequently used for preserving the activity of dried proteins for months [148, 149]. Phenylalanine crystalizes when it freezes [150] and forms a scaffold covered by a layer of trehalose [148]. The reasons for the preservation effect of trehalose and other sugars are still beeing discussed in literature [151]. The most common complementary hypotheses are the water substitution model [152] and the glassy state model [152, 153]. The water substitution model suggests the stabilization of antibodies via the formation of hydrogen bonds with free hydroxyl-groups of the trehalose for example. The glassy state model suggests the formation of a glass in which the proteins are immobilized and thereby have their reaction kinetics of degradation and denaturation highly retarded.

We used a volume of 0.5 µL and a concentration of 125 µg mL^{-1} dAbs in 60 mM trehalose and 20 mg mL^{-1} phenylalanine to ensure that dAbs would be present at least in a 10 fold excess of CRP at a high concentration range in clinical samples without using too a large microfluidic volume element of the CS. Key steps for the deposition of the dAbs were to pipet the dAbs solution into a main pad of each CS, freeze the chip and the reagents, and then freeze-dry the chip and reagents overnight.

Figure 7.3a shows a lyophilisate of the dAb solution, which was frozen at -18 °C. The lyophilisate is not distributed equally in the cross section of the channel. Freeze-concentration occurred while the liquid was beeing frozen [154, 155]. Approximately one quarter of the cross section of the microchannel is not filled with the freeze-dried material. Thus reconstitution of the dAbs suffers from the entrapment of numerous gas bubbles. Lowering the temperature to -196 °C increases the speed of freezing the reagents and results in a finely structured lyophilisate, Fig. 7.3b. The small pore size of the lyophilisate results in general in a slow drying process [148] but because of to the large surface-to-volume ratio of the small quantities and the overnight drying, no difference was observed. The micrographs in Fig. 7.3c and d show the redissolution and reconstitution of a lyophilisate in human serum. This lyophilisate was prepared using a 150 nL solution of dAbs. The

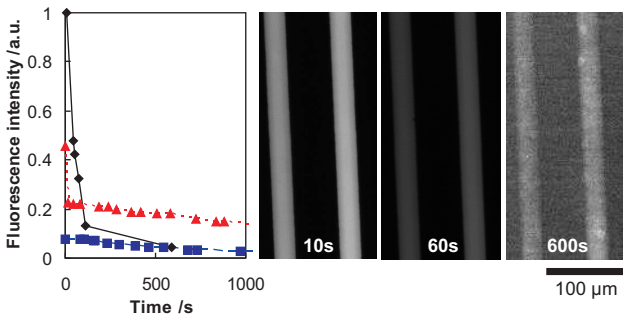

Figure 7.4. Time dependence of the relative concentration of labeled dAbs measured at the entrance of the 20 µm deep reaction chamber of a CS. The three intensity series shown in the graph correspond to volumes of freeze-dried detection antibody of 0.15 µL in a 30 µm deep reconstitution chamber (◆), 0.15 µL and 0.5 µL in a 180 µm deep reconstitution chamber (■, ▲), which were redissolved and reconstituted in human serum. The optical micrographs show the fluorescence intensity corresponding to dissolved dAbs (◆) flowing in the reaction chamber. The exposure time was 50 ms.

dAbs in Fig. 7.3c are almost completely wetted after 8.25 min and partially redissolved. Some fragments of the dAb-phenylalanine-trehalose complex are visible in the image, and the filling front moves at a rate of approximately 0.15 mm s^{-1}. The filling front accelerates to ∼0.5 mm s^{-1} as soon as it reaches the end of the lyophilisate. All fragments are dissolved, and the dAbs are reconstituted in ∼50 nL of human serum at a concentration of ∼375 µg mL^{-1} 45 s later, Fig. 7.3d. For the highest concentration of 3 µg mL^{-1} CRP used here, dAbs were >100× in excess. During and shortly after the reconstitution step, dAbs bind to analytes present in the sample and the analyte-dAb complexes proceed to the reaction chamber. Typically, solutions of 0.15 µL (0.5 µL) of dAbs that were put into 180 µm deep and 2 µL large reconstitution chambers reconstituted in human serum in a volume of 0.3 µL (1 µL).

The flow rate and volume of solution containing the dAb-analyte complexes define the incubation time for capturing the complexes in the reaction chamber. We therefore monitored the fluorescence intensity of a solution of reconstituted dAbs passing at the entrance of the reaction chamber, Fig. 7.4. Timing of the measurements started when the solution entered the reaction chamber. In a first experiment, dAbs were deposited on the CS using a volume of 0.15 µL of dAb solution and a 30 µm deep reconstitution chamber. The flu-

orescence intensity corresponding to the dissolved dAbs decayed to less than 5 % of the initial intensity after the serum had been flowing for 600 s. Increasing the depth of the reconstitution chamber to 180 µm significantly reduced its hydraulic resistance and accelerated the flow of solution of dAbs at the entrance of the reaction chamber. In this case, dAbs were reconstituted in a larger volume of human serum. The fluorescence intensity corresponding to dAbs passing at the entrance of the chamber initially decayed to below 10 % of the maximum intensity in 30 s when 0.15 µL of solution of dAbs were used. The fluorescence intensity decreased slowly to ∼2 % after 1000 s. Depositing 0.5 µL of dAbs in a similar reconstitution chamber significantly increased the time needed to pass the dAbs through the reaction chamber: the fluorescence diminished to 25 % of the maximum intensity in 30 s but remained as high as 14 % after 1000 s.

7.4.2. Functionality of the reconstituted detection antibodies

The experiments described above show that reconstitution chambers and volumes of dAbs can be varied to obtain a short or long-lasting flow of dAb-analyte complexes through the reaction chamber. The next experiments focus on one-step assays for CRP in which 2 µL and 0.15 µL large reconstitution chambers have been used. In both cases, the depth of these chambers was 180 µm, and 0.15 µL of solution of dAbs was deposited and freeze-dried in these chambers. The 0.15 µL reconstitution chambers essentially correspond to the flow resistor and connecting channel placed between loading pad and reaction chamber. CSs having such reconstitution chambers were directly designed to hold 0.15 µL of dAbs solution and were not appended to an overflow or secondary pad.

CRP-free human serum that was spiked with CRP (1 and 3 µg mL^{-1}) was directly loaded into the loading pad of these CSs. The transparency and low autofluorescence of PDMS for the excitation and emission wavelengths used for Alexa-647 allow the fluorescence signals to be measured over the capture areas through the PDMS substrate. Fig. 7.5 shows the surface-bound and free analyte-dAb complexes in the reaction chambers 10 and 25 min after loading

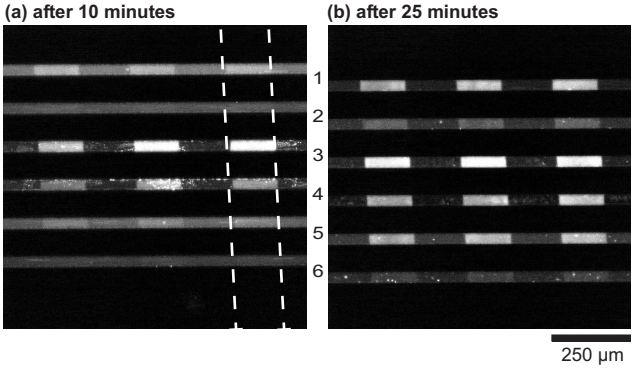

Figure 7.5. Optical fluorescence micrographs of the reaction chamber of a one-step chip in which a CRP immunoassay was performed. Capture antibodies were patterned on PDMS as three vertical lines, indicated by dashed lines in (a), and crossed horizontally by six reaction chambers in which the CRP-dAbs complexes were flowing. The six lines had alternating concentration of 3 and 1 µg mL^{-1} CRP. Imaging the reaction chamber (a) 10 min and (b) 25 min after the sample was injected into the loading pad of the CSs illustrates how signal originates in the areas of PDMS having cAbs. The exposure time was 50 ms.

the samples. Human serum reached the reaction chambers of CSs 3 and 4, which had 0.15 µL reconstitution chambers, after a few seconds, whereas it took approximately 8 min for the other CSs. Within 10 min, the binding reaction was completed and a larger fraction of unbound dAbs had been washed out of the reaction chamber. Both analyte concentrations of 1 and 3 µg mL^{-1} could be detected. The incubation time in reaction chambers 1, 2, 5 and 6 was 2 min and only the high concentration of CRP could be detected within 10 min of loading the sample. In these CSs, the background signal from unbound dAbs in the reaction chamber was still high, but 15 min later the binding reaction had proceeded and concentration of unbound dAbs had decayed such that also the concentration of 1 µg mL^{-1} could be detected, Fig. 7.3b.

These results suggest that for the concentrations used here a small reconstitution chamber and a high flow rate provide faster results, mainly because the analyte needs less time to reach the reaction chamber where it is captured. Nevertheless, for smaller concentrations that required longer incubation times, the CSs having larger reconstitution chambers and slow flow rates might be better.

7.5. Conclusions

CSs enabling one-step immunoassays reduce the handling overhead of the end-user from several pipetting step to a single one. Due to the small footprint of these CSs, several CSs might be integrated one a single chip to perform different assays in parallel. Multiple CSs can in principle be connected to one loading pad and be linked to various reconstitution chambers, the geometries of which can be used to optimize the time needed for reconstituting the dAbs and binding dAbs to analytes for a given concentration of analyte. Alternatively, different types of dAbs can be positioned on independent flow paths for performing multiplexed assays and for minimizing the risk of cross reactivity between dAbs and cAbs. Besides performing independent assays in parallel CSs, several assays may be performed in one CS exposing analytes to different, patterned cAbs. Pipetting robots or inkjet printers, which are able to dose small volumes of solution of dAbs into reconstitution chambers, should prove valuable for preparing CSs for fast analysis. The work presented here suggests that the performance characteristics of CSs that we previously reported, i.e., small volume of samples and reagents used, highly integrated signals, multiplexed and fast assays, can also be achieved with one-step immunoassays.

8. Valves for Autonomous Capillary Systems

Autonomous capillary systems (CSs), which are microfluidics inside which liquids move owing to capillary forces, can in principle bring the high-performances of microfluidic-based analytical devices to near patient and environmental testing applications. In this chapter,[1] we show how wettable capillary valves can enhance CSs with novel functionalities, such as delaying and stopping liquids in microchannels. The valves employ an abruptly changing geometry of the flow path to delay a moving liquid filling front in a wettable microchannel. We show how to combine delay valves with capillary pumps, prevent shortcuts of liquid along the corners of microfluidic channels, stop liquids filling microchannels from a few seconds to over 30 min, trigger valves using two liquid fronts merging, and time a liquid using parallel microfluidic paths converging to a trigger valve. All together, these concepts should add functionality to passive microfluidics without departing from their initial simplicity of use.

8.1. Introduction

Microfluidics have become increasingly used as high-end bio-analytical research platforms [156, 157, 158], portable diagnostic devices [137], and in many other applications [159, 160]. In general, microfluidics tend to be complex compared to non-miniaturized bio-analytical instruments and they incorporate functional elements such as pumps, flow resistances, and valves for controlling the flow of liquid. We have developed microfluidic autonomous

[1] M. Zimmermann, P. Hunziker and E. Delamarche, Valves for autonomous capillary systems, first published in *Microfluidics and Nanofluidics*, **5**, 395–402, **2008**.

capillary systems (CSs) for performing miniaturised surface immunoassays for both research and diagnostic applications [33, 49]. A CS comprises at least a loading pad, a reaction chamber and a capillary pump, wherein liquids move owing to capillary forces. We recently reported the concept of advanced capillary pumps for encoding the displacement of defined volumes of liquids with various flow rates in CSs for optimising the individual steps of an immunoassay, Chapter 5. In this chapter, we show how to enhance CSs with more functionalities and valve-based actuation principles focusing on passive valves for the control of liquids filling wettable CSs.

Valves are functional elements that are used to control the flow of a liquid. A large number of different valves are commonly used in microfluidics [161] and they are either actuated or non-actuated. Actuated valves usually have moving parts and use electrostatic, electromagnetic, pneumatic, hydraulic or thermal power to open or close [161]. These valves are most suitable for repeated dosing of the same liquid, controlling pressurised liquids, or for pumping liquids [51]. Typically non-actuated valves having moving parts cannot be opened or closed without changing the geometry of flow paths such as with check valves, pressure control valves or flap valves. The most interesting valves for combination with CSs are non-actuated valves that have no moving parts such as hydrophobic valves [20, 162], diffuser valves [163], phase change valves [117], and capillary valves [164, 165, 166, 167, 168], for example. These valves are for single use: they influence how a liquid fills the region of the valve but not how a liquid afterward flows through the valve. Capillary valves can, in principle, withstand pressures in the order of 10 kPa [164, 169]. Melin et al. have demonstrated wettable capillary valves for fluidic AND-gates, but suction at the valve outlet had to be applied in order to release the valve after the valve inlets were filled [170]. Passive microfluidic logic gates can also be based on the surface tension of bubbles moving in a liquid [171] or liquid droplets [172]. Actuated valves that have no moving parts such as electrowetting-based valves [173] might also be integrated in CSs, but require additional fabrication steps and electric circuits to operate the valve which might be costly for ultimately disposable CSs.

The passive valves used in this paper, referred to as “valves”, are non-actuated, do not have moving parts, but instead capillary forces propel or stop

liquids filling these valves. These valves can be integrated seamlessly into CSs and combined with different capillary pumps. A liquid pipetted into a loading pad of a CS typically flows into the CS until the loading pad becomes empty or the CS becomes filled [33]. Sequential pipetting of multiple reagents allows to perform surface immunoassays in such CSs [34, 35]: different geometries in a CS can tailor the flow rate of the liquid to optimise the conditions for the different steps of the immunoassay, Chapter 5, but realizing a stop-and-go flow is challenging. We present implementations of valves enabling such functionalities.

8.2. Principle

The capillary pressure propelling liquids in wettable CSs originates from the contact angle of liquids to the surface of CSs and the curvature of the meniscus at the liquid-solid-gas interface (filling front) of the liquids in CSs. Valves alter the curvature of the meniscus and in doing so the capillary pressure in the liquid. The filling front can slow down or even stop depending on how strong the meniscus is varied. The pressure barrier in such valves can be estimated based on the total interfacial energy of the liquid-solid-gas interface system. Energy changes at the interface modulate the capillary pressure and thus the filling rate of a liquid in valves. The capillary pressure P in a liquid flowing in a CS is [164]

$$P = -\frac{\delta E_{\mathrm{T}}}{\delta V_{\mathrm{l}}} = \gamma_{\mathrm{la}}(\cos\Theta_{\mathrm{c}}\frac{\delta A_{\mathrm{sl}}}{\delta V_{\mathrm{l}}} - \frac{\delta A_{\mathrm{la}}}{\delta V_{\mathrm{l}}}) \tag{8.1}$$

with the total interfacial energy E_{T} of the capillary system, the volume of liquid V_{l} in the CS, surface tension γ_{la} and the area A_{la} of the liquid-air interface, contact angle Θ_{c} of the liquid with the walls of the CS, and the wetted surface area A_{sl} of the CS. The curvature of the meniscus in a straight channel is $\alpha = \frac{\pi}{2} - \Theta_{\mathrm{c}}$. At an abrupt enlargement having an angle β between the old and new direction of the microchannel wall, the meniscus changes its curvature in order to achieve the equilibrium contact angle. The curvature disappears for $\beta = \frac{\pi}{2} - \Theta_{\mathrm{c}} = \alpha$ and the capillary pressure drops to $P = 0$. For larger β the curvature becomes negative and the sign of P changes. The pressure barrier ΔP for a 2-dimensional valve (depth $\gg$ width) can be

calculated to [164]

$$\Delta P = \frac{2\gamma_{\mathrm{la}}}{w}\left(\frac{\cos\Theta_{\mathrm{c}} - \frac{\alpha}{\sin\alpha}\sin\beta}{\cos\beta + \frac{\sin\beta}{\sin\alpha}\left(\frac{\alpha}{\sin\alpha} - \cos\alpha\right)}\right) \tag{8.2}$$

with the width w of the meniscus in the valve. Using this equation Man et al. determined the pressure barrier ΔP to be in the order of ∼10 kPa for water ($w = 5$ µm, $\Theta_{\mathrm{c}} = 20°, \beta = 90°$) [164].

8.3. Experimental

The valves were fabricated in silicon using photolithography and dry etching. A photoresist was exposed through photoplotted polymer masks (Selba S.A., Versoix, Switzerland) with a resolution of 25400 dpi (minimum feature size ∼10 µm) and laser written soda lime chrome masks (Delta Mask V.O.F., Enschede, Netherlands) with a minimum feature size of 1.5 µm. The polymer masks were used for delay valves and chrome masks for stop valves. A deep reactive ion etcher (STS ICP, Surface Technology Systems plc. Newport, U.K.) was used to etch the valves 30 and 60 µm deep in silicon. After removal of the photoresist, the wafers were coated with Ti (10 nm) and Au (150 nm), and then diced to produce individual chips having each 11–24 valves connected with loading pads large enough for pipetting.

Before testing valves on a chip, the Au surface of the chip was cleaned in a UV-ozone chamber (UV-Ozone Photoreactor PR-100, Ultra-Violet Products, Upland, CA) for at least 20 min after the lamps had warmed up. The chip was then immersed for 2 min in a 2 mM ethanolic solution of thiolated poly(ethylene glycol) (HS-PEG 12750-4, Rapp Polymere, Tübingen, Germany) to make the Au surface hydrophilic. The chips were then rinsed with ethanol and blown dry under a stream of N_2. The resulting Au surface had an advancing contact angle of 40° with deionised water, which was coloured with a food colorant (Werna W. Schweizer AG, Wollerau, Switzerland). A 1–2 mm thick layer of cured PDMS (Sylgard-184, Dow Corning, Midland, MI) was used to seal the valves.

The valves were tested within 30 to 90 min after derivatization of their surface and sealing with PDMS. Coloured deionised water and coloured human

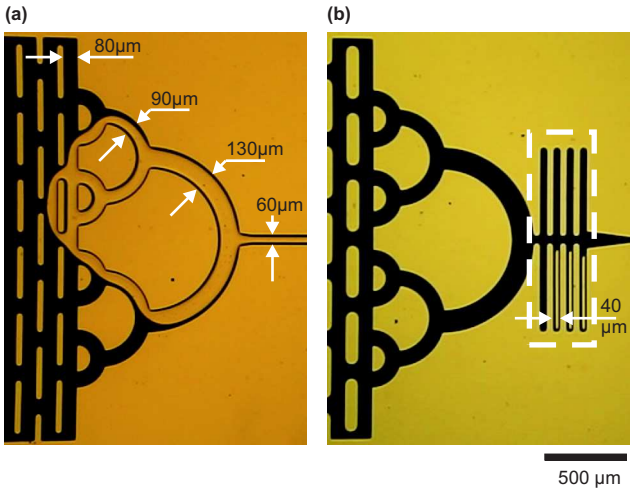

Figure 8.1. Optical micrographs showing how a liquid arriving at the end of a capillary pump can be collected into one output microchannel. (a) The merging of smaller channels into larger ones defines delay valves, the purpose of which is to gradually collect a liquid at the end of a pump. (b) Adding a resistance (outlined by the dashed rectangle) further reduces the risks of having liquids wetting walls and short cutting programmed microfluidic paths.

serum were used as liquids in this chapter. To prevent evaporation of liquid from the loading pads, the chips with the sealed valves were placed in a humidified chamber. The chamber was briefly opened to pipette liquid into the loading pads. The performance of the valves was determined based on the time until the valve released the liquid. The filling of liquids in the valves was observed using a stereomicroscope (MZ16, Leica) and a microscope having a 10× objective (Eclipse 90i, Nikon) equipped with digital photo and video cameras (DCR-SR100E, Sony and DXM 1200C, Nikon).

8.4. Results and Discussion

The three functionalities that we want to integrate into CSs using valves are preventing shortcut of liquids along the edges of microfluidic structures and at the end of capillary pumps in particular, delaying a filling front, and stopping a flow in wettable microfluidic elements.

8.4.1. Delay valves

Fig. 8.1 shows valves for merging a wide filling front of liquid exiting multiple microchannels into a single microchannel. Such delay valves retard one of at least two filling fronts by increasing the size of the meniscus of the filling front and thereby reducing its capillary pressure. A delay valve changes the ratio of flow rates of two parallel flow paths. The velocity of a filling front in a wide microchannel is lower than a filling front moving in a narrow microchannel. The menisci of the filling fronts in Fig. 8.1a move from a region of high capillary pressure (width of microchannel 80 µm) into regions of reduced capillary pressure (width of microchannel 90 and 130 µm). A single meniscus proceeding through one of the delay valves gets retarded in its progression until it merges with an adjacent filling front. Delay valves can be added in a serial and parallel configuration to occupy a small footprint as shown in Fig. 8.1. In some cases, when microchannels have highly wettable surfaces, very smooth corners, or the outlet channel is very narrow, liquid might flow along the corners of the microstructures more easily. In this case, delay valves can be supplemented by increasing the roughness of the structures using a lower resolution microfabrication process (e.g. polymeric photomasks) or by adding structures having a large flow resistance. In Fig. 8.1b, a flow resistance having 4-mm-long microchannels and a small total dead volume reduces the chance of a liquid to shortcut the delay valves.

The same principle of delaying filling fronts can also be used for sequentially filling parallel microfluidic elements, Fig. 8.2. The six rhombohedric elements shown in the figure form a capillary pump and are placed above and below a main inlet. The elements are numbered based on the filling sequence. Each element is connected by a 30 µm wide microchannel to the 60 µm wide main inlet at an angle of 45°. The elements themselves comprise a network of 30 µm wide parallel microchannels also connected at angles of 45°. The liquid front moves forward in the main inlet until it reaches a zone comprising the inlet for an element and a delay valve (see inset in Fig. 8.2). The delay valves ensure that each element fills entirely before the liquid moves further in the main inlet and fills the next element. A supplementary video [174] exemplifies how a liquid fills the elements one after each other in a highly controlled manner.

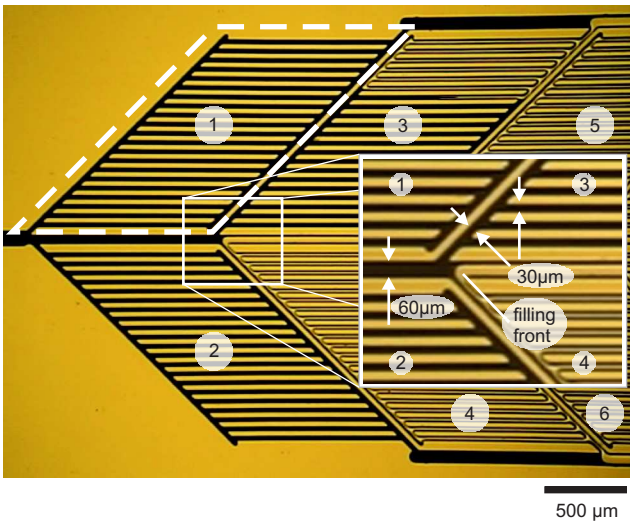

Figure 8.2. Optical micrograph of an assembly of delay valves forming a capillary pump. A liquid entering the pump by the inlet microchannel on the left will sequentially fill regions (1), delineated by the dashed rhombus, to (6). Each region can have a specific pumping power and volume capacity and a liquid filling one region is prevented from proceeding to the next region by a delay valve (see inset). The filling of such a pump can be seen in a supporting real time video [174].

This concept is important for capillary-based microfluidics because a filling element can impose specific filling conditions (volume and flow rate) until it becomes filled and is bypassed by the main inlet. As a result, filled elements do not add hydraulic resistance to the CS. Using this principle, a large capillary pump can have specific elements and can dictate the duration and volume used for the individual steps of a biological assay even if the assay necessitates a large number of incubation and rinsing steps. As shown above, delay valves can significantly slow down one filling front by placing it into competition with a second filling front, which is moving in a zone of comparatively higher capillary pressure. We discuss next how the inner geometry of microchannels can be changed to stop a filling front.

8.4.2. Stop valves

The principle of a stop valve is to eliminate the curvature of a meniscus of a filling front so that the capillary pressure $P = 0$. This is done by reducing the width of a microfluidic path using a restriction and enlarging it abruptly, Fig. 8.3a, similarly to the end of a glass capillary. In the region of enlargement, the microchannel wall changes its direction by the angle β. The liquid follows the changed direction of the microchannel wall, trying to keep its typical contact angle to the microchannel wall. If $\beta \geq \frac{\pi}{2} - \Theta_c$ the meniscus flattens or inverts its curvature and the filling front is pinned.

We have implemented a number of stop valves in silicon having different angles at the abrupt enlargement and also two different widths of the restriction, Fig. 8.3b. Ideally, the abrupt enlargement should occur on all 4 walls of a microchannel. This would require a complex fabrication process based on multilayer lithography or rapid prototyping. A large aspect-ratio (depth/width) of ∼10 at the abrupt enlargement can be considered as a simplified 2-dimensional system in which the influence of the bottom and top channel walls on the liquid-solid-air interface system of the meniscus at the filling front is negligible.15 Various types of stop valves, having such aspect-ratios at a restriction, were designed in microchannels and tested. In Fig. 8.3b, all microchannels are filled with black coloured water and the valves in microchannels 1, 2 and 5 stopped the liquid for at least a few seconds at the

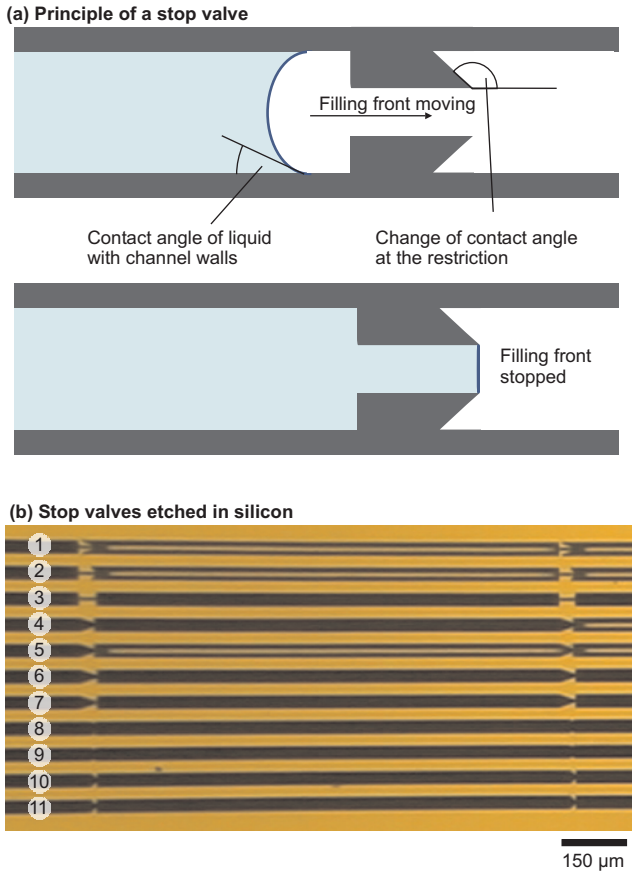

Figure 8.3. Principle and implementation of stop valves. (a) A restriction in a microchannel having an abrupt enlargement is filled with liquid. The meniscus at the filling front moves with a steady contact angle to the microchannel wall. At the abrupt enlargement the contact angles change and the meniscus flattens and stops. (b) Optical micrograph showing 30 µm wide wettable microchannels each having two stop valves in series. The microchannels are covered with PDMS. Microchannel 1, 2 and 5 are filled with black coloured water up to the first stop valve.

first stop valve. The valves in these microchannels were the ones having the largest angles and smallest widths at the abrupt enlargement. These stop valves were selected as the most promising ones for designing trigger valves.

8.4.3. Trigger valves

Stop valves can be assembled to form trigger valves where at least two liquids must meet in the valve to trigger it and move forward in a common outlet. Trigger valves can encode logical functions in CSs. Figure 8.4 shows trigger valves each composed of two equivalent stop valves mirroring each other. The two flow paths meet at different angles of 20° and 90°. Therefore, the angles β of the merged filling fronts are different, which influences the triggering function of the valve. The spacing of the two stop valves reduces the risk of liquid leaking from an already filled stop valve into the neighbouring empty stop valve. The high fabrication accuracy, the sharp vertical edges, and narrow restrictions at the abrupt enlargement, Fig. 8.4a, are important in order to stop the filling front at an accurate position. We have implemented 12 different types of trigger valves and tested their functionality with coloured water. Fig. 8.4b shows the 4 best working types of valves. These valves were able to retain liquid filled in one inlet for 15 min on average but the liquid was occasionally not retained at all, maybe owing to imperfect microfabrication of the valve or chemical functionalisation of its surface. Valves stable for 30 min had their second inlet filled with coloured water to assess their triggering functionality. In some cases triggering failed owing to a separation distance of the adjacent filling fronts that was too large. An asymmetric design of the trigger valve solves this problem by making it easier for the liquid to pass by the valve in the second inlet.

Trigger valves, in which the first inlet has a stop valve and the second inlet has a flow resistance, are shown in Fig. 8.5. The flow resistances designed here lead to equal flow from each inlet once the trigger valve is actuated but asymmetric flow rates can also be programmed. Six types of trigger valves were tested. In view of using CSs for rapid *in vitro* diagnostics, trigger valves were tested using coloured human serum. Serum has similar or slightly smaller surface tension, [175] similar viscosity, and similar contact angles on

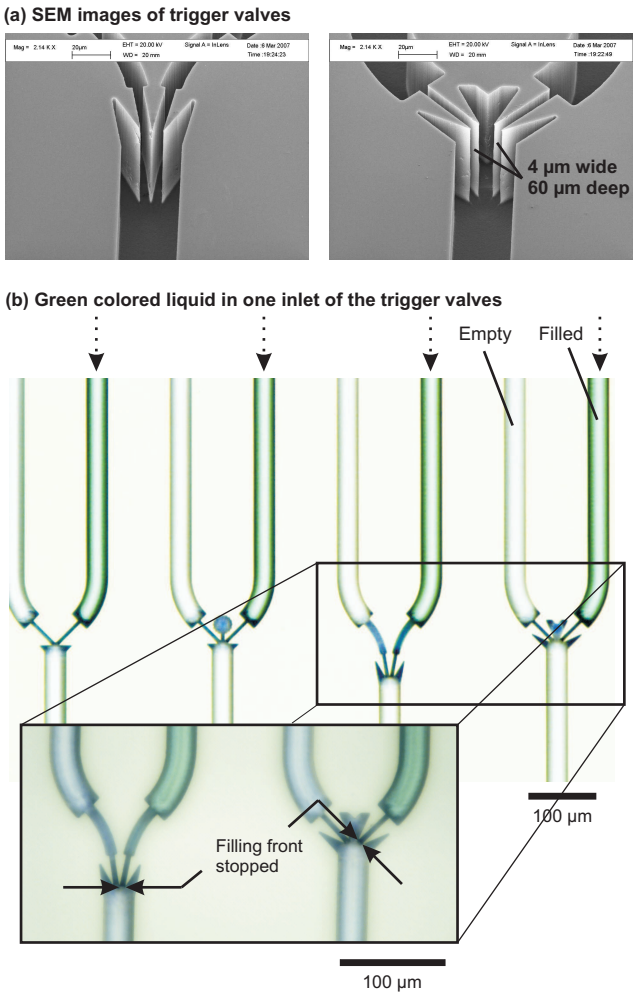

Figure 8.4. Examples of trigger valves microfabricated in Si. (a) These SEM images show trigger valves composed of two symmetric inlets, which meet at stop valves, and of one outlet channel. (b) Optical micrograph of trigger valves having different types of stop valves and having each an inlet filled with water coloured in green. The filling of the empty inlet can be seen in a supporting real time video [174].

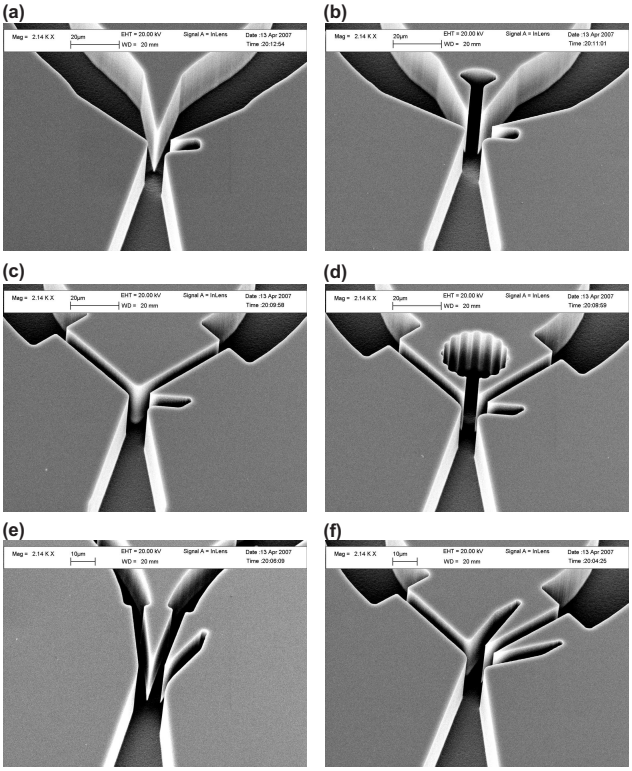

Figure 8.5. SEM images of asymmetric, 30 μm deep trigger valves microfabricated in Si. These six types of valves differ in the opening width and the change of contact angle at the restriction. From (a) to (f), narrow openings, a large change of contact angle and the asymmetry improve the performance of the trigger valve.

the surfaces of CSs as water. The valves were evaluated by filling human serum in the first inlet of trigger valves and monitored if the valves were able to hold the liquid for 5 min and to be triggered, Table 8.1. We found that triggering the valve by adding liquid in the second inlet was not an issue but that the success rate of the experiments depended on the retention of the serum for at least five minutes. Valves having a 7 μm wide and short restriction, Fig. 8.5a and b, were less efficient in stopping the first incoming liquid than valves having longer and 5 μm wide restrictions, Fig. 8.5b and c. Valves having narrow, 5 μm wide restrictions and a large angle β performed best. In 69 % and 85 % of the tests done with the valves shown in Fig. 8.5e and f, human serum stopped for at least five minutes and proceeded satisfactorily upon triggering of the valves. Reducing the width of the restrictions further and increasing their depth might improve the performance of the valves.

Type of valve	Change of contact angle /°	Width of restriction / µm	Success rate /%
a	155	7	7.7
b	155	7	7.7
c	135	5	15.4
d	135	5	23.1
e	160	5	69.2
f	160	5	84.6

Table 8.1. Geometry and chance of stopping human serum for $\geq$ 5 min for six types of trigger valves shown in Fig. 8.5.

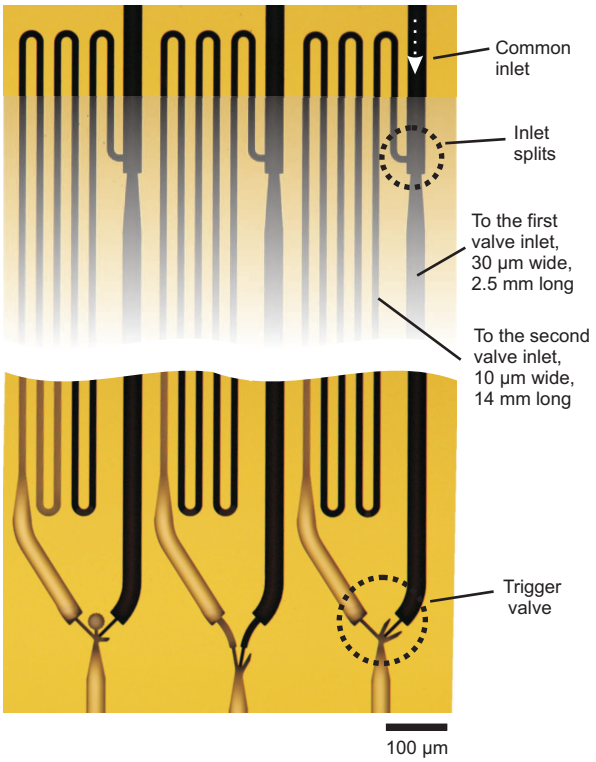

Figure 8.6. Optical micrographs of microfluidic timers. Trigger valves are assembled with microchannels to have a common inlet that splits via a short and a long flow path to the two inlets of the trigger valve. This microfluidic timer prevents the liquid from entering the common outlet for 5 s.

8.4.4. Microfluidic timers

Stopping a liquid in a CS for 5 minutes is a long time compared to the timescale of biological assays previously performed in CSs. Fluorescence sandwich surface immunoassays performed using a CS have taken from a few minutes [35] up to 24 min [34] in the case of high sensitivity assays. Rinsing steps can be as brief as a few seconds whereas incubation steps are on the order of 3 to 6 minutes. Delaying a liquid in a microfluidic structure for one minute should be long enough for mixing liquids and reagents, dissolving reagents dried in some microfluidic areas, stimulating cells in microfluidic chambers, and metering a liquid. A microfluidic timer comprising a trigger valve connected to microchannels having different lengths was realized, Fig. 8.6. The timer has a common inlet that splits into a 30 µm wide and 2.5 mm long microchannel and a 10 µm wide and 14 mm long microchannel. The shorter microchannel is connected to the first inlet of the trigger valve and supplies the liquid to the stopping element of the valve. The longer microchannel draws liquid to the trigger element of the valve. A liquid entering the valve will be delayed for a precise time until both filling fronts meet and trigger the valve. In the microfluidic timer shown in Fig. 8.6, an aliquot of coloured water needs 5 s to pass the timer. Both the width and length of the microchannel connected to the second inlet of the trigger valve can be easily varied to yield a timer having the desired time scale. Microfluidic timers can prevent a liquid from filling the remainder of the CS for a certain time without substantially increasing the overall hydraulic resistance of the CS.

8.5. Conclusions

Miniaturization and lab-on-a-chip concepts have brought impressive performances in terms of short time to results, sensitivity, and parallelization to a number of bio-analytical platforms. Commercialized point-of-care diagnostics and analytical instruments for environmental testing have yet only marginally benefited from miniaturization. The reasons might be the cost of miniaturized bioanalytical devices, the degree of expertise needed from users, and the fragility of these devices. By developing microfluidics for immunoassays

wherein capillary forces draw liquids through functional microfluidic elements, we hope to combine the performances of microfluidic-based systems with the needs of end users for point-of-care applications. The passive valves shown here enhance CSs with a range of functionalities such as safety features (delay valves and flow resistances), timing features (delay and stop valves), and basic logical functions (trigger valves). The volume and time characteristics of these elements range from nanolitres to picolitres of liquid and from seconds to minutes, respectively. No complex microfabrication strategy is needed for these valves and the designs reported here are in reach of conventional plastic molding or embossing techniques used for mass fabrication of microfluidic components. We therefore think that CSs incorporating valves represent a promising tool for microfluidic-based bio-analytical tests to be used by non-technical experts.

9. Conclusions

Microfluidic CSs are a powerful technology for transporting minute volumes of liquids through a micrometer-sized reaction chamber without any tubing or electrical connections to peripheral instruments. Immunoassays in such CSs can be optimized to obtain a maximum sensitivity, minimal sample consumption or fast results by choosing an optimal flow rate as discussed in Chapter 2. Flow rates can be programmed in CSs by selecting appropriate combinations of flow resistors and capillary pumps. A solution for the problem of having a sequence of fast and slow flow rates in the same CS has also been demonstrated in Chapter 5.

An important criterion for medical diagnostic assays are fast results. CSs are capable to generate large flow rates to capture enough analytes and generate a large fluorescence signal within a few minutes, Chapter 6. Stencils minimize the effort for fabricating accurate and dense patterns of several cAbs should allow performing of high-sensitive multiplexed surface immunoassays efficiently in such CSs. We think that the open and flexible approach of patterning cAbs and using the CSs will allow to develop a large variety of immunoassays in CSs. The approach of a one-step immunoassay in CSs greatly simplifies performing of immunoassays and exemplifies the versatility of CSs, Chapter 7. Such CSs for one-step immunoassays might not only be suited for medical diagnostics, but also for other applications such as monitoring of food and water quality, where immunoassays are preferably performed in the field and fast results are desired.

Additional functionalities such as temperature control in the CSs might be used to perform temperature sensitive assays, or to program the flow rate at the time of use instead at the time of fabrication, Chapter 3. For assay developments aiming at short development cycles this method might be a good option. Other functions such as timing, metering, or triggering of liquids can

be integrated directly in the flow paths of CSs using valves, Chapter 8. Such valves enable digital microfluidic functions such as logic microfluidic AND-gates, for instance.

We think that the methods and tools developed in this work are promising for being used by biological experts in life science research and are key steps for developing one-step immunoassays in CSs for the ultimate benefit in diagnostics at the point-of-care.

A. Supplementary Information to Chapter 2

A.1. Implementation of the model

The model was implemented using the method described in [43] and is divided in two parts: the first part calculates the velocity vector field and the second calculates the convection-diffusion-equation and the binding kinetics to the concentration field.

The velocity vector field is calculated using the finite difference form of the *Navier-Stokes* equation. The general impulse equations

$$\frac{\partial u}{\partial t} + \frac{\partial p}{\partial x} = \frac{1}{Re}\left(\frac{\partial^2 u}{\partial x^2} + \frac{\partial^2 u}{\partial y^2}\right) - \frac{\partial\left(u^2\right)}{\partial x} - \frac{\partial\left(uv\right)}{\partial y} \tag{A.1}$$

$$\frac{\partial u}{\partial t} + \frac{\partial p}{\partial y} = \frac{1}{Re}\left(\frac{\partial^2 v}{\partial x^2} + \frac{\partial^2 v}{\partial y^2}\right) - \frac{\partial\left(uv\right)}{\partial x} - \frac{\partial\left(v^2\right)}{\partial y} \tag{A.2}$$

are discretized on a regular staggered grid, Fig. A.1. To prevent numerical oscillations the different variables for velocity in the x- and y-direction, u, v, and the pressure P are localized at diverse positions on the grid cells. The boundary conditions are "no-slip" ($u = 0$) on the channel walls, "inflow" ($u =$ const.) at the inlet and "outflow" ($\frac{\partial(u,v)}{dn} = 0$) at the channel end. Furthermore we have to prevent stability problems occurring in discretized second-order differential equations at convection-dominated flow conditions. For this, a variety of different methods are described in literature. From these methods, we chose the donor-cell scheme [176]:

$$\begin{aligned}\left[\frac{d\left(ku\right)}{dx}\right] = {} & \frac{1}{2\,\delta x}\left(k_{\mathrm{r}}\left(u_{\mathrm{i}} + u_{\mathrm{i+1}}\right) - k_{\mathrm{l}}\left(u_{\mathrm{i-1}} + u_{\mathrm{i}}\right)\right) + \\ & \frac{1}{2\,\delta x}\left(\left|k_{\mathrm{r}}\right|\left(u_{\mathrm{i}} - u_{\mathrm{i+1}}\right) - \left|k_{\mathrm{l}}\right|\left(u_{\mathrm{i-1}} - u_{\mathrm{i}}\right)\right)\ ,\end{aligned} \tag{A.3}$$

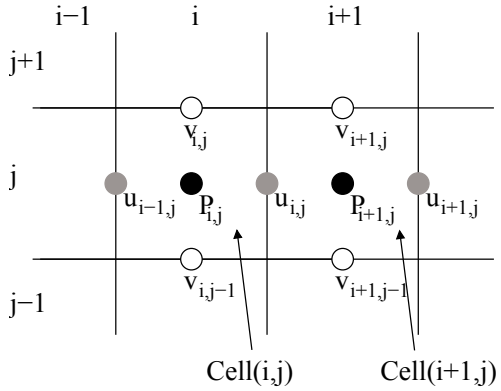

Figure A.1. 2D staggered grid used to model the flow by diffusion and convection.

which has a good stability performance and combined it with the central difference scheme [177]:

$$\left[\frac{du^2}{dx}\right]_{\mathrm{i}} = \frac{1}{\delta x}\left(\left(\frac{u_{\mathrm{i}} + u_{\mathrm{i+1}}}{2}\right)^2 - \left(\frac{u_{\mathrm{i-1}} + u_{\mathrm{i}}}{2}\right)^2\right) , \tag{A.4}$$

which has a higher approximation performance than the donor-cell scheme. Equations A.3 and A.4 are shown as a one-dimensional example. They are averaged using a real parameter γ chosen from the interval [0, 1]:

$$\gamma \cdot \text{Donor Cell} + (1-\gamma) \cdot \text{Central Difference} . \tag{A.5}$$

We have to introduce another stability condition for the time step to guaranty the stability of the numerical algorithm. We use a time-step control which includes the *Courant-Friedrichs-Levi* conditions:

$$\delta t = \tau min\left(\frac{Re}{2}\left(\frac{1}{\delta x^2} + \frac{1}{\delta y^2}\right)^{-1}, \frac{\delta x}{|u_{\max}|}, \frac{\delta y}{|v_{\max}|}\right), \ \tau \in]0, 1] . \tag{A.6}$$

These conditions prevent volume elements of liquid from moving further than one cell width, δx or δy, during the time δt.

The second part of the model applies only the convection-diffusion equation, Eqn. 2.3, and the binding kinetics, Eqn. 2.4, to the concentration field. These equations have been discretized using the same models. The boundary conditions for Eqn. 2.3 are a "constant concentration" at the inlet, "no flow" across the channel wall, and a simple "outflow" condition. For boundary cells next to the capture area, Eqn. 2.4 is linked to Eqn. 2.3 via the source term

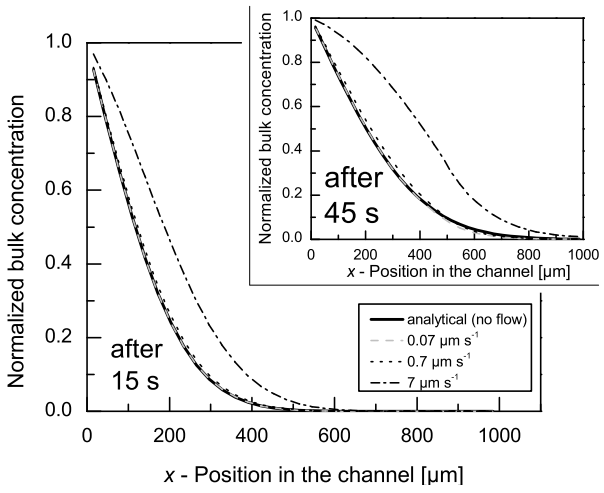

Figure A.2. Verification of the diffusion model using a slow convection in the x-direction. The graphs show the concentration profile along the channel after 15 and 45 s, starting from infinite source at inlet $x = 0$ μm into the initially empty channel. At flow velocities ≤ 0.07 μm s^{-1}, diffusion predominates mass transport. Convection starts to have an effect on the transport of analyte in the microchannel for a flow velocity of 0.7 μm s^{-1}, and substantially contributes to the transport for velocities > 7 μm s^{-1}.

which can reduce or increase the analyte concentration in this boundary cell depending on the saturation of the capture area and the binding constants.

A.2. Validation of the implemented numerical model

Specific problems that can be described by analytical solutions are compared with the simulated results. Figure A.2 shows the validation of the diffusion of the analyte during the assay. In this case, the flow velocity of the liquid in the microchannel is reduced to a minimal value to suppress convection. The mass transport then results from diffusion. The analytical solution is given as a reference. The correlation between the numerical and the analytical solutions is excellent for the two graphs shown in Fig. A.2.

The flow velocity and the parabolic profile also have an important effect on the mass transport of analyte within the microchannel. Figure A.3 gives an example of the capabilities of the model to describe the flow in the mi-

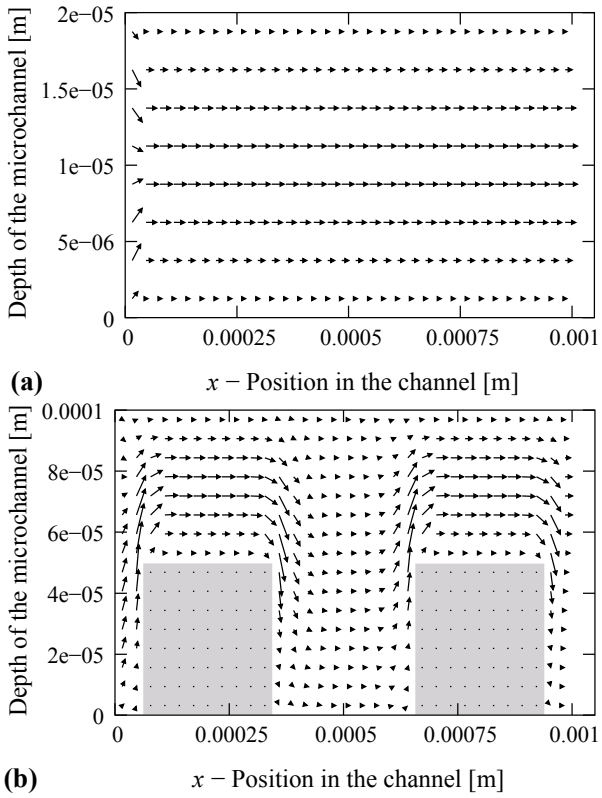

Figure A.3. Visualization of the self-established laminar flow profile for (a) a short zone of flow development (at the inlet on the left-hand side) where the boundary conditions are "constant inflow" (left), "no-slip" (top, bottom) and "outflow" (right), and (b) for a channel having two obstacles.

crochannel. Figure A.4 shows the agreement between the analytical and the numerical solution describing the self-established flow profile.

The correctness of the ligand-receptor binding model is shown in Fig. A.5. No significant analyte exploitation occurs at high flow velocities. The curves describing the saturation of the binding sites obtained with the numerical and the analytical model are in agreement.

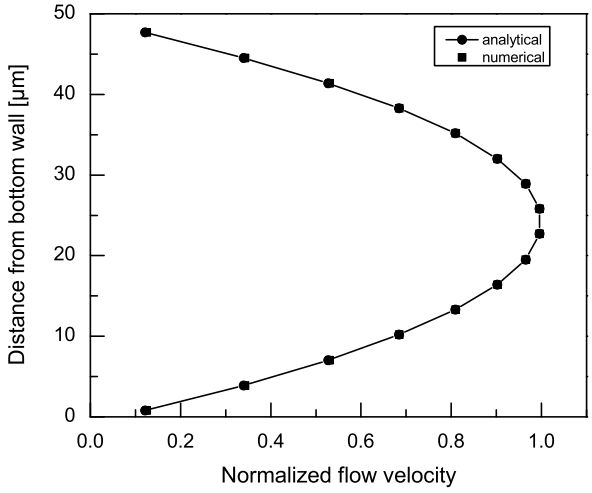

Figure A.4. The resemblance of the flow profiles obtained with the analytical and numerical model validates the numerical model describing the velocity flow profile. The flow profile here occurs at a x-position outside the flow development zone for a 50 μm deep channel.

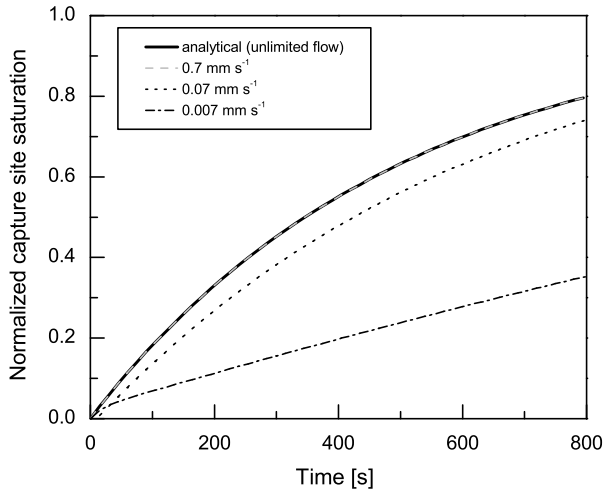

Figure A.5. Saturation of immobilized capture sites on a channel wall segment at 1 nM analyte concentration. The binding reaction, represented by a ligand receptor model, is not slowed down at flow velocities of 0.7 mm s^{-1}. The lines are provided as guides to the eye.

B. Fabrication of microfluidic chips in plastics

Microfluidic capillary systems (CSs) can be used for patterning (bio-)molecules on surfaces and to perform fluorescence assays with sub-microliter volumes of sample and picomolar sensitivity. Typically, a CS comprises a loading pad, a capillary retention valve, a microchannel wherein an assay can be done, and a capillary pump. CSs can be cloned on a microfluidic chip for performing independent assays in parallel. In our previous work, we utilized CSs that were microfabricated in Si, coated with Au, and derivatized with a wettable, thiolated poly(ethylene glycol). These chips fill spontaneously owing to capillary forces. Here, we report two strategies to fabricate CSs in plastic using hot embossing of cyclic olefin copolymer (COC). These strategies might prove useful for the mass fabrication of CS regarding applications in diagnostics, where disposable microfluidic chips are favoured. In addition, COC is highly resistant to many organic solvents, non-permeable to water, transparent, and has low auto-fluorescence.

B.1. Concept

Figure B.1 describes a first strategy for hot embossing COC using a Ni master, which is obtained by electroplating Ni on a deep reactive ion etching (DRIE)-micromachined Si wafer. With this strategy, it takes approximately one week to fabricate the Ni master, and the cycle time to emboss one COC wafer is only a few minutes. Figures B.1B-F show a profile and images of some areas of a 30 μm deep embossed chip. Although these areas are very smooth, the depth profile of the Si structures made the release of the COC chip after embossing somewhat challenging: the DRIE process generated a slight undercut

(∼0.5°) of the Si structures which was conserved in the Ni master and interlocked with the COC replica. Since it can be difficult and time consuming to adjust the profile of structures obtained using DRIE, we also used an alternative method to optimize the profile of the master by fabricating it using a high temperature resistant epoxy and SU-8 photoresist, Fig. B.2A. SU-8, a negative resist, was here exposed from the backside and developed, which resulted in SU-8 structures having ∼7° tilted sidewalls. After an intermediate replication step using PDMS, the tilted structures were replicated into the epoxy master. Fabrication of an epoxy master required approximately 3 days. The profile and images of COC structures that have been fabricated using this strategy show accurate COC replicas, Fig. B.2B-G. Similarly to Si microfluidic chips, the COC chips were diced, coated with Au, and made wettable. These replicas could easily seal with PDMS and showed spontaneous filling by capillarity, Fig. B.3.

B.2. Outlook

The replication of autonomous CSs in COC is promising for the miniaturization of immunoassays using low cost, disposable microfluidic chips. In addition, the SU-8 structures may be used to generate electroplated Ni masters, instead of epoxy masters, featuring high robustness and long lifetimes necessary for hot embossing.

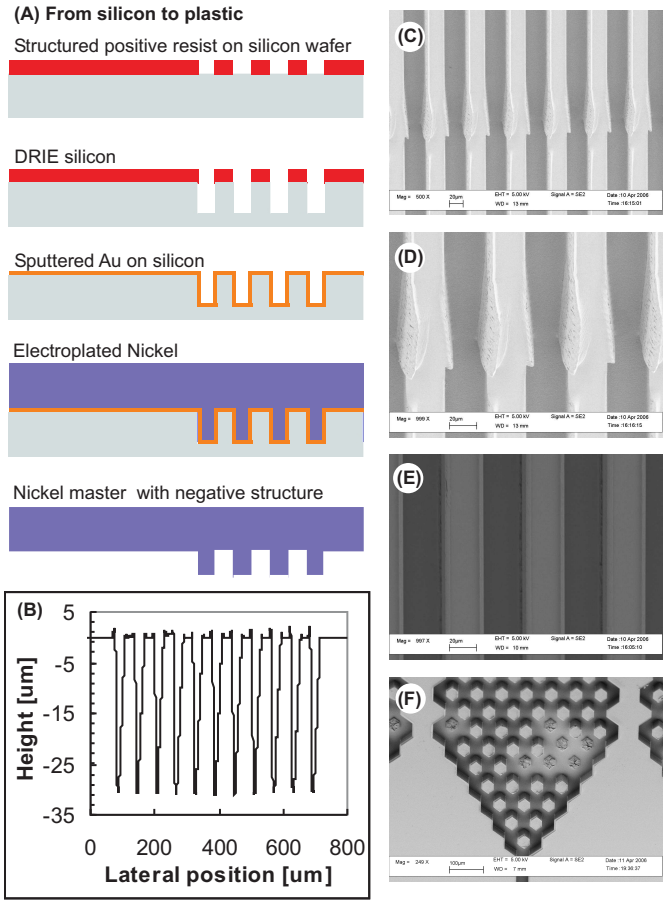

Figure B.1. Hot embossing of 30 µm deep CSs in COC using a Nickel master fabricated from a Si wafer template. (A) The Si master is structured using photolithography and DRIE, and then coated with an Au seed layer for electroplating Ni. The Ni replica is released by wet etching the Si wafer. (B) Depth profile of the 30 µm wide microchannels of the 11 CSs composing one microfluidic chip. (C-F) SEM images of the 15 µm wide capillary retention valves (C and D), microchannels (E), and capillary pumps (F) of the CSs. A general difficulty in the preparation of electroplated masters for hot embossing is found in the DRIE-derived profile of the Si master, which does not always have vertical walls, but show a slight undercut of 0.5°. During release of the embossed plastic wafer from the Ni master, this can lead to minor imperfections such as the ∼2 µm high protrusions on the edges of the channels (B), or missing posts in (F). The replicated structures otherwise show smooth surfaces and good contour accuracy.

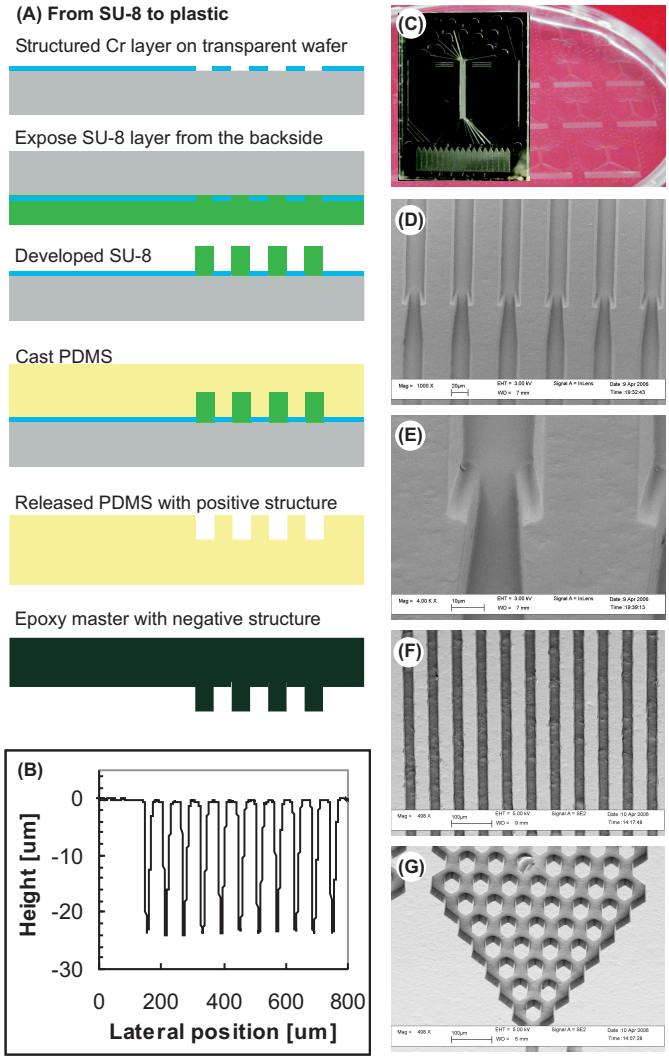

Figure B.2. Hot embossing of 25 µm deep CSs in COC using an epoxy master fabricated from a SU-8 structure. (A) A Cr layer on a transparent substrate is used to expose a SU-8 layer from the backside, resulting in ∼7° slanted sidewalls. The SU-8 structure is molded in PDMS and a high-temperature resistant aluminum-filled epoxy is then filled in the PDMS cast. (B) Profile of 11 microchannels replicated in COC. (C) Photograph of a hot embossed COC wafer and a single chip with 11 capillary systems (inset). (D-G) SEM images of molded capillary retention valves (D, E), straight microchannels (F), and posts in a capillary pump (G). The tilted walls of the master, especially visible in (E), enable an accurate replication by facilitating release of the molded COC wafer from the master.

Figure B.3. Optical micrographs showing the capillary pump of one CS being filled by a colored (red) solution of PBS. Here, the microfluidic chip was hot embossed in COC (SU-8 process) and coated with Au derivatized with self-assembled monolayers. The chip is sealed with a layer of PDMS except for the loading pads at the beginning of the CSs. The PBS solution added to the loading pads spontaneously fills the CSs due to capillarity, as well as the capillary pumps ending each CS. The tight sealing between PDMS and the COC chip prevents leaks and crosstalk between adjacent CSs from occuring. The scale bar is 400 µm.

C. Datasheet “Assay Development Chip”

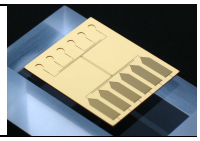

Assay Development v.2 Chip	*AD v.2.10*	*AD v.2.20*	*AD v.2.30*
Outer dimensions	22.5 × 27.5 × 0.5 [mm]		
Number of capillary systems	6		
Capacity of loading pad	1 µL		
Depth of loading pad	180 µm		
Volume of channel in front of reaction chambers	0.15 µL		
Volume of reaction chamber	2.7 nL	5.4 nL	8.1 nL
Depth of reaction chamber	10 µm	20 µm	30 µm
Width of reaction chamber	30 µm		
Length of reaction chamber	9 mm		
Volume of capillary pump	2 µL		
Depth of capillary pump	180 µm		
Vent at end of capillary pump	x		
Pitch of loading pads	3.5 mm		
Pitch of reaction chambers	100 µm		
Bulk/Surface material	Si/Au		
Surface monolayer	HS-PEG (750 Da)		

Table 1. Dimensions.

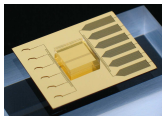

A. Block of PDMS (8 × 8 mm) sealing the reaction chambers of the capillary systems. Optional: The entire surface of the PDMS, which is in contact with the chip can be coated with capture antibodies in advance.

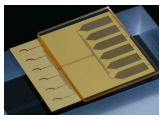

B. Block of PDMS (24 × 20 mm) sealing the reaction chambers and the capillary pumps. The loading pads remain open for pipetting. No undesired evaporation of sample in the capillary pumps anymore.

Figure 1. Assay development chips sealed with PDMS.

Average Flow Rates in the Reaction Chambers	Viscosity [mPa s]	Setup as in	AD v.2.20 [nL s^{-1}]	AD v.2.20 CV (%)	AD v.2.30 [nL s^{-1}]	AD v.2.30 CV (%)
Water	1	Fig. 1B	1.85	4.7	4.16	4.8
PBS + 1% BSA	1	Fig. 1B	1.85	5.0	3.96	3.4
Solution of 20% hum. albumin	4	Fig. 1A	0.51	12.0	1.51	11.9

Table 2. Characteristic flow rates of liquids in the “Assay development v.2” chip.

Bibliography

[1] H. Unger and B. Willms. Self-control of blood sugar with a new blood sugar test strip. *Dtsch. Med. Wochenschr.*, 105(16):566–570, 1980.

[2] K. May. Home tests to monitor fertility. *Am. J. Obstet. Gynecol.*, 165(6 Pt 2):2000–2002, 1991.

[3] D. Wild, editor. *The Immunoassay Handbook*. Elsevier Ltd., Oxford, UK, 2005.

[4] R.S. Yalow and S.A. Berson. Assay of plasma insulin in human subjects by immunological methods. *Nature*, 184(Suppl 21):1648–1649, 1959.

[5] A. Manz, N. Graber, and H.M. Widmer. Miniaturized total analysis systems: A novel concept for chemical sensors. *Sens. Actuators B*, 1(1):244–248, 1990.

[6] A. Manz, D.J. Harrison, E.M.J. Verpoorte, J.C. Fettinger, H. Lüdi, and H.M. Widmer. Miniaturization of Chemical Analysis Systems A Look into Next Century's Technology or Just a Fashionable Craze? *CHIMIA*, 45(4):103–105, 1991.

[7] K.A. Erickson and P. Wilding. Evaluation of a novel point-of-care system, the i-STAT portable clinical analyzer. *Clinical Chemistry*, 39(2):283–287, 1993.

[8] F. Hoffmann-La Roche Ltd., Diagnostics division, Cardiac Reader, http://www.roche.com/home/products/, accessed August 2007.

[9] Biosite Inc., Triage Cardiac Panel, http://www.biosite.com/products/, accessed August 2007.

[10] C. Gallery, S. Content, C. Technology, and S. Matter. Microfluidics in commercial applications; an industry perspective. *Lab Chip*, 6:1118–1121, 2006.

[11] E.P. Kartalov, J.F. Zhong, A. Scherer, S.R. Quake, C.R. Taylor, and W.F. Anderson. High-throughput multi-antigen microfluidic fluorescence immunoassays. *BioTechniques*, 40(1):85–90, 2006.

[12] M.J. Madou and R. Cubicciotti. Scaling issues in chemical and biological sensors. *Proc. of the IEEE*, 91(6):830–838, 2003.

[13] E.M. Purcell. Life at low Reynolds number. *Am. J. Phys*, 45(1):3–11, 1977.

[14] A. Bernard, B. Michel, and E. Delamarche. Micromosaic immunoassays. *Anal. Chem.*, 73(1):8–12, 2001.

[15] L. M. Amzel and R. J. Poljak. Three-dimensional structure of immunoglobulins. *Annu. Rev. Biochem.*, 48:961–997, 1979.

[16] E. Delamarche. *Nanobiotechnology*, pages 31–52. Wiley-VCH Verlag, Weinheim, 2004.

[17] Genetix. *aQuire microarray scanner specification sheet*. Genetix Ltd., http://www.genetix.com, 2004.

[18] L.W. Schwartz and S. Garoff. Contact angle hysteresis on heterogeneous surfaces. *Langmuir*, 1(2):219–230, 1985.

[19] S.K. So, W.K. Choi, C.H. Cheng, L.M. Leung, and C.F. Kwong. Surface preparation and characterization of indium tin oxide substrates for organic electroluminescent devices. *Appl. Phys. A*, 68(4):447–450, 1999.

[20] H. Andersson, W. van der Wijngaart, P. Griss, F. Niklaus, and G. Stemme. Hydrophobic valves of plasma deposited octafluorocyclobutane in drie channels. *Sens. Actuators B Chem.*, 75:136–141, 2001.

[21] V. Namasivayam, R.G. Larson, D.T. Burke, and M.A. Burns. Transpiration-based micropump for delivering continuous ultra-low flow rates. *J. Micromech. Microeng.*, 13(2):261–271, 2003.

[22] T. Young. Cohesion of fluids. *Phil. Trans.*, page 65, 1805.

[23] P.S. Laplace. *Traité de Mécanique Céleste, Supplement to the Theory of Capillary Action*. 1806.

[24] O. Reynolds. An experimental investigation of the circumstances which determine whether the motion of water shall be direct or sinuous, and of the law of resistance in parallel channels. *Proc. Royal Soc. London*, 35:84–99, 1883.

[25] J.H. Spurk. *Strömungslehre*. Springer, Berlin, 4 edition, 2004. J. H. Spurk, Ströhmungslehre, 4th Ed.; Springer: Berlin, 1996, pp. 160–167.

[26] R. Brown. A brief account of microscopical observations made in the months of june, july and august, 1827, on the particles contained in the pollen of plants; and on the general existence of active molecules in organic and inorganic bodies. *Edinburgh new Philosophical Journal*, pages 358–371, 1828.

[27] P. W. Atkins. *Physical Chemistry*. Oxford University Press, Oxford, 1990.

[28] E. F. H. Tay, editor. *Microfluidics and BioMEMS Applications*. Kluwer Academic Publishers, Boston, 2002.

[29] R.P. Ekins. Ligand assays: from electrophoresis to miniaturized microarrays. *Clin. Chem.*, 44(9):2015–2030, 1998.

[30] A. Manz and H. Becker. *Microsystem Technology in Chemistry and Life Science*. Springer-Verlag, Heidelberg, 1998.

[31] N.T. Nguyen and S.T. Wereley. *Fundamentals and Applications of Microfluidics*. MEMS series. Artech House, Boston, 2002.

[32] F.S. Apple, R.H. Christenson, R. Valdes, A.J. Andriak, A. Berg, S.H. Duh, Y.J. Feng, S.A. Jortani, N.A. Johnson, B. Koplen, et al. Simultaneous Rapid Measurement of Whole Blood Myoglobin, Creatine Kinase MB, and Cardiac Troponin I by the Triage Cardiac Panel for Detection of Myocardial Infarction. *Clinical Chemistry*, 45(2):199–205, 1999.

[33] D. Juncker, H. Schmid, U. Drechsler, H. Wolf, M. Wolf, B. Michel, N. de Rooij, and E. Delamarche. Autonomous microfluidic capillary system. *Anal. Chem.*, 74(24):6139–6144, 2002.

[34] S. Cesaro-Tadic, G. Dernick, D. Juncker, G. Buurman, H. Kropshofer, B. Michel, C. Fattinger, and E. Delamarche. High-sensitivity miniaturized immunoassays for tumor necrosis factor alpha using microfluidic systems. *Lab Chip*, 4(6):563–569, 2004.

[35] M. Wolf, D. Juncker, B. Michel, P. Hunziker, and E. Delamarche. Simultaneous detection of c-reactive protein and other cardiac markers in human plasma using micromosaic immunoassays and self-regulating microfluidic networks. *Biosens. Bioelectron.*, 19(10):1193–1202, 2004.

[36] R. Vijayendran, F.S. Ligler, and D.E. Leckband. A computational reaction-diffusion model for the analysis of transport-limited kinetics. *Anal. Chem.*, 71:5405–5412, 1999.

[37] D.G. Myszka, X. He, M. Dembo, T.A. Morton, and B. Goldstein. Extending the Range of Rate Constants Available from BIACORE: Interpreting Mass Transport-Influenced Binding Data. *Biophys. J.*, 75(2):583–594, 1998.

[38] D.A. Edwards. Estimating rate constants in a convection-diffusion system with a boundary reaction. *J. Appl. Math.*, 63:89–112, 1999.

[39] D.A. Edwards, B. Goldstein, and D.S. Cohen. Transport effects on surface-volume biological reactions. *J. Math. Biol.*, 39:533–561, 1999.

[40] J. Jenkins, B. Prabhakarpandian, K. Lenghaus, J. Hickman, and S. Sundaram. Fluidics-resolved estimation of protein adsorption kinetics in a biomicrofluidic system. *Anal. Biochem.*, 331:207–215, 2004.

[41] K.E. Sapsford, Z. Liron, Y.S. Shubin, and F.S. Ligler. Kinetics of antigen binding to arrays of antibodies in different sized spots. *Anal. Chem.*, 73:5518–5524, 2001.

[42] G. Balgi, DE Leckband, and JM Nitsche. Transport effects on the kinetics of protein-surface binding. *Biophysical Journal*, 68(6):2251–2260, 1995.

[43] M. Griebel, T. Dornseifer, and T. Neunhoeffer. *Numerische Simulation in der Strömungsmechanik*. Vieweg, Braunschweig/Wiesbaden, 1995.

[44] K.L. Prime and G.M. Whitesides. Self-assembled organic monolayers: model systems for studying adsorption of proteins at surfaces. *Science*, 252:1164–1167, 1991.

[45] S. Metsämuuronen, S. Reinikainen, and M. Nyström. Analysis of protein filtration data by pls regression. *Desalination*, 149:453–458, 2002.

[46] W. Koenig, M. Sund, B. Filipiak, A. Döring, H. Löwel, and E. Ernst. Plasma viscosity and the risk of coronary heart disease results from the monica-augsburg cohort study, 1984 to 1992. *Arterioscler. Thromb. Vasc. Biol.*, 18:768–772, 1998.

[47] L.C. Santora, Z. Kaymakcalan, P. Sakorafas, I.S. Krull, and K. Grant. Characterization of Noncovalent Complexes of Recombinant Human Monoclonal Antibody and Antigen Using Cation Exchange, Size Exclusion Chromatography, and BIAcore. *Anal. Biochem.*, 299(2):119–129, 2001.

[48] A. Bernard, D. Fitzli, P. Sonderegger, E. Delamarche, B. Michel, H. R. Bosshard, and H. Biebuyck. Affinity capture of proteins from solution and their dissociation by contact printing. *Nat. Biotechnol.*, 19(9):866–869, 2001.

[49] E. Delamarche, D. Juncker, and H. Schmid. Microfluidics for processing surfaces and miniaturizing biological assays. *Adv. Mater.*, 17:2911–2933, 2005.

[50] B. Bhushan, editor. *Handbook of Nanotechnology*. Springer Verlag, Berlin/Heidelberg, 2004.

[51] P. Woias. Micropumps—past, progress and future prospects. *Sens. Actuators B*, 105(1):28–38, 2005.

[52] Harvard Apparatus, Inc., http://www.harvardapparatus.com, accessed July 2006.

[53] A. Homsy, S. Koster, J.C.T. Eijkel, A. van den Berg, F. Lucklum, E. Verpoorte, and N.F. de Rooij. A high current density DC magnetohydrodynamic (MHD) micropump. *Lab Chip*, 5(4):466–471, 2005.

[54] Roche Diagnostics AG, http://www.roche-diagnostics.com, accessed August 2007.

[55] T.A. Neff, C. Fellmann, R.M. Fuechslin, A.C. Gerber, and M. Weiss. The Panomat P-10 micro-volumetric infusion pump is suitable for continuous drug administration at minimal flow rates. *Can. J. Anaesth.*, 49(10):1048–1052, 2002.

[56] http://www.microjet.it, accessed July 2006.

[57] http://www.mantsch-medizintechnik.de, accessed July 2006.

[58] N. Goedecke and A. Manz. Towards evaporation-driven hplc on a chip: an alternative transport process for microanalysis systems. In *5th International Conference on Micro Total Analysis Systems (uTAS)*, Monterey, CA, 2001.

[59] N. Goedecke, J. Eijkel, and A. Manz. Evaporation driven pumping for chromatography application. *Lab Chip*, 2(4):219–223, 2002.

[60] V. Namasivayam, K. Handique, D.T. Burke, R.G. Larson, and M.A. Burns. A microfabricated valveless pump for delivering non-pulsatile flow. In *Proc. SPIE: Micromachining, Micromanufacturing and Microelectronic Manufacturing*, Santa Clara, CA, 2000.

[61] K. Handique, D.T. Burke, C.H. Mastrangelo, and M.A. Burns. On-chip thermopneumatic pressure for discrete drop pumping. *Anal. Chem.*, 73(8):1831–1838, 2001.

[62] C.S. Effenhauser, H. Harttig, and P. Kramer. An evaporation-based disposable micropump concept for continuous monitoring applications. *Biomed. Microdev.*, 4(1):27–32, 2002.

[63] J.A. Schonberg, S. DasGupta, and P.C. Wayner. An augmented young-laplace model of an evaporating meniscus in a microchannel with high heat-flux. *Exp. Therm. Fluid Sci.*, 10(2):163–170, 1995.

[64] V. Babin and R. Holyst. Evaporation of a thin liquid film. *J. Chem. Phys.*, 122(2):024713, 2005.

[65] R.M. Rowan, O.W. Van Assendelft, and F.E. Preston. *Advances in Laboratory Methods: General Haematology.* Oxford University Press Inc., New York, 2002.

[66] D. Mattanovich and N. Borth. Applications of cell sorting in biotechnology. *Microb. Cell. Fact.*, 5:12, 2006.

[67] A. Persidis. High-throughput screening. Advances in robotics and miniturization continue to accelerate drug lead identification. *Nat. Biotechnol.*, 16(5):488–489, 1998.

[68] N. Li, A. Tourovskaia, and A. Folch. Biology on a chip: microfabrication for studying the behavior of cultured cells. *Crit. Rev. Biomed. Eng.*, 31(5-6):423–488, 2003.

[69] A. Prokop, Z. Prokop, D. Schaffer, E. Kozlov, J. Wikswo, D. Cliffel, and F. Baudenbacher. Nanoliterbioreactor: Long-term mammalian cell culture at nanofabricated scale. *Biomed. Microdev.*, 6(4):325–339, 2004.

[70] A.R. Wheeler, W.R. Throndset, R.J. Whelan, A.M. Leach, R.N. Zare, Y.H. Liao, K. Farrell, I.D. Manger, and A. Daridon. Microfluidic device for single-cell analysis. *Anal. Chem.*, 75(14):3581–3586, 2003.

[71] J. Pihl, J. Sinclair, E. Sahlin, M. Karlsson, F. Petterson, J. Olofsson, and O. Orwar. Microfluidic gradient-generating device for pharmacological profiling. *Anal. Chem.*, 77(13):3897–3903, 2005.

[72] C.R. Poulsen, C.T. Culbertson, S.C. Jacobson, and J. M. Ramsey. Static and dynamic acute cytotoxicity assays on microfluidic devices. *Anal. Chem.*, 77(2):667–672, 2005.

[73] A. Khademhosseini, J. Yeh, G. Eng, J. Karp, H. Kaji, J. Borenstein, O.C. Farokhzad, and R. Langer. Cell docking inside microwells within reversibly sealed microfluidic channels for fabricating multiphenotype cell arrays. *Lab Chip*, 5(12):1380–1386, 2005.

[74] D.T. Chiu, N.L. Jeon, S. Huang, R.S. Kane, C.J. Wargo, I.S. Choi, D.E. Ingber, and G.M. Whitesides. Patterned deposition of cells and proteins onto surfaces by using three-dimensional microfluidic systems. *Proc Natl Acad Sci U S A*, 97(6):2408–2413, 2000.

[75] S. Takayama, J.C. McDonald, E. Ostuni, M.N. Liang, P.J. Kenis, R.F. Ismagilov, and G.M. Whitesides. Patterning cells and their environments using multiple laminar fluid flows in capillary networks. *Proc. Natl. Acad. Sci. U. S. A.*, 96(10):5545–5548, 1999.

[76] A. Tourovskaia, X. Figueroa-Masot, and A. Folch. Differentiation-on-a-chip: a microfluidic platform for long-term cell culture studies. *Lab Chip*, 5(1):14–19, 2005.

[77] N. Li Jeon, H. Baskaran, S.K.W. Dertinger, G.M. Whitesides, L. Van De Water, and M. Toner. Neutrophil chemotaxis in linear and complex gradients of interleukin-8 formed in a microfabricated device. *Nat. Biotech.*, 20(8):826–830, 2002.

[78] E. Delamarche, A. Bernard, H. Schmid, B. Michel, and H. Biebuyck. Patterned delivery of immunoglobulins to surfaces using microfluidic networks. *Science*, 276(5313):779–781, 1997.

[79] E. Delamarche, A. Bernard, H. Schmid, A. Bietsch, B. Michel, and H. Biebuyck. Microfluidic networks for chemical patterning of substrate: Design and application to bioassays. *J. Am. Chem. Soc.*, 120(3):500–508, 1998.

[80] C.A. Rowe, S.B. Scruggs, M.J. Feldstein, J.P. Golden, and F.S. Ligler. An array immunosensor for simultaneous detection of clinical analytes. *Anal. Chem.*, 71(2):433–439, 1999.

[81] C. A. Rowe, L. M. Tender, M. J. Feldstein, J. P. Golden, S. B. Scruggs, B. D. MacCraith, J. J. Cras, and F. S. Ligler. Array biosensor for simultaneous identification of bacterial, viral, and protein analytes. *Anal. Chem.*, 71(17):3846–3852, 1999.

[82] V. Kanda, J.K. Kariuki, D.J. Harrison, and M.T. McDermott. Label-free reading of microarray-based immunoassays with surface plasmon resonance imaging. *Anal. Chem.*, 76(24):7257–7262, 2004.

[83] B.P. Nelson, T.E. Grimsrud, M.R. Liles, R.M. Goodman, and R.M. Corn. Surface plasmon resonance imaging measurements of DNA and RNA hybridization adsorption onto DNA microarrays. *Anal. Chem.*, 73(1):1–7, 2001.

[84] X. Jiang, J.M.K. Ng, A.D. Stroock, S.K.W. Dertinger, and G.M. Whitesides. A miniaturized, parallel, serially diluted immunoassay for analyzing multiple antigens. *J. Am. Chem. Soc.*, 125(18):5294–5295, 2003.

[85] G.C. Koo and J.R. Peppard. Establishment of monoclonal anti-Nk-1.1 antibody. *Hybridoma*, 3(3):301–303, 1984.

[86] S.K. Kung, R.C. Su, J. Shannon, and R.G. Miller. Characterization of four new monoclonal antibodies that recognize mouse natural killer activation receptors. *Hybridoma*, 20(2):91–101, 2001.

[87] K. Miyake, C.B. Underhill, J. Lesley, and P.W. Kincade. Hyaluronate can function as a cell adhesion molecule and CD44 participates in hyaluronate recognition. *J. Exp. Med.*, 172(1):69–75, 1990.

[88] Comment. Danger: piranha solution is a strong oxidizer and explosions can occur when it is mixed with organic compounds/solvents. A safer alternative for cleaning microfluidic chips is to use a UV/ozone reactor.

[89] S. Chen, R. Alon, R.C. Fuhlbrigge, and T.A. Springer. Rolling and transient tethering of leukocytes on antibodies reveal specializations of selectins. *Proc Natl Acad Sci U S A*, 94(7):3172–3177, 1997.

[90] A.O. Eniola, P.J. Willcox, and D.A. Hammer. Interplay between rolling and firm adhesion elucidated with a cell-free system engineered with two distinct receptor-ligand pairs. *Biophys. J.*, 85(4):2720–2731, 2003.

[91] The time serie of Fig. 4.3 is available as real time video immunoassay.mov on http://www.zurich.ibm.com/st/video.

[92] E. Fitzpatrick, S. McBride, J. Yavelow, S. Najmi, P. Zanzucchi, and R. Wieder. Microfluidic techniques for single-cell protein expression analysis. *Clin. Chem.*, 52(6):1080–1088, 2006.

[93] N.D. Gallant, J.R. Capadona, A.B. Frazier, D.M. Collard, and A.J. Garcia. Micropatterned surfaces to engineer focal adhesions for analysis of cell adhesion strengthening. *Langmuir*, 18(14):5579–5584, 2002.

[94] J.P. Shelby, J. White, K. Ganesan, P.K. Rathod, and D.T. Chiu. A microfluidic model for single-cell capillary obstruction by Plasmodium falciparum-infected erythrocytes. *Proc. Natl. Acad. Sci. U. S. A.*, 100(25):14618–14622, 2003.

[95] A.Y. Fu, C. Spence, A. Scherer, F.H. Arnold, and S.R. Quake. A microfabricated fluorescence-activated cell sorter. *Nat. Biotechnol.*, 17(11):1109–1111, 1999.

[96] D. Huh, W. Gu, Y. Kamotani, J.B. Grotberg, and S. Takayama. Microfluidics for flow cytometric analysis of cells and particles. *Physiol. Meas.*, 26(3):R73–R98, 2005.

[97] J. Ducree and R. Zengerle. *Microfluidics*. Springer, Berlin, 2006.

[98] T.M. Squires and S.R. Quake. Microfluidics: Fluid physics at the nanoliter scale. *Rev. Mod. Phys.*, 77:977–1026, 2005.

[99] J.P. Brody, P. Yager, R.E. Goldstein, and R.H. Austin. Biotechnology at low Reynolds numbers. *Biophys J*, 71(6):3430–3441, 1996.

[100] K. Hosokawa, K. Sato, N. Ichikawa, and M. Maeda. Power-free poly(dimethylsiloxane) microfluidic devices for gold nanoparticle-based DNA analysis. *Lab Chip*, 4(3):181–185, 2004.

[101] G.C. Randall and P.S. Doyle. Permeation-driven flow in poly(dimethylsiloxane) microfluidic devices. *Proc. Natl. Acad. Sci. U. S. A.*, 102(31):10813–10818, 2005.

[102] P.G. de Gennes, F. Brochard-Wyart, and D. Quere. *Capillarity and Wetting Phenomena*. Springer-Verlag, New York, 2004.

[103] J. Bico and D. Quere. Rise of liquids and bubbles in angular capillary tubes. *J Colloid Interface Sci*, 247(1):162–166, 2002.

[104] C.H. Ahn, J. Choi, G. Beaucage, J.H. Nevin, J. Lee, A. Puntambekar, and J.Y. Lee. Disposable smart lab on a chip for point-of-care clinical diagnostics. *Proc. IEEE*, 92:154–173, 2004.

[105] E. Kim, Y. Xia, and G.M. Whitesides. Polymer microstructures formed by moulding in capillaries. *Nature*, 376(6541):581–584, 2002.

[106] F.G. Tseng, K.H. Lin, H.T. Hsu, and C.C. Chieng. A surface-tension-driven fluidic network for precise enzymenext term batch-dispensing and glucose detection. *Sens. Actuators A*, 111:107–117, 2004.

[107] R.G. Cox. The dynamics of the spreading of liquids on a solid-surface. 1. viscous-flow. *J. Fluid. Mech.*, 168:169–194, 1986.

[108] G. Martic, T. D. Blake, and J. De Coninck. Dynamics of imbibition into a pore with a heterogeneous surface. *Langmuir*, 21(24):11201–11207, 2005.

[109] S. Hardt, T. Baier, and F. Schönfeld. Computational models and methods for microfluidics: From flow distribution to mixing. Jyväskylä, 2004. ECCOMAS 2004, European Congress on Computational Methods in Applied Sciences and Engineering.

[110] D. Erickson. Towards numerical prototyping of labs-on-chip: modeling for integrated microfluidic devices. *Microfluid Nanofluid*, 1:301–308, 2005.

[111] I. Treise, N. Fortner, B. Shapiro, and A. Hightower. Efficient energy based modeling and experimental validation of liquid filling in planar micro-fluidic components and networks. *Lab Chip*, 5(3):285–297, 2005.

[112] V. Linder, H. Wu, X. Jiang, and G.M. Whitesides. Rapid prototyping of 2D structures with feature sizes larger than 8 microm. *Anal. Chem.*, 75(10):2522–2527, 2003.

[113] S. He, G.L.M.K.S. Kahanda, and P. Wong. Roughness of wetting fluid invasion fronts in porous media. *Phys. Rev. Lett.*, 69(26):3731–3734, 1992.

[114] M. Tuller and D. Or. Hydraulic conductivity of variably saturated porous media: film and corner flow in angular pore space. *Wat. Resour. Res.*, 37:1257–1276, 2001.

[115] The time series of Fig. 5.4 are available as real time videos b609813d-v1a.mov, b609813d-v1b.mov and b609813d-v1c.mov on http://dx.doi.org/10.1039/b609813d.

[116] S.K. Sia, V. Linder, B.A. Parviz, A. Siegel, and G.M. Whitesides. An integrated approach to a portable and low-cost immunoassay for resource-poor settings. *Angew. Chem. Int. Ed.*, 43(4):498–502, 2004.

[117] D.J. Beebe, J.S. Moore, J.M. Bauer, Q. Yu, R.H. Liu, C. Devadoss, and B. Jo. Functional hydrogel structures for autonomous flow control inside microfluidic channels. *Nature*, 404(6778):588–590, 2000.

[118] M. Diaz-Gonzalez, M.B. Gonzalez-Garcia, and A. Costa-Garcia. Recent advances in electrochemical enzyme immunoassays. *Electroanalysis*, 17(21):1901–1918, 2005.

[119] J. Homola. Present and future of surface plasmon resonance biosensors. *Anal. Bioanal. Chem.*, 377(3):528–539, 2003.

[120] D. R. Baselt, G. U. Lee, and R. J. Colton. Biosensor based on force microscope technology. *J. Vac. Sc. Tech. B*, 14(2):789–793, 1996.

[121] U. Bilitewski. Protein-sensing assay formats and devices. *Anal. Chim. Acta*, 568(1-2):232–247, 2006.

[122] P.M. Ridker. Clinical application of c-reactive protein for cardiovascular disease detection and prevention. *Circulation*, 107(3):363–369, 2003.

[123] G.K. Hansson. Mechanisms of disease - inflammation, atherosclerosis, and coronary artery disease. *N. Engl. J. Med.*, 352(16):1685–1695, 2005.

[124] A. Bietsch and B. Michel. Conformal contact and pattern stability of stamps used for soft lithography. *J. Appl. Phys.*, 88(7):4310–4318, 2000.

[125] A.C. Guyton and J.E. Hall. *Textbook of Medical Physiology.* Saunders, Philadelphia, 2000.

[126] R.H. Haynes and A.C. Burton. Role of the non-Newtonian behavior of blood in hemodynamics. *American Journal of Physiology*, 197(5):943–950, 1959.

[127] V.C. Rucker, K.L. Havenstrite, B.A. Simmons, S.M. Sickafoose, A.E. Herr, and R. Shediac. Functional Antibody Immobilization on 3-Dimensional Polymeric Surfaces Generated by Reactive Ion Etching. *Langmuir*, 21:7621–7625, 2005.

[128] E. Ostuni, R. Kane, C.S. Chen, D.E. Ingber, and G.M. Whitesides. Patterning Mammalian Cells Using Elastomeric Membranes. *Langmuir*, 16(7819):7811–7819, 2000.

[129] A. Folch, B.H. Jo, O. Hurtado, D.J. Beebe, and M. Toner. Microfabricated elastomeric stencils for micropatterning cell cultures. *J. Biomed. Mat. Res.*, 52(2):346–353, 2000.

[130] G.M. Kim, M.A.F. van den Boogaart, and J. Brugger. Fabrication and application of a full wafer size micro/nanostencil for multiple length-scale surface patterning. *Microelectron. Eng.*, 67:609–614, 2003.

[131] Diagnostics Systems Laboratories Inc., Ultra-sensitive CRP assay No DSL-10-42100, http://www.dslabs.com/kits, accessed August 2007.

[132] K. Hosokawa, M. Omata, and M. Maeda. Immunoassay on a power-free microchip with laminar flow-assisted dendritic amplification. *Anal. Chem.*, 79(15):6000–6004, 2007.

[133] M. Vanderlaan, B.E. Watkins, and L. Stanker. Environmental monitoring by immunoassay. *Environ. Sci. Technol.*, 22(3):247–254, 1988.

[134] J. Mair, F. Dienstl, and B. Puschendorf. Cardiac troponin-t in the diagnosis of myocardial injury. *Crit. Rev. Clin. Lab. Sci.*, 29(1):31–57, 1992.

[135] U. Samarajeewa, C.I. Wei, T.S. Huang, and M.R. Marshall. Application of immunoassay in the food-industry. *Crit. Rev. Food Sc. Nutr.*, 29(6):403–434, 1991.

[136] M.J. Pugia, G. Blankenstein, R.P. Peters, J.A. Profitt, K. Kadel, T. Willms, R. Sommer, H.H. Kuo, and L.S. Schulman. Microfluidic Tool Box as Technology Platform for Hand-Held Diagnostics. *Clin. Chem.*, 51(10):1923–1932, 2005.

[137] P. Yager, T. Edwards, E. Fu, K. Helton, K. Nelson, M.R. Tam, and B.H. Weigl. Microfluidic diagnostic technologies for global public health. *Nature*, 442(7101):412–418, 2006.

[138] Clearblue pregnancy tests. Unipath Ltd., Clearblue Pregnancy Tests, http://www.invernessmedical.com/consumer/, accessed August 2007.

[139] F. Hoffmann-La Roche Ltd., Diagnostics division, Accu-check, http://www.roche.com/home/products/, accessed August 2007.

[140] D. Wild, editor. *The Immunoassay Handbook*. Elsevier Ltd., Oxford, UK, 2005, pp. 424–430.

[141] Axon Lab AG, Cardiac Status, http://www.axonlab.com, accessed August 2007.

[142] E. Garcia, J.R. Kirkham, A.V. Hatch, K.R. Hawkins, and P. Yager. Controlled microfluidic reconstitution of functional protein from an anhydrous storage depot. *Lab Chip*, 4(1):78–82, 2004.

[143] M. Madou, J. Zoval, G. Jia, H. Kido, J. Kim, and N. Kim. Lab on a CD. *Annu. Rev. Biomed. Eng.*, 8:601–628, 2006.

[144] K.E. Nelson, J.O. Foley, and P. Yager. Concentration gradient immunoassay. 1. an immunoassay based on interdiffusion and surface binding in a microchannel. *Anal. Chem.*, 79(10):3542–3548, 2007.

[145] J.O. Foley, K.E. Nelson, A. Mashadi-Hossein, B.A. Finlayson, and P. Yager. Concentration gradient immunoassay. 2. computational modeling for analysis and optimization. *Anal. Chem.*, 79(10):3549–3553, 2007.

[146] S. Thorslund, O. Klett, F. Nikolajeff, K. Markides, and J. Bergquist. A hybrid poly(dimethylsiloxane) microsystem for on-chip whole blood filtration optimized for steroid screening. *Biomed. Microdev.*, 8(1):73–79, 2006.

[147] X. Yang, A. Hibara, K. Sato, M. Tokeshi, K. Morishima, Y. Kikutani, H. Kimura, and T. Kitamori. Interchannel microstructure for separation and analyses of plasma from whole blood. In *8th International Conference on Miniaturized Systems for Chemistry and Life Sciences, Malmo, Sweden*, pages 120–122. Royal Society of Chemistry, 2005.

[148] C. Roth, G. Winter, and G. Lee. Continuous measurement of drying rate of crystalline and amorphous systems during freeze-drying using an in situ microbalance technique. *J. Pharm. Sci.*, 90(9):1345–1355, 2001.

[149] J.L. Cleland, X. Lam, B. Kendrick, J. Yang, T.H. Yang, D. Overcashier, D. Brooks, C. Hsu, and J.F. Carpenter. A specific molar ratio of stabilizer to protein is required for storage stability of a lyophilized monoclonal antibody. *Journal Of Pharmaceutical Sciences*, 90(3):310–321, 2001.

[150] M. Mattern, U. Kohnert, G. Winter, and G. Lee. Stabilization of proteins in vacuum-dried glasses. ii: Process and storage stability in sugar-free amino acid systems. *Pharm. Devel. Technol.*, 4:199–208, 1999.

[151] J.K. Kaushik and R. Bhat. Why is trehalose an exceptional protein stabilizer? an analysis of the thermal stability of proteins in the presence of the compatible osmolyte trehalose. *J. Biol. Chem.*, 278(29):26458–26465, 2003.

[152] D.Q.M. Craig, P.G. Royall, V.L. Kett, and M.L. Hopton. The relevance of the amorphous state to pharmaceutical dosage forms: glassy drugs and freeze dried systems. *Int. J. Pharm.*, 179(2):179–207, 1999.

[153] W.Q. Sun, P. Davidson, and H.S.O. Chan. Protein stability in the amorphous carbohydrate matrix: relevance to anhydrobiosis. *Biochimica Biophysica Acta*, 1425(1):245–254, 1998.

[154] M.J. Pikal. Freeze-drying of proteins, part 1: Process design. *Biopharm.*, 3:18–27, 1990.

[155] K. Izutsu and S. Kojima. Freeze-concentration separates proteins and polymer excipients into different amorphous phases. *Pharmaceutical Research*, 17(10):1316–1322, 2000.

[156] D.J. Beebe, G.A. Mensing, and G.M. Walker. Physics and applications of microfluidics in biology. *Annu. Rev. Biomed. Eng.*, 4:261–286, 2002.

[157] J. Khandurina and A. Guttman. Bioanalysis in microfluidic devices. *J. Chromatogr. A*, 943(2):159–183, 2002.

[158] D.N. Bresslauer, P.J. Lee, and L.P. Lee. Microfluidics-based systems biology. *Mol. BioSyst.*, 2:97–112, 2006.

[159] A.J. DeMello. Control and detection of chemical reactions in microfluidic systems. *Nature*, 442(7101):394–402, 2006.

[160] P.S. Dittrich, K. Tachikawa, and A. Manz. Micro total analysis systems. latest advancements and trends. *Anal. Chem.*, 78(12):3887–3907, 2006.

[161] K.W. Oh and C.H. Ahn. A review of microvalves. *J. Micromechan. Microeng.*, 16:R13–R39, 2006.

[162] C.M. Lu, Y.B. Xie, Y. Yang, M.M.C. Cheng, C.G. Koh, Y.L. Bai, and L.J. Lee. New valve and bonding designs for microfluidic biochips containing proteins. *Anal. Chem.*, 79(3):994–1001, 2007.

[163] E. Stemme and G. Stemme. A valveless/nozzle-based fluid pump. *Sens. Actuators A Phys.*, 39:159–167, 1993.

[164] F.P. Man, C.H. Mastrangelo, M.A. Burns, and D.T. Burke. Microfabricated capillarity-driven stop valve and sample injector. In *Proceedings of The Eleventh Annual International Workshop on Micro Electro Mechanical Systems.*, 1998.

[165] T.S. Leu and P.Y. Chang. Pressure barrier of capillary stop valves in micro sample separators. *Sens. Actuators A Phys.*, 115:508–515, 2004.

[166] V. Siljegovic, N. Milicevic, and P. Griss. Passive, programmable flow control in capillary force driven microfluidic networks. *TRANSDUCERS '05. The 13th International Conference on Solid-State Sensors, Actuators and Microsystems. Digest of Technical Papers (IEEE Cat. No. 05TH8791)*, pages 1565–8 Vol. 2, 2005.

[167] H. Cho, H.Y. Kim, J.Y. Kang, and T.S. Kim. How the capillary burst microvalve works. *J. Colloid Interface Sci.*, 306(2):379–385, 2007.

[168] J. Chen, P. Huang, and M. Lin. Analysis and experiment of capillary valves for microfluidics on a rotating disk. *Microfluid Nanofluid*, pages DOI:10.1007/s10404–007–0196–x.

[169] A. Gliere and C. Delattre. Modeling and fabrication of capillary stop valves for planar microfluidic systems. *Sens. Actuators A Phys.*, 130–131:601–608, 2006.

[170] J. Melin, N. Roxhed, G. Gimenez, P. Griss, W. van der Wijngaart, and G. Stemme. A liquid-triggered liquid microvalve for on-chip flow control. *Sens. Actuators B Chem.*, 100(3):463–468, 2004.

[171] M. Prakash and N. Gershenfeld. Microfluidic bubble logic. *Science*, 315(5813):832–835, 2007.

[172] L.F. Cheow, L. Yobas, and D.L. Kwong. Digital microfluidics: Droplet based logic gates. *Appl. Phys. Lett.*, 90(5):054107, 2007.

[173] J.Y. Cheng and L.C. Hsiung. Electrowetting (ew)-based valve combined with hydrophilic teflon microfluidic guidance in controlling continuous fluid flow. *Biomed. Microdev.*, 6(4):341–347, 2004.

[174] The real time videos 10404_2007_256_moesm1_esm.mov and 10404_2007_256_moesm2_esm.mov corresponding to Fig. 8.2 and Fig. 8.4 are available on http://dx.doi.org/10.1007/s10404-007-0256-2.

[175] A. Krishnan, A. Wilson, J. Sturgeon, C.A. Siedlecki, and E.A. Vogler. Liquid-vapor interfacial tension of blood plasma, serum and purified protein constituents thereof. *Biomaterials*, 26(17):3445–3453, 2005.

[176] R. Gentry, R. Martin, and B. Daly. An eulerian differencing method for unsteady compressible flow problems. *J. Comp. Phys.*, 1:87–118, 1966.

[177] C. Hirt, B. Nichols, and N. Romero. Sola: A numerical solution algorithm for transient fluid flows. Technical Report LA-5852, LA–5852, Los Alamos Scientific Lab., N. Mex.(USA), 1975.

Acknowledgments

This work would not have been possible without the support of many people. It is my pleasure to thank each and every one of them for their valuable contributions and support in the last years.

My special thanks go to Prof. Dr. Hans-Joachim Güntherodt for supporting my work as an external PhD student and always helping out when necessary. Furthermore I thank Prof. Dr. Nico de Rooij for kindly acting as co-referee and evaluating my thesis.

I express my deepest gratitude to Dr. Emmanuel Delamarche for his dedication and superintendence, his patience in correcting and writing, and his knowledgeable and diplomatic guidance. His support and reams of exciting discussions were simply invaluable.

I also express my sincere gratitude to PD Dr. Patrik Hunziker without whom the project would not have been kicked off. His fascinating visionary spirit and his profound command of physics in medicine made it a pleasure to work for him.

It was a great pleasure to work in this interdisciplinary environment with experts in the fields of medicine, biology, microfabrication technology and chemistry at the University Hospital in Basel and the IBM Zurich Research Laboratory in Rüschlikon. My sincere thanks are given to the managers at IBM, Dr. Paul Seidler, the head of the Science & Technology Department, and Dr. Walter Riess for making this cooperation possible and giving me the opportunity to benefit from the substantial skills and expertise, and infrastructure available in the lab.

I thank all my colleagues at the ZRL for their generous support. Ute Drechsler, Michel Dupont and Richard Stutz for help with the fabrication of many microstructures, Heinz Schmid, Dr. David Juncker, Dr. Daniel Solis, Jörg Ziegler and Sean Coyer for many interesting discussions and technical help,

as well as Urs Bapst, Meinrad Tschudy, Marilyne Sousa Petit, the staff of the publication and purchasing departments, and in the library.

I acknowledge support and many useful discussions from Dr. Jakob Weber, Dr. Andreas Abel and Thomas Jermann from Bühlmann Laboratories in Schönenbuch. I am also grateful to Dr. Christoph Fattinger and Dr. Gregor Dernick from F. Hoffmann-La Roche in Basel for helpful discussions. I thank Reinhold Jurischka and Prof. Dr. Holger Reinecke from the University of Freiburg i. Br. for providing their know-how in microfabrication of microstructures in plastics and fabricating samples for us.

Finally, I thank my office and lab mates in Rüschlikon and Basel, which have already been and which have not yet been mentioned, for sharing their experiences, many discussions and the pleasant time we had together at work or at leisure: Corinne von Arx, Steven Bentley, Dr. Michael Björk, Dr. Marco Dorrestijn, Jennifer Foley, Luc Gervais, Dr. Oliver Hayden, Dr. Christian Jansen, Dr. Tobias Kraus, Robert Lovchik, Dr. Laurent Malaquin, Dr. Heiko Wolf, and Dr. Marc Wolf.

I acknowledge financial support from the Swiss Commission for Technology and Innovation (KTI).

Last but not least I like to thank my family for giving me all the assistance I needed. I thank my parents for making my studies possible. Most of all I thank my wife, Kirsten, for enriching my life with her love.